MS Analysis Report

Ribolytix Project Number: Internal

Ribolytix Report Number: Internal-MS-3v3

Client / laboratory: Internal

Report date: 2026-11-15

Report status: Final

Prepared By:

Ribolytix, Inc.

701 West Main Street, Suite 200

Durham, NC, 27701

QUALITY CONTROL STATEMENT

It is the objective of Ribolytix, Inc., that all studies conducted by our facility shall be of the highest quality to ensure the integrity of the data generated.

The MS analysis report for project Internal was reviewed before finalization.

JohnCarlo Kristofich, PhD

Founder & CEO

Ribolytix, Inc.

1. Purpose and Scope

This study profiles cellular responses to RBP-targeting compounds in HCT116 cells. It identifies compound-responsive proteins and potential markers of cellular activity, examines relationships among their responses, and interprets the observed patterns in the context of the compounds' reported mechanisms.

This report summarizes the results from LC–MS/MS analysis of the sample fractions identified in Section 4, including protein coverage, sample variability, differential analysis, and functional annotation of differentially abundant proteins. The supporting data package contains results and figures for all protein panels defined below. This report focuses on the filtered GO RNA-binding protein panel, which includes proteins with annotated RNA-binding functions while excluding those with historical evidence that free protein contributed more than 25% of their measured signal.

Protein panel	Definition
Total identified proteins	Proteins identified by LC–MS/MS in the analyzed sample fractions, excluding contaminants and technical standards.
GO RNA-binding proteins	Identified proteins with Gene Ontology annotations for RNA binding (GO:0003723).
Filtered GO RNA-binding proteins	GO RNA-binding proteins excluding those with previously reported free-protein contributions greater than 25% of their measured signal ($S/N < 3$). Proteins without previously reported S/N measurements remain included.

2. Abbreviations and Definitions

The following abbreviations and definitions are aligned with terminology previously defined by Kristofich and Nicchitta (*Nature Communications*, 2023; *RNA*, 2024; *Bio-protocol*, 2024).

RBP: RNA-binding protein.

Ribonucleoprotein (RNP) fractions: Sample fraction containing total RNA and RNA-bound protein.

Total protein (Input) fractions: Sample fraction containing total protein.

Fragmented RNP (frag RNP) fractions: Sample fraction containing both protein-bound and protein-free RNA fragments (fragment-size peak: approximately 200 nt).

Fragmented and free RNA depleted RNP (frag clRNP) fractions: Sample fraction containing protein-bound RNA fragments (fragment-size peak: approximately 200 nt).

PK: Proteinase K.

PK-treated, fragmented RNP (PK frag RNP) fractions: RNA fraction recovered following proteinase K treatment of a frag RNP fraction.

PK-treated, fragmented, and free RNA depleted RNP (PK frag clRNP) fractions: RNA fraction recovered following proteinase K treatment of a frag clRNP fraction.

Signal (*S*): RNA-bound protein.

Noise (*N*): Unbound counterpart of an RNA-bound protein.

Background (*B*): Protein without an RNA-bound counterpart.

Signal-to-noise ratio (*S*/*N*): The ratio of RNA-bound protein to its unbound counterpart.

Yield: Quantity of RNA or protein recovered by a given process expressed as micrograms per one percent of starting sample fraction (e.g., µg/% fraction).

RNP composition: The ratio of protein to RNA in RNP fractions, estimated by dividing protein yields by their corresponding RNA yields.

LC-MS/MS: Liquid chromatography-tandem mass spectrometry.

GO: Gene Ontology, a reference system describing molecular functions, biological processes, and cellular components.

Sum peptide intensities (SPI): The sum of MS peptide intensities assigned to a protein; used to estimate protein quantity.

Total Protein Approach (TPA): An approach for estimating protein abundances from protein SPI values relative to total MS signal of the sample (total SPI).

Protein abundance (%TP): Protein abundance estimated as 100 × protein SPI divided by total SPI across all eligible proteins in the sample. Protein panels retain this complete eligible-protein denominator.

Fold change (FC): In this report, the ratio of geometric mean protein abundances (%TP) in the numerator and denominator groups.

Differentially abundant protein: A protein showing a statistically significant difference in abundance between the compared sample groups after correction for multiple testing.

False discovery rate (FDR): The expected proportion of significant results that are actually false positives.

Coefficient of variation (CV): Standardized measure of dispersion of a probability distribution or frequency distribution, calculated as the ratio of the standard deviation to the mean.

Principal component analysis (PCA): A method that summarizes variation across many measurements using uncorrelated components, ordered by the amount of variation they explain, to display similarities and differences among samples.

MA plot: A plot of M (minus, or the difference between log-transformed values) versus A (average). In this report, M represents the $\log_2$ ratio of protein abundances (%TP), and A represents the average $\log_{10}$(%TP) across all samples.

Over-representation analysis (ORA): A statistical analysis testing whether a functional category is represented more frequently in a selected gene or protein list than expected relative to a defined reference background.

Gene set enrichment analysis (GSEA): An analysis testing whether members of a predefined gene set are concentrated toward the top or bottom of a gene list ranked by a specified measurement or statistic.

Normalized enrichment score (NES): A GSEA enrichment score scaled relative to permutation-derived scores to account for differences in gene-set size. Positive and negative values indicate enrichment toward the top and bottom of the ranked list, respectively. Statistical significance is assessed separately.

3. Study and Sample Metadata

3.1 Experimental Sample List

Sample group	Biological replicate	Cell line	UV irradiation	Treatment / condition
H3B-8800	R1	HCT116	0.4 J/cm²; 254 nm	10 µM H3B-8800; 90 min
H3B-8800	R2	HCT116	0.4 J/cm²; 254 nm	10 µM H3B-8800; 90 min
H3B-8800	R3	HCT116	0.4 J/cm²; 254 nm	10 µM H3B-8800; 90 min
RK-33	R1	HCT116	0.4 J/cm²; 254 nm	10 µM RK-33; 90 min
RK-33	R2	HCT116	0.4 J/cm²; 254 nm	10 µM RK-33; 90 min
RK-33	R3	HCT116	0.4 J/cm²; 254 nm	10 µM RK-33; 90 min
Untreated	R1	HCT116	0.4 J/cm²; 254 nm	Untreated; 90-min timepoint
Untreated	R2	HCT116	0.4 J/cm²; 254 nm	Untreated; 90-min timepoint
Untreated	R3	HCT116	0.4 J/cm²; 254 nm	Untreated; 90-min timepoint

4. Sample Fractions Covered by This Report

The following table identifies the sample fractions included in this MS analysis and accompanying data package.

Client-provided sample ID	Internally assigned sample ID	Sample fraction type	Sample fraction ID
Not provided	Not provided	Not provided	Not provided
Not provided	Not provided	Not provided	Not provided
Not provided	Not provided	Not provided	Not provided
Not provided	Not provided	Not provided	Not provided
Not provided	Not provided	Not provided	Not provided
Not provided	Not provided	Not provided	Not provided
Not provided	Not provided	Not provided	Not provided
Not provided	Not provided	Not provided	Not provided
Not provided	Not provided	Not provided	Not provided

5. Execution and Source-Data Traceability

Execution records, source files, internal software versions, and reference dates used for this report are summarized below.

Component	Execution and source information
MS sample submission	Aliquots for the 9 analyzed sample fractions were prepared on July 27, 2026, following SOP-P-0029-0001. Supporting equipment, material, and reagent records are provided in 05_Traceability.
LC–MS/MS acquisition and database searching	Acquisition and search methods are summarized in Methods_and_Data_Analysis.docx. Additional details may be requested from the facility.
MS data analysis	Ribolytix MS analysis workflow 3.4.5; executed November 14, 2026.
Databases and annotations	Accessed November 14, 2026: UniProtKB 2026_04 for protein functions, KEGG 2026, Reactome 98, InterPro domains 111.0, GO biological process 2026-11-13, GO molecular function 2026-11-13, GO cellular component 2026-11-13, STRING 12.5 (functional associations). Reference check November 14, 2026: UniProtKB 2026_04, Pfam 39.0, InterPro 111.0 (protein features). Accessed November 14, 2026: GOA/QuickGO annotations; GO release 2026-11-13.
Report assembly	Ribolytix Deliverable builder 1.12.19; report assembled November 15, 2026.

Supporting data and traceability records are provided in the data package.

6. Protein Coverage

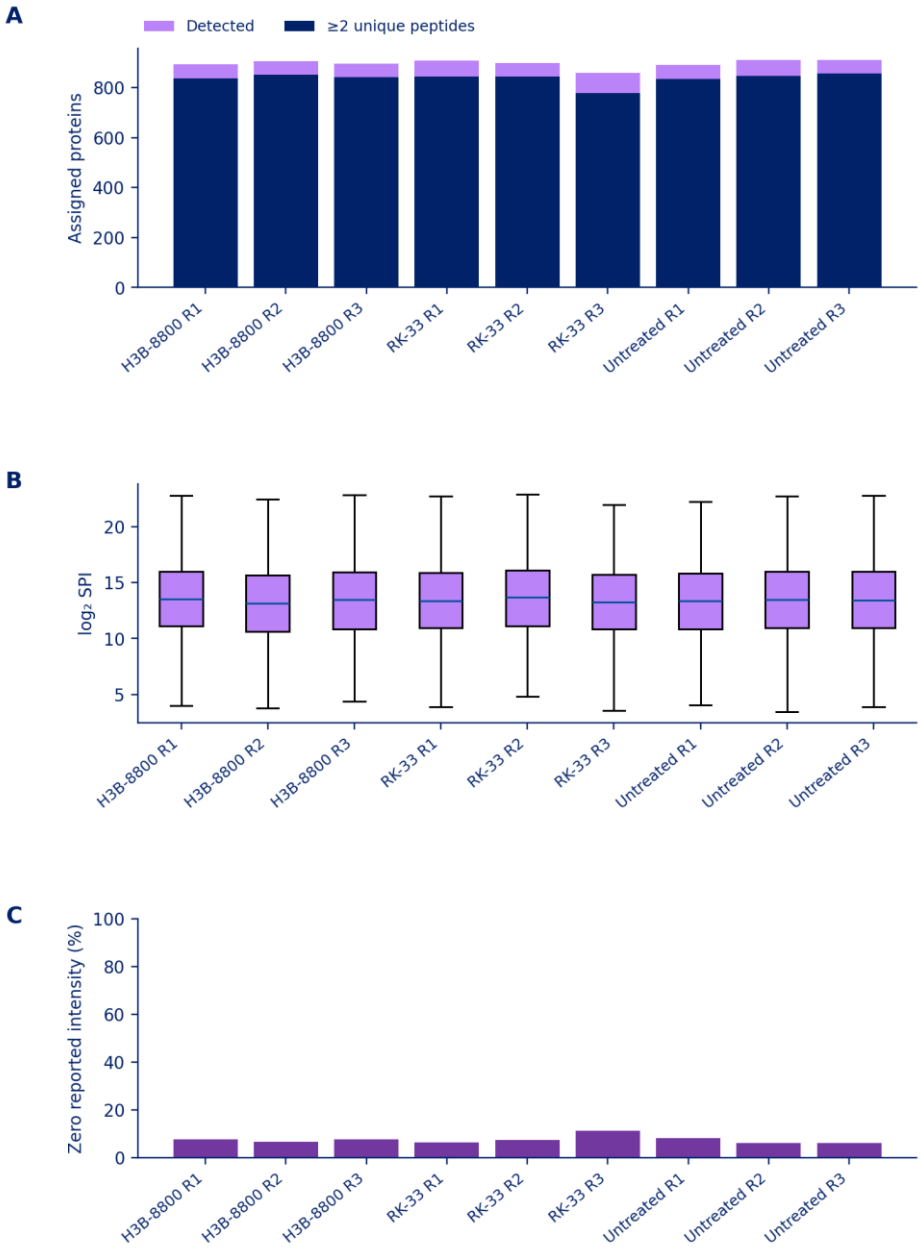
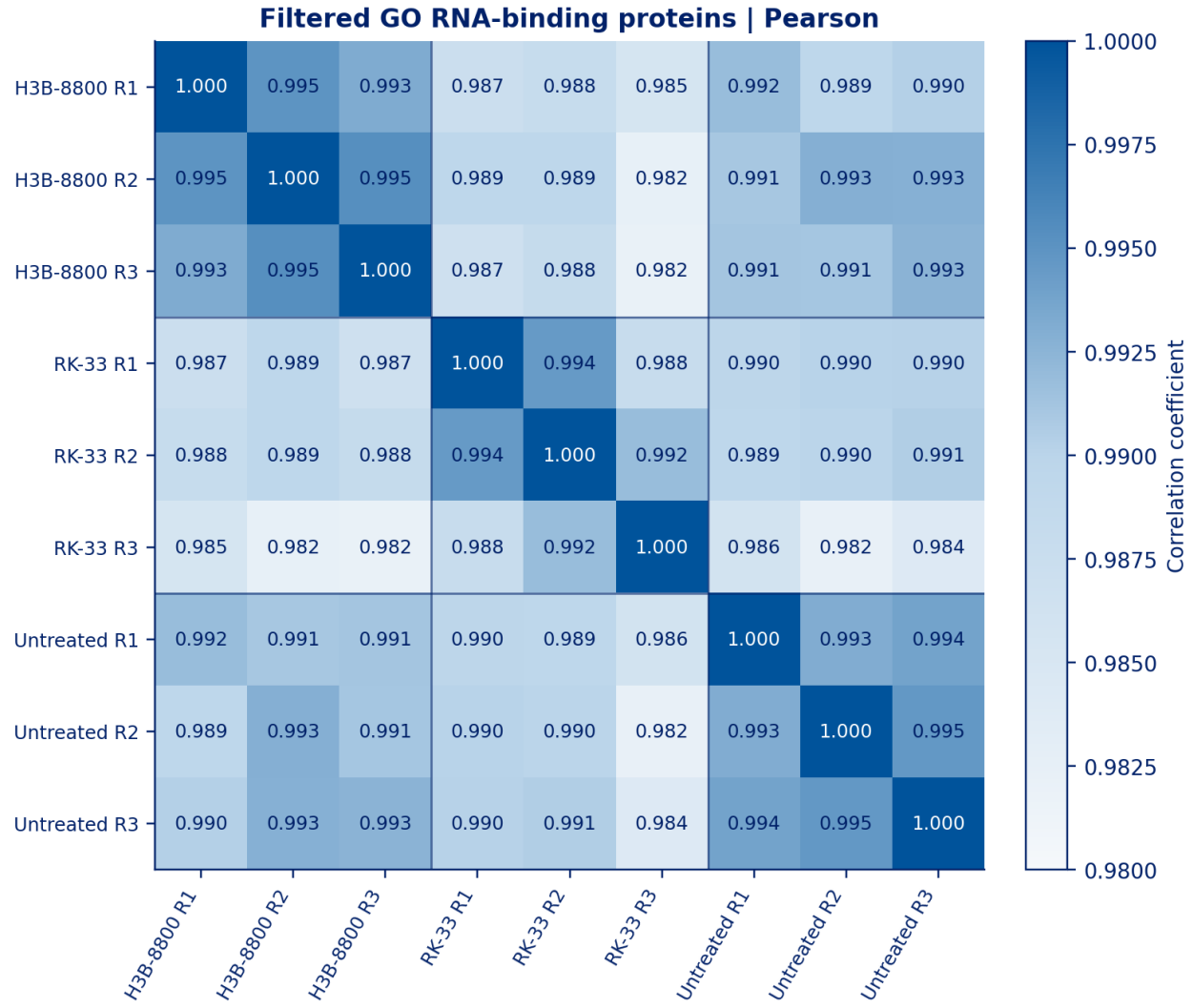


Figure 1. Protein coverage and signal distributions for filtered GO RNA-binding proteins. (A) Numbers of proteins detected per sample. Total bar height represents proteins detected with ≥1 unique peptide; dark blue indicates the subset supported by ≥2 unique peptides. **(B)** Distributions of positive protein intensities after $\log_2$ transformation, before sample normalization. Boxes span the interquartile range (IQR), horizontal lines indicate medians, and whiskers extend to the most extreme values within 1.5 × IQR of the box edges. Outliers are not displayed. **(C)** Percentage of proteins in the panel with zero reported intensity in each sample. Differential-abundance testing requires ≥2 unique peptides per protein in every included replicate of both comparison groups.

Across samples, 859–911 proteins were identified, including 779–857 identified with ≥2 unique peptides.

7. Within- and Between-Group Variability



750 common proteins; color scale: 0.98–1.00; diagonal: self-correlation; gray: undefined.

Figure 2. Pairwise Pearson correlations among samples. Correlations were calculated using $\log_2$(%TP) values in the analyzed RNP fractions for filtered GO RNA-binding proteins identified with at least two unique peptide matches in every included sample. Each cell shows Pearson's *r* for the corresponding sample pair; diagonal cells represent self-correlations.

Principal component analysis

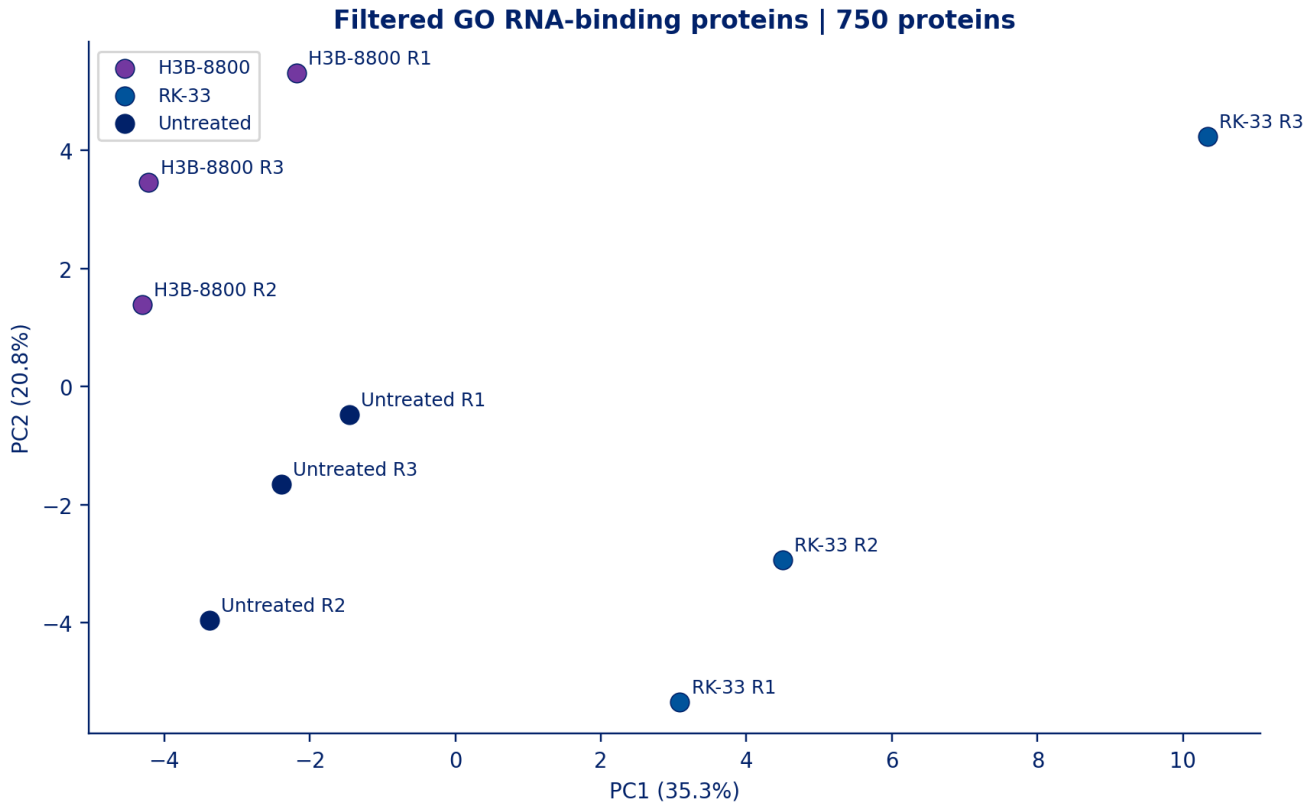


Figure 3. Principal component analysis of filtered GO RNA-binding proteins. PCA was performed using $\log_2$(%TP) values in the analyzed RNP fractions for proteins identified with at least two unique peptide matches in every included sample. Points represent individual biological replicates, colored by sample group. Axis labels indicate the percentage of total variance explained by each principal component.

The first two principal components accounted for 56.1% of the total variance (PC1, 35.3%; PC2, 20.8%).

8. Differential Analysis

Common contaminants and spike-ins were excluded, and sum peptide intensities (SPI) were calculated by summing the intensities of unique peptides assigned to each protein. Proteins identified with at least two unique peptide matches in every included sample were retained. Samples were mean-normalized to total SPI across these proteins. Protein abundances (%TP) were estimated using the Total Protein Approach and expressed as a percentage of total SPI across all eligible proteins. Protein panels retained this complete eligible-protein denominator.

Within the filtered GO RNA-binding proteins panel, $\log_2$(%TP) values in the analyzed RNP fractions were used to test for differences in protein abundance using independent, two-tailed, homoscedastic *t* tests. The Benjamini–Hochberg procedure was used to correct for multiple hypothesis testing across all proteins tested in this panel within each comparison, with a false discovery rate of 5%. The adjusted *p* values are reported as *q* values ($q < .05$). Fold changes represent ratios of geometric mean protein abundances (%TP) between groups. No minimum fold-change threshold was applied.

Short protein function and feature descriptions accompany the heatmaps. Descriptions summarize recorded UniProtKB functions, selected positive Gene Ontology annotations, and Pfam/InterPro features. They are independent of the observed abundance differences. Complete annotations, source evidence, database releases, and selection rules for every retained identified protein are provided in the supporting Protein_Annotations folder.

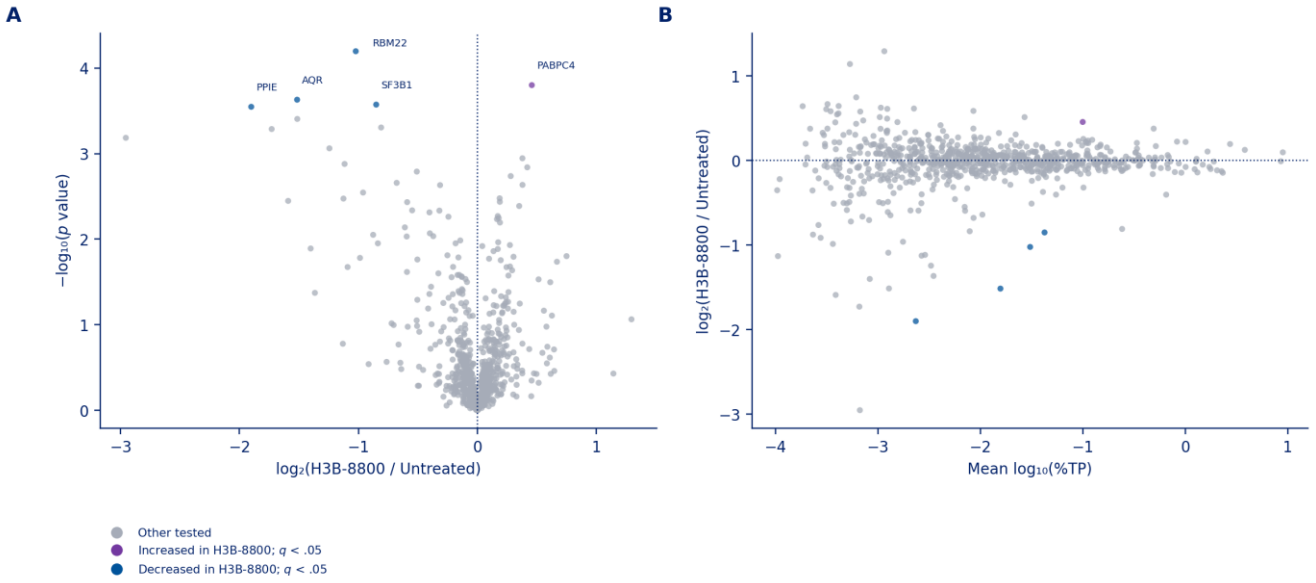


Figure 4. Differential analyses of filtered GO RNA-binding proteins between H3B-8800 and Untreated. 5 of 790 tested proteins met $q < .05$. **(A)** Volcano plot showing $-\log_{10}$-transformed *p* values before FDR correction as a function of $\log_2$(H3B-8800/Untreated). Point colors indicate differential abundance after Benjamini–Hochberg correction ($q < .05$) in both panels. **(B)** MA plot showing $\log_2$(H3B-8800/Untreated) as a function of mean $\log_{10}$(%TP) across all samples.

Of the 790 proteins tested, 5 (0.6%) differed significantly in abundance, including 1 with increased and 4 with decreased abundance in H3B-8800 relative to Untreated.

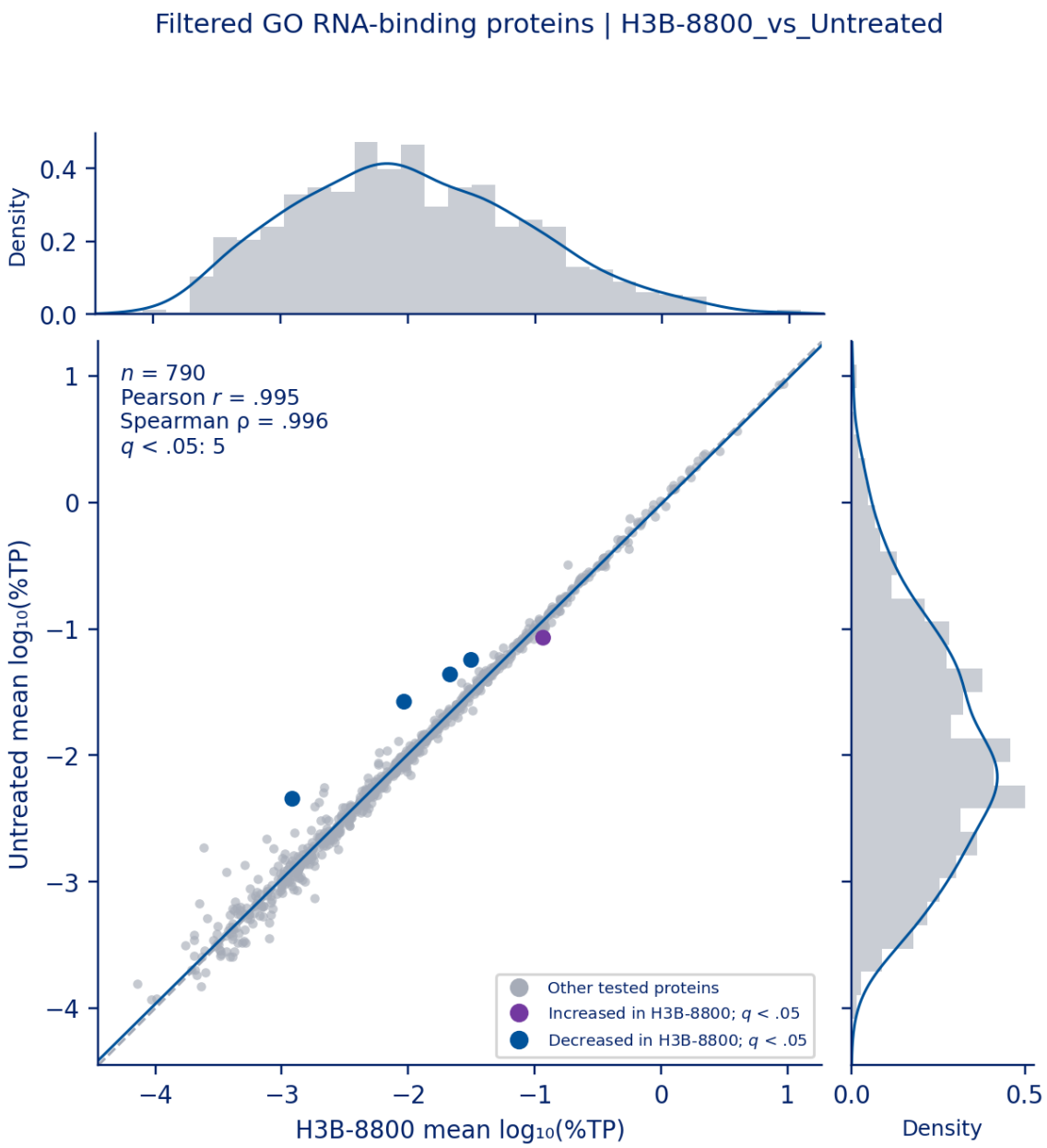


Figure 5. Comparison of observed protein abundances between H3B-8800 and Untreated. Scatterplot comparing group means of $\log_{10}$(%TP) for filtered GO RNA-binding proteins. Each point represents a protein tested for differential abundance. Corresponding histograms and probability density curves show the distributions for the horizontal-axis group (top) and vertical-axis group (right). Purple and blue identify proteins with significantly increased and decreased abundance, respectively, in H3B-8800 relative to Untreated after Benjamini–Hochberg correction ($q < .05$). Other tested proteins are shown in gray. The dashed line indicates equal abundance, and the solid blue line shows the linear regression fit.

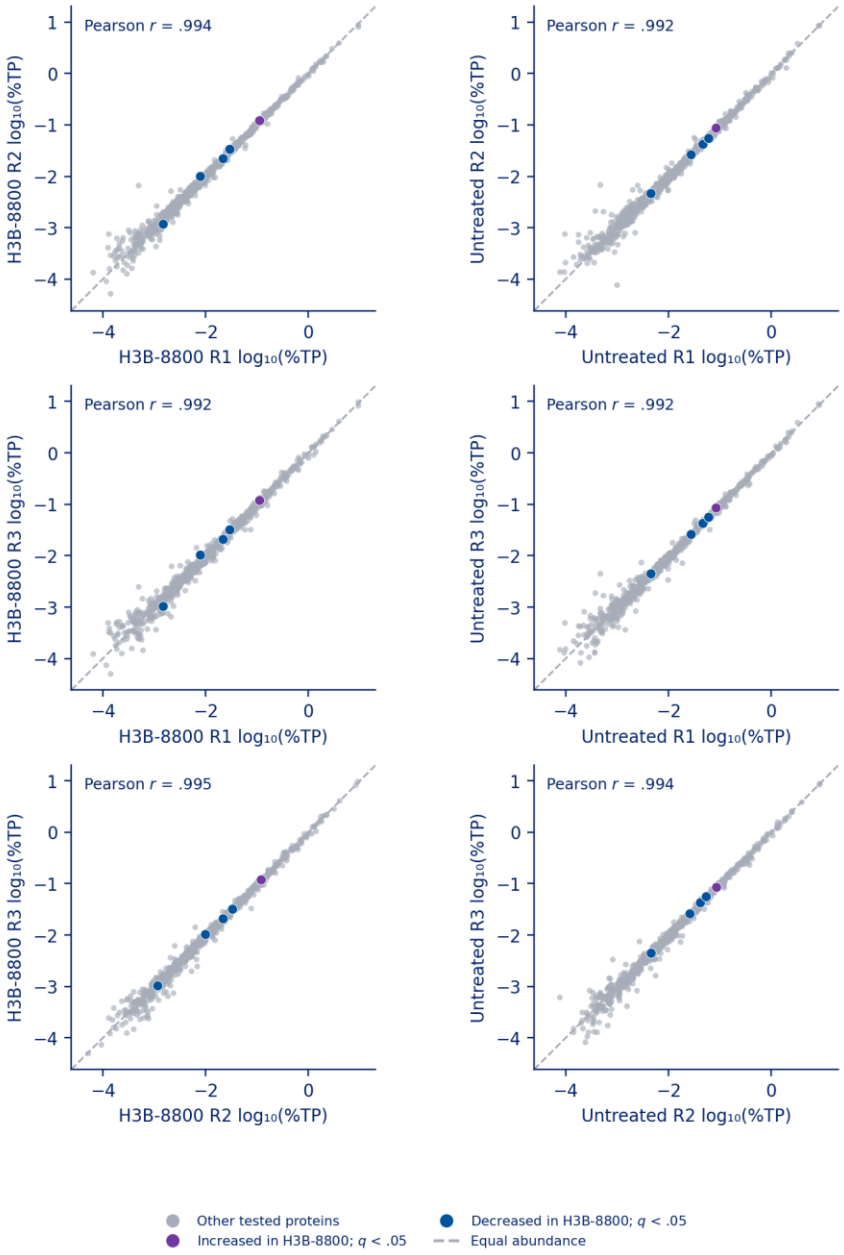


Figure 6. Within-group comparisons of biological replicates for H3B-8800 and Untreated. Each point represents a protein tested in the filtered GO RNA-binding proteins panel; axes show $\log_{10}$(%TP) in the analyzed RNP fractions for individual replicates. Pearson *r* summarizes all plotted proteins. The dashed line indicates equal abundance. Purple and blue identify proteins with significantly increased and decreased abundance, respectively, in H3B-8800 relative to Untreated (BH-adjusted $q < .05$). Other tested proteins are gray. The colors refer to the between-group comparison, not a within-group test.

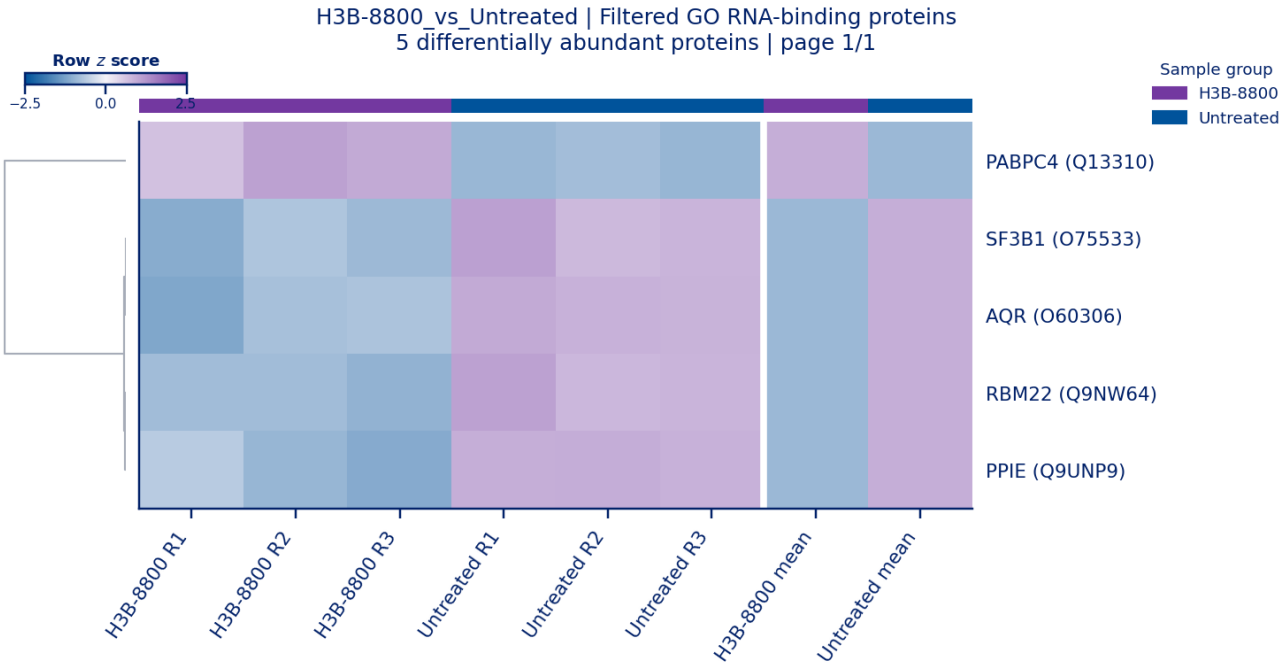


Figure 7. Protein abundance patterns of differentially abundant proteins. Heatmap showing $\log_2$(%TP) values in the analyzed RNP fractions, standardized within each protein across biological replicates (row *z* scores). Purple and blue indicate abundances above and below the mean for each protein, respectively; the color scale is limited to ±2.5. Rows were clustered using average linkage and correlation distance across replicate samples. The dendrogram branches show the hierarchical clustering of proteins by their abundance patterns; the merge positions reflect average correlation distances, not evidence of direct interactions. Sample columns retain their experimental order. The final columns show the group means of the row *z* scores and were excluded from clustering. All proteins meeting $q < .05$ are included.

Protein functions and features (Figure 7)

PABPC4 (Q13310). Binds the poly(A) tail of mRNA; GO annotations include poly(A) binding; RNA catabolic process. Annotated features: MLLE domain; RNA recognition motif.

SF3B1 (O75533). Component of the 17S U2 SnRNP complex of the spliceosome, a large ribonucleoprotein complex that removes introns from transcribed pre-mRNAs. Annotated features: Splicing factor 3B subunit 1; PPP2R1A-like HEAT repeat (repeat).

AQR (O60306). Involved in pre-mRNA splicing as component of the spliceosome; GO annotations include 3'-5' RNA helicase activity; mRNA splicing, via spliceosome. Annotated features: AAA domain; Intron-binding protein aquarius insert domain.

RBM22 (Q9NW64). Required for pre-mRNA splicing as component of the activated spliceosome; GO annotations include U6 snRNA binding; positive regulation of protein import into nucleus. Annotated features: RBM22 CCCH zinc finger domain; RNA recognition motif.

PPIE (Q9UNP9). Involved in pre-mRNA splicing as component of the spliceosome; GO annotations include poly(A) binding; mRNA splicing, via spliceosome. Annotated features: Cyclophilin type peptidyl-prolyl cis-trans isomerase/CLD; RNA recognition motif.

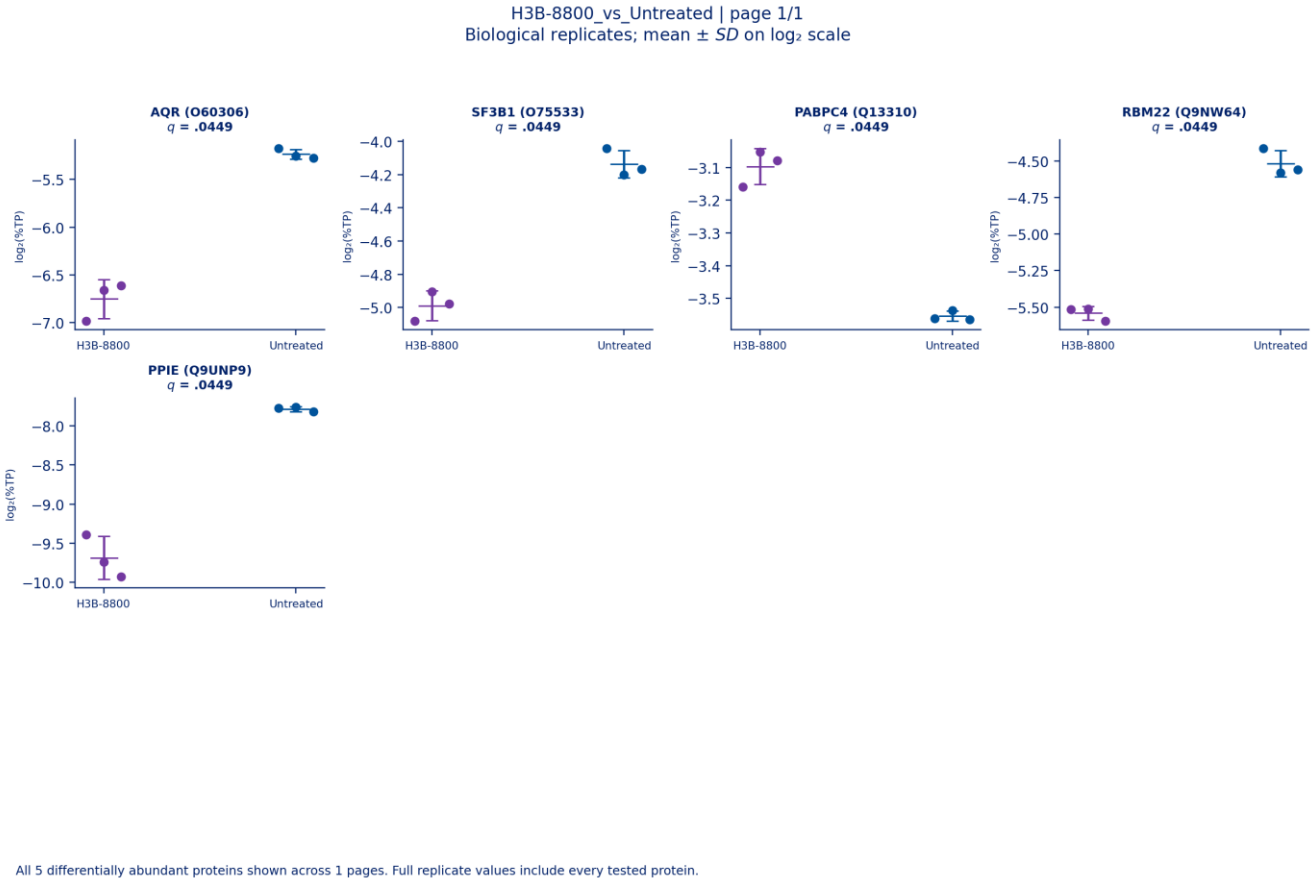


Figure 8. Replicate abundances of differentially abundant proteins between H3B-8800 and Untreated. Points show $\log_2$(%TP) for individual biological replicates (n = 3 per sample group); horizontal bars and whiskers show the group mean and standard deviation on this scale. Panels identify the protein by gene symbol and UniProt accession and report its q value. All significant proteins are shown across 1 pages (page 1 of 1).

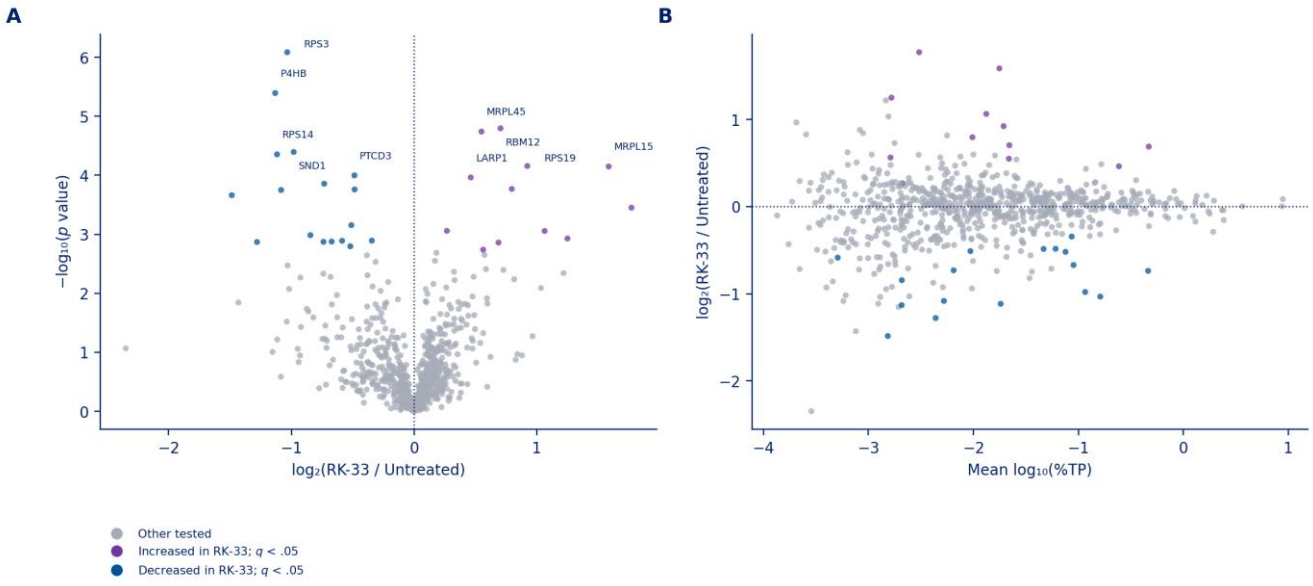


Figure 9. Differential analyses of filtered GO RNA-binding proteins between RK-33 and Untreated. 29 of 757 tested proteins met q < .05. **(A)** Volcano plot showing $-\log_{10}$-transformed p values before FDR correction as a function of $\log_2$(RK-33/Untreated). Point colors indicate differential abundance after Benjamini–Hochberg correction (q < .05) in both panels. **(B)** MA plot showing $\log_2$(RK-33/Untreated) as a function of mean $\log_{10}$(%TP) across all samples.

Of the 757 proteins tested, 29 (3.8%) differed significantly in abundance, including 12 with increased and 17 with decreased abundance in RK-33 relative to Untreated.

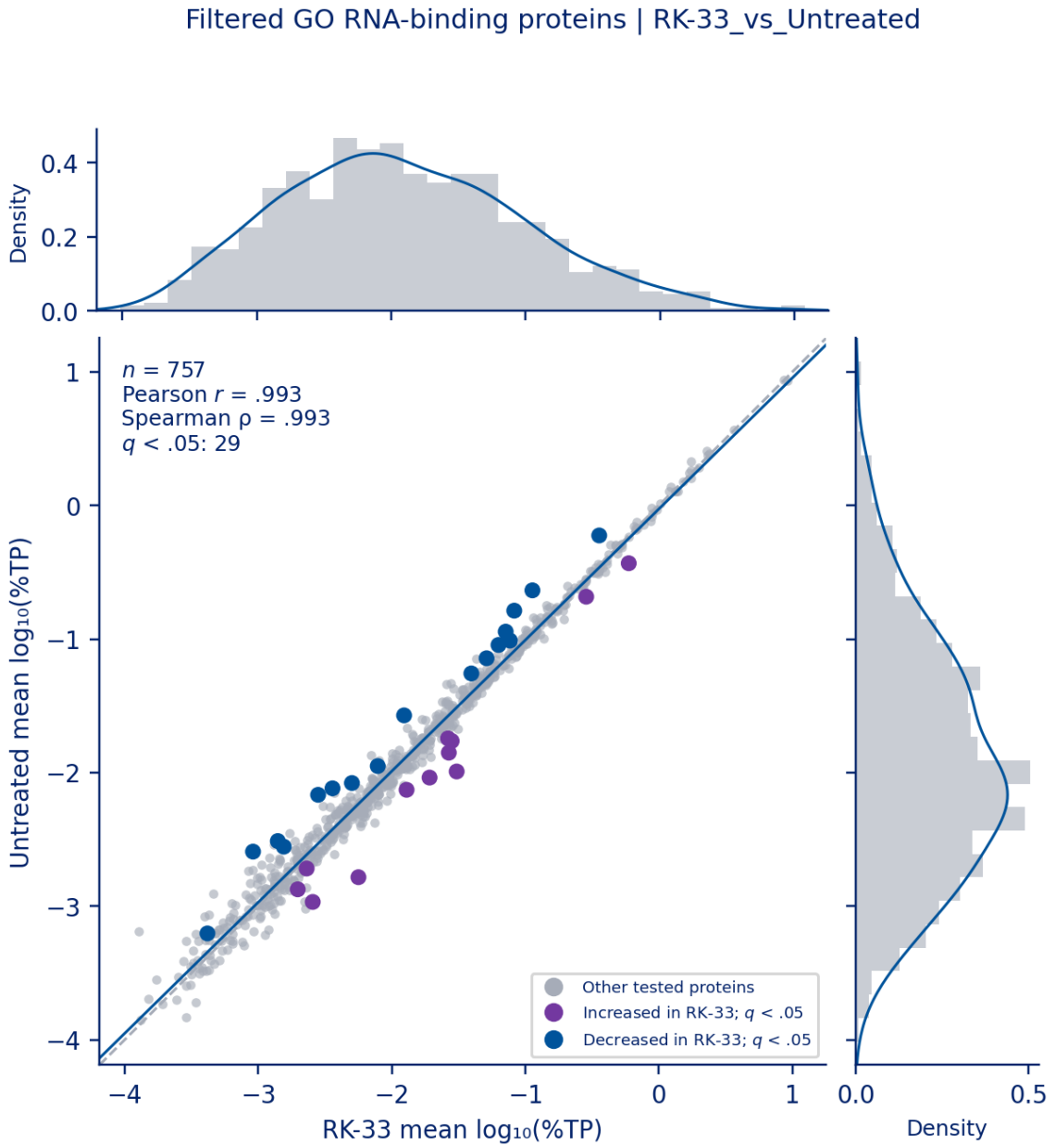


Figure 10. Comparison of observed protein abundances between RK-33 and Untreated. Scatterplot comparing group means of $\log_{10}$(%TP) for filtered GO RNA-binding proteins. Each point represents a protein tested for differential abundance. Corresponding histograms and probability density curves show the distributions for the horizontal-axis group (top) and vertical-axis group (right). Purple and blue identify proteins with significantly increased and decreased abundance, respectively, in RK-33 relative to Untreated after Benjamini–Hochberg correction ($q < .05$). Other tested proteins are shown in gray. The dashed line indicates equal abundance, and the solid blue line shows the linear regression fit.

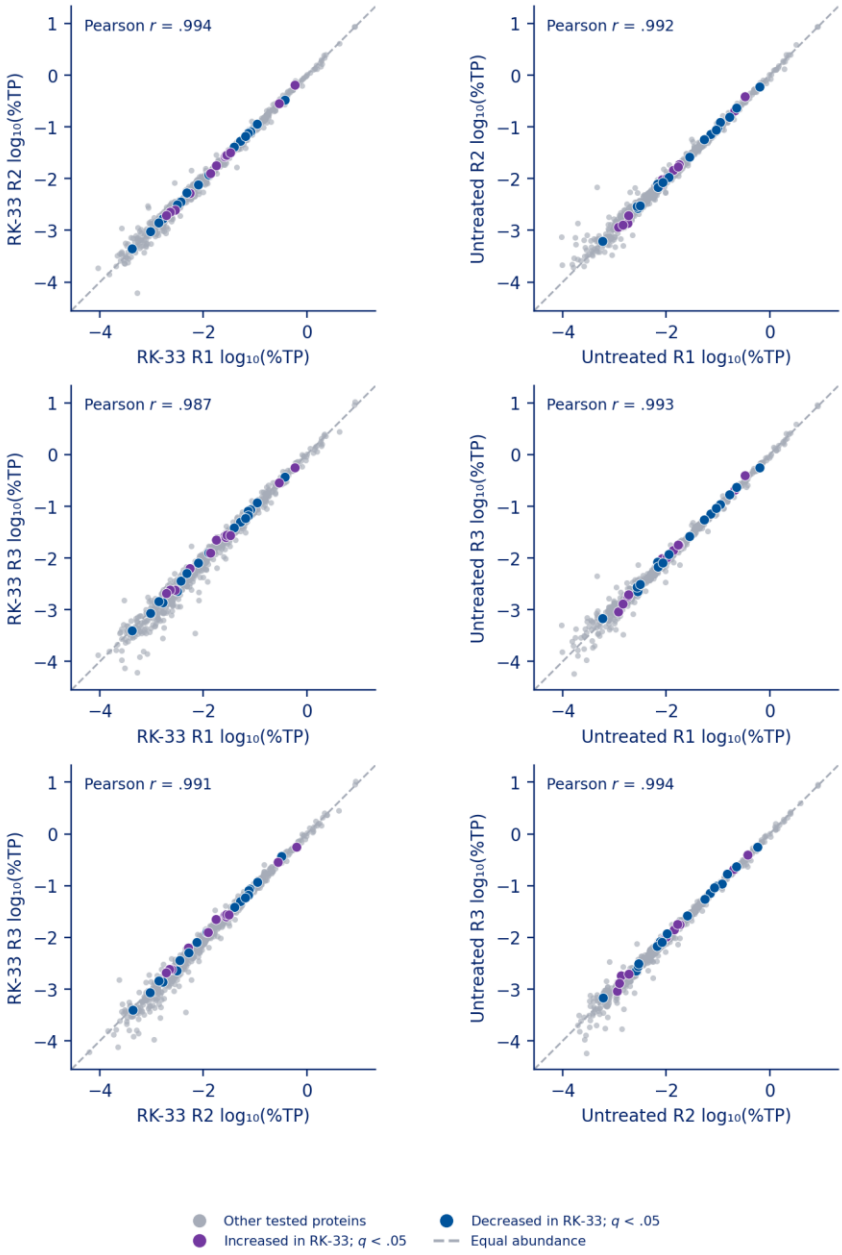


Figure 11. Within-group comparisons of biological replicates for RK-33 and Untreated. Each point represents a protein tested in the filtered GO RNA-binding proteins panel; axes show $\log_{10}$(%TP) in the analyzed RNP fractions for individual replicates. Pearson *r* summarizes all plotted proteins. The dashed line indicates equal abundance. Purple and blue identify proteins with significantly increased and decreased abundance, respectively, in RK-33 relative to Untreated (BH-adjusted $q < .05$). Other tested proteins are gray. The colors refer to the between-group comparison, not a within-group test.

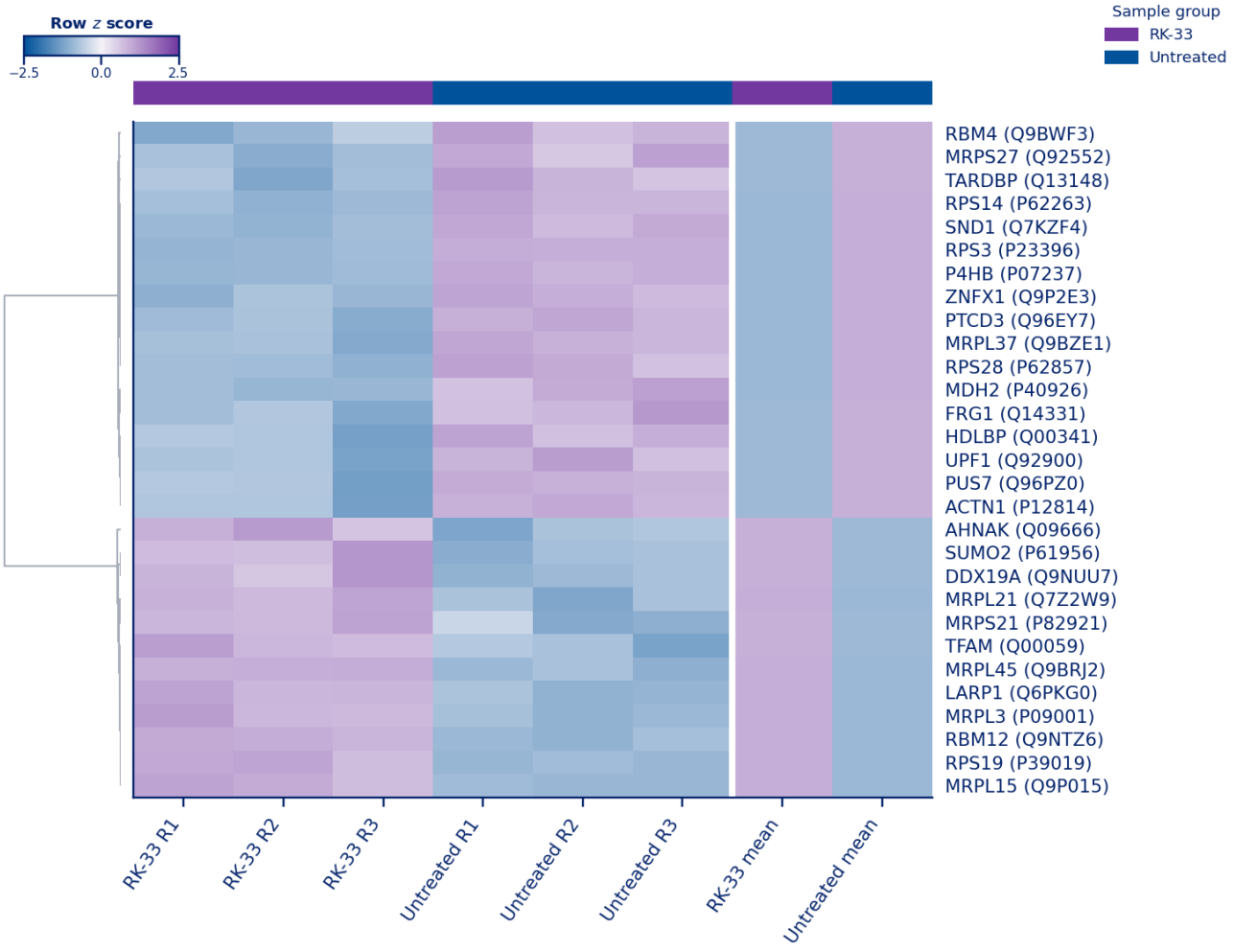


Figure 12. Protein abundance patterns of differentially abundant proteins. Heatmap showing $\log_2$(%TP) values in the analyzed RNP fractions, standardized within each protein across biological replicates (row *z* scores). Purple and blue indicate abundances above and below the mean for each protein, respectively; the color scale is limited to ±2.5. Rows were clustered using average linkage and correlation distance across replicate samples. The dendrogram branches show the hierarchical clustering of proteins by their abundance patterns; the merge positions reflect average correlation distances, not evidence of direct interactions. Sample columns retain their experimental order. The final columns show the group means of the row *z* scores and were excluded from clustering. All proteins meeting $q < .05$ are included.

Protein functions and features (Figure 12)

RBM4 (Q9BWF3). RNA-binding factor involved in multiple aspects of cellular processes like alternative splicing of pre-mRNA and translation regulation. Annotated features: RNA recognition motif; Zinc knuckle.

MRPS27 (Q92552). RNA-binding component of the mitochondrial small ribosomal subunit (mt-SSU) that plays a role in mitochondrial protein synthesis. Annotated features: Mitochondrial 28S ribosomal protein S27 (repeat); Pentatricopeptide repeat (repeat).

TARDBP (Q13148). RNA-binding protein that is involved in various steps of RNA biogenesis and processing. Annotated features: RNA recognition motif; TAR DNA-binding protein 43, N-terminal domain.

RPS14 (P62263). Component of the small ribosomal subunit; GO annotations include mRNA 5'-UTR binding; negative regulation of transcription by RNA polymerase II. Annotated features: Ribosomal protein S11 (family).

SND1 (Q7KZF4). Endonuclease that mediates miRNA decay of both protein-free and AGO2-loaded miRNAs; GO annotations include 3' overhang single-stranded DNA endonuclease activity; mRNA catabolic process. Annotated features: Staphylococcal nuclease homologue; Tudor domain.

RPS3 (P23396). Component of the small ribosomal subunit; GO annotations include class I DNA-(apurinic or apyrimidinic site) endonuclease activity; positive regulation of intrinsic apoptotic signaling pathway in response to DNA damage. Annotated features: KH domain; Ribosomal protein S3, C-terminal domain.

P4HB (P07237). This multifunctional protein catalyzes the formation, breakage and rearrangement of disulfide bonds. Annotated features: Thioredoxin; Thioredoxin-like domain.

ZNFX1 (Q9P2E3). RNA-activated non-canonical E3 ubiquitin ligase required for cell survival during interferon (IFN) responses. Annotated features: AAA domain; RZ type zinc finger domain.

PTCD3 (Q96EY7). Mitochondrial RNA-binding protein that has a role in mitochondrial translation. ; GO annotations include ribosomal small subunit binding; mitochondrial translation. Annotated features: Pentatricopeptide repeat domain (repeat); Small ribosomal subunit protein mS39, PPR (repeat).

MRPL37 (Q9BZE1). GO annotations include structural constituent of ribosome; mitochondrial translation. Annotated features: Mitochondrial 28S ribosomal protein S30 (PDCD9) (family).

RPS28 (P62857). Component of the small ribosomal subunit; GO annotations include structural constituent of ribosome; cytoplasmic translation. Annotated features: Ribosomal protein S28e.

MDH2 (P40926). Mitochondrial malate dehydrogenase that catalyzes the reversible conversion of malate to oxaloacetate using NAD(+) as a cofactor. Annotated features: lactate/malate dehydrogenase, NAD binding domain; lactate/malate dehydrogenase, alpha/beta C-terminal domain.

FRG1 (Q14331). Binds to mRNA in a sequence-independent manner; GO annotations include mRNA splicing, via spliceosome. Annotated features: FRG1-like domain.

HDLBP (Q00341). Appears to play a role in cell sterol metabolism; GO annotations include cadherin binding; cholesterol metabolic process. Annotated features: KH domain; Vigilin KH domain.

UPF1 (Q92900). RNA-dependent helicase required for nonsense-mediated decay (NMD) of aberrant mRNAs containing premature stop codons and which modulates the expression level of normal mRNAs. Annotated features: AAA domain; RNA helicase (UPF2 interacting domain).

PUS7 (Q96PZ0). Pseudouridylate synthase that catalyzes pseudouridylation of RNAs; GO annotations include tRNA pseudouridine(13) synthase activity; negative regulation of translation. Annotated features: Pseudouridine synthase, TruD, insertion domain.

ACTN1 (P12814). F-actin cross-linking protein which is thought to anchor actin to a variety of intracellular structures. Annotated features: Ca2+ insensitive EF hand; Calponin homology (CH) domain.

AHNAK (Q09666). May be required for neuronal cell differentiation; GO annotations include cadherin binding; positive regulation of plasma membrane repair. Annotated features: PDZ domain.

SUMO2 (P61956). Ubiquitin-like protein that can be covalently attached to proteins as a monomer or as a lysine-linked polymer. Annotated features: Rad60/SUMO-like domain; Ubiquitin-like domain.

DDX19A (Q9NUU7). ATP-dependent RNA helicase involved in mRNA export from the nucleus (inferred by similarity). Annotated features: DEAD/DEAH box helicase; Helicase conserved C-terminal domain.

MRPL21 (Q7Z2W9). GO annotations include structural constituent of ribosome; mitochondrial translation. Annotated features: Ribosomal prokaryotic L21 protein (family).

MRPS21 (P82921). GO annotations include structural constituent of ribosome; mitochondrial translation. Annotated features: Ribosomal protein S21 (family).

TFAM (Q00059). Binds to the mitochondrial light strand promoter and functions in mitochondrial transcription regulation. Annotated features: HMG (high mobility group) box; HMG-box domain.

MRPL45 (Q9BRJ2). Component of the mitochondrial large ribosomal subunit (mt-LSU); GO annotations include mitochondrial translation. Annotated features: Tim44-like domain.

LARP1 (Q6PKG0). RNA-binding protein that regulates the translation of specific target mRNA species downstream of the mTORC1 complex, in function of growth signals and nutrient availability. Annotated features: La domain; LARP1 HEAT repeat region (repeat).

MRPL3 (P09001). GO annotations include structural constituent of ribosome; mitochondrial translation. Annotated features: Ribosomal protein L3 (family).

RBM12 (Q9NTZ6). RNA binding protein; GO annotations include nucleic acid binding; negative regulation of cAMP/PKA signal transduction. Annotated features: RNA recognition motif; RRM domain.

RPS19 (P39019). Component of the small ribosomal subunit; GO annotations include fibroblast growth factor binding; antimicrobial humoral immune response mediated by antimicrobial peptide. Annotated features: Ribosomal protein S19e (family).

MRPL15 (Q9P015). GO annotations include structural constituent of ribosome; mitochondrial translation. Annotated features: Ribosomal proteins 50S-L15, 50S-L18e, 60S-L27A.

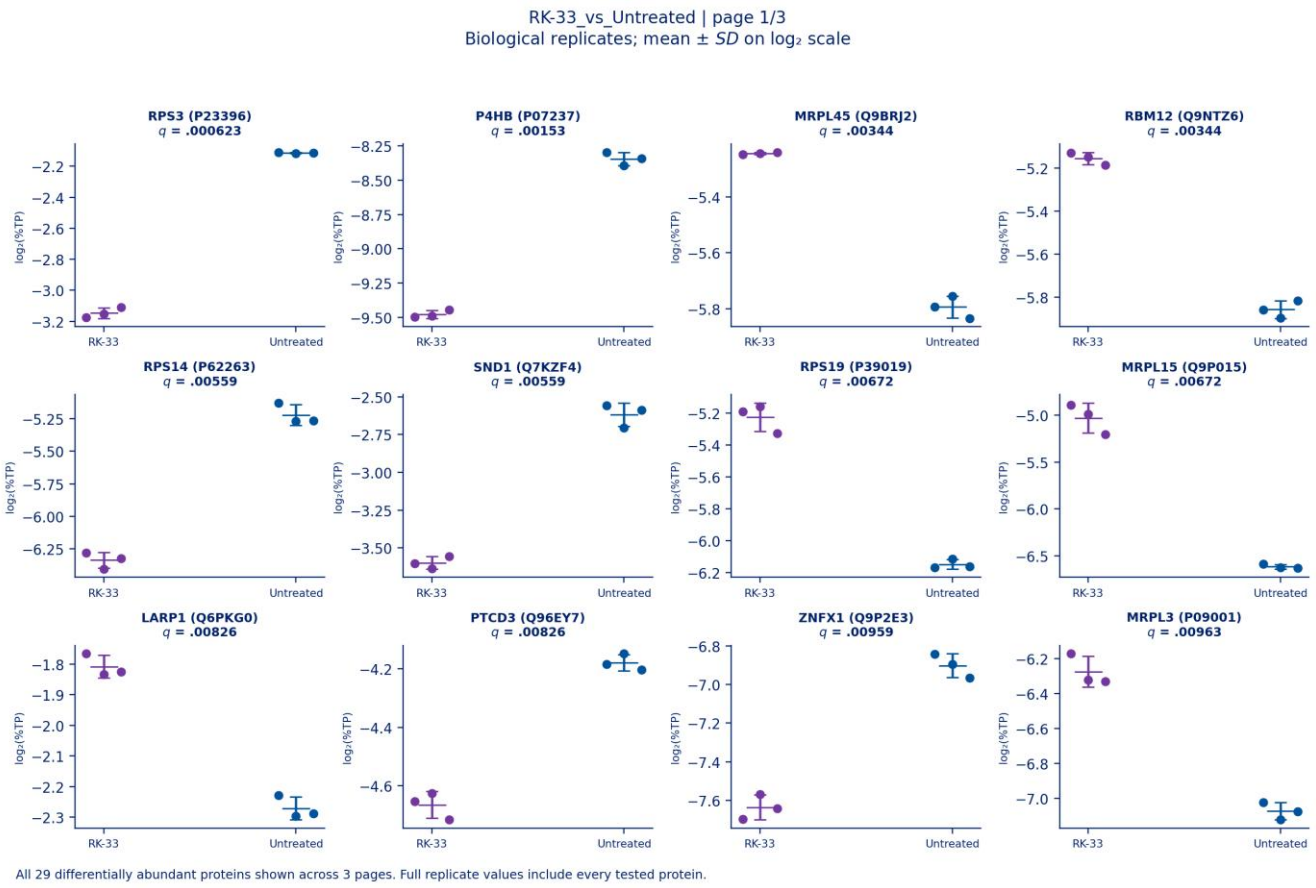


Figure 13. Replicate abundances of differentially abundant proteins between RK-33 and Untreated. Points show $\log_2$(%TP) for individual biological replicates (n = 3 per sample group); horizontal bars and whiskers show the group mean and standard deviation on this scale. Panels identify the protein by gene symbol and UniProt accession and report its q value. All significant proteins are shown across 3 pages (page 1 of 3).

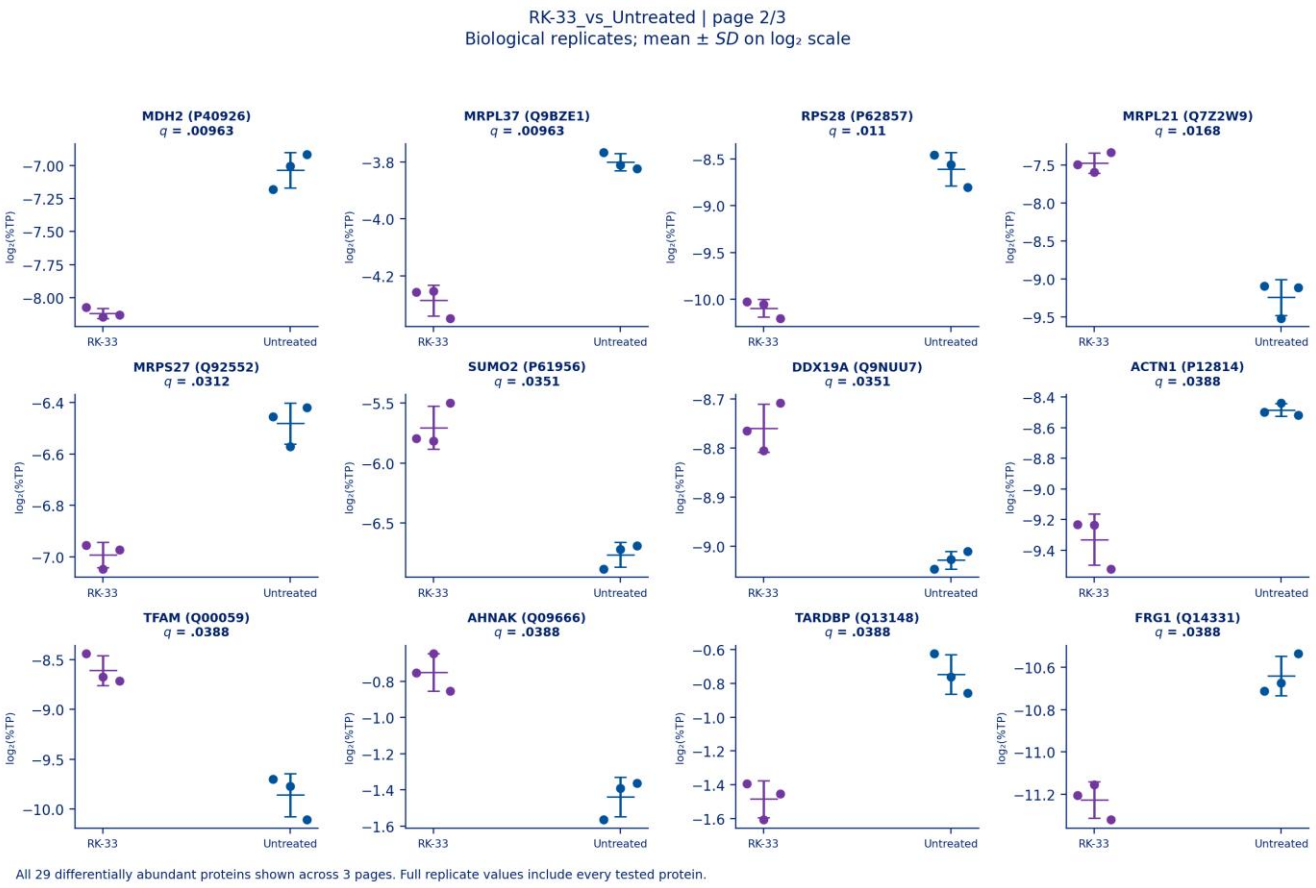


Figure 14. Replicate abundances of differentially abundant proteins between RK-33 and Untreated. Points show $\log_2$(%TP) for individual biological replicates (n = 3 per sample group); horizontal bars and whiskers show the group mean and standard deviation on this scale. Panels identify the protein by gene symbol and UniProt accession and report its q value. All significant proteins are shown across 3 pages (page 2 of 3).

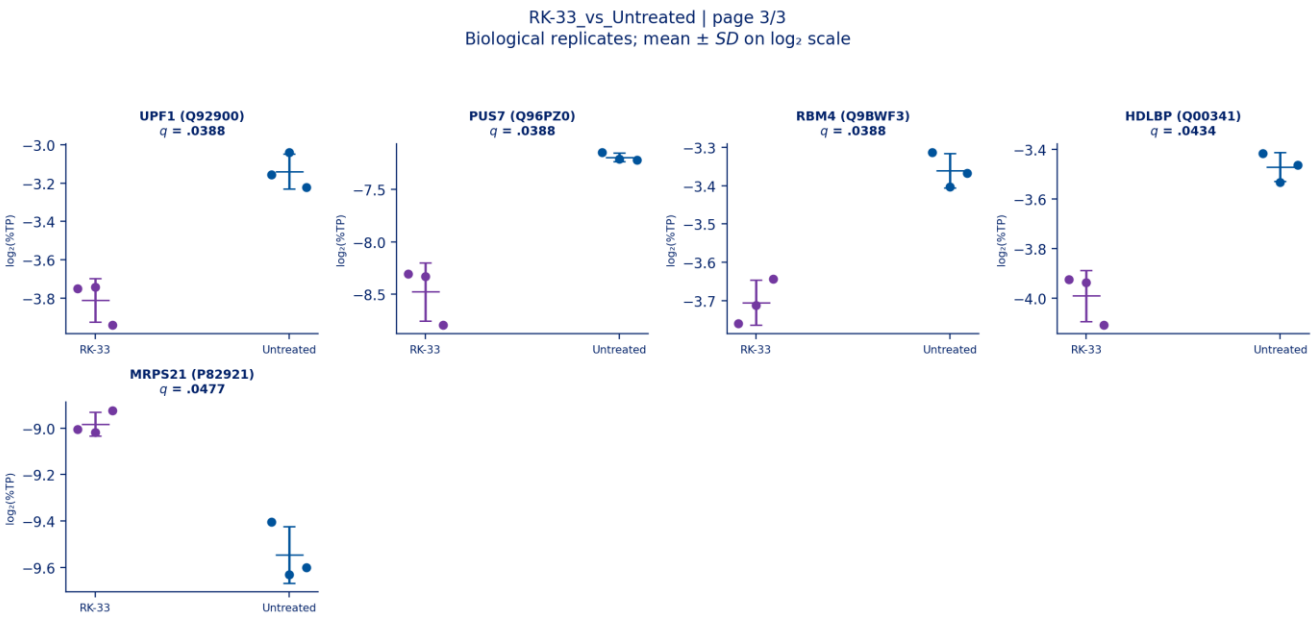


Figure 15. Replicate abundances of differentially abundant proteins between RK-33 and Untreated. Points show $\log_2$(%TP) for individual biological replicates (n = 3 per sample group); horizontal bars and whiskers show the group mean and standard deviation on this scale. Panels identify the protein by gene symbol and UniProt accession and report its q value. All significant proteins are shown across 3 pages (page 3 of 3).

9. Functional Annotations

Functional categories were curated in-house using UniProtKB Gene Ontology annotations and keywords. Proteins could be assigned to more than one category. The classification approach is described in Methods_and_Data_Analysis.docx; category assignments and supporting database annotations are provided in the 06_Functional_Annotations folders.

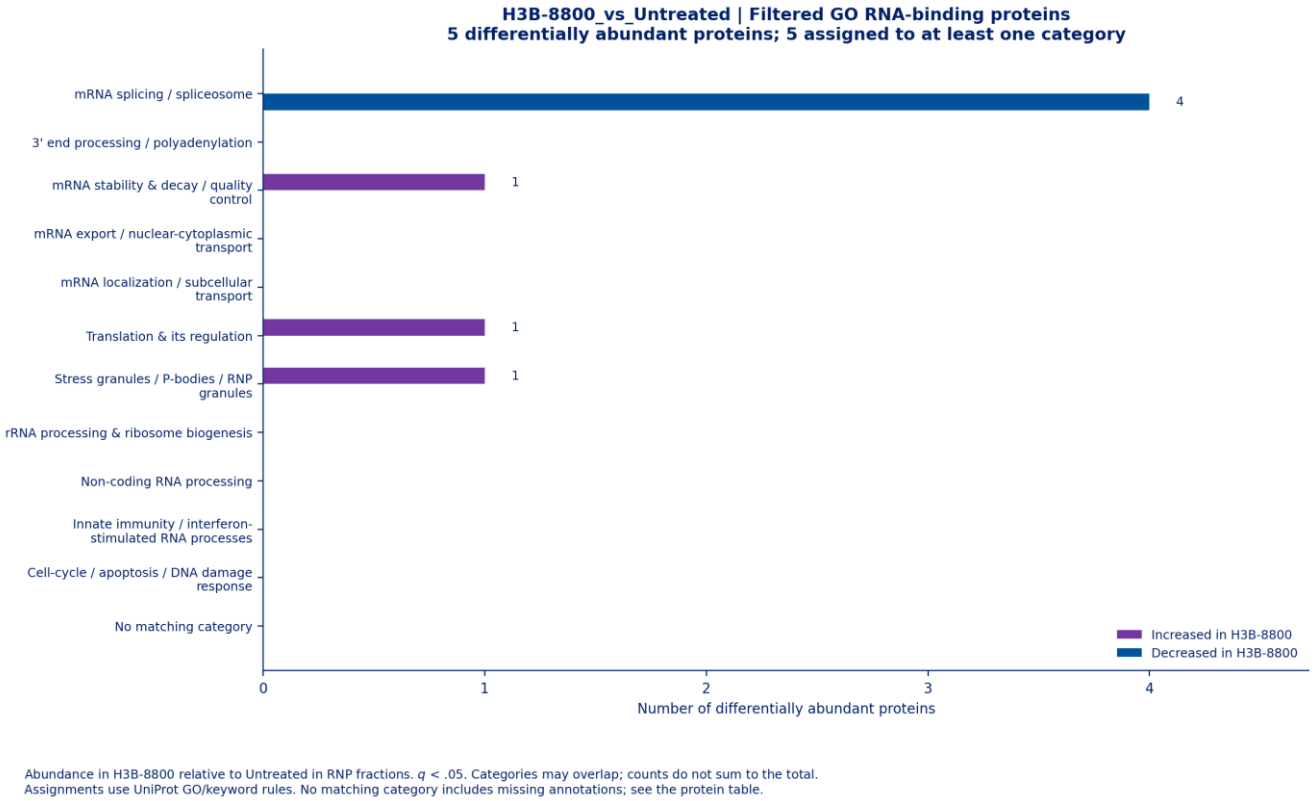


Figure 16. Annotated functions of differentially abundant proteins. Bar chart showing the numbers of differentially abundant filtered GO RNA-binding proteins assigned automatically to categories defined in-house using UniProtKB Gene Ontology annotations and keywords. Purple and blue bars indicate proteins with increased and decreased abundance in H3B-8800 relative to Untreated, respectively ($q < .05$). Categories overlap, and individual proteins may contribute to multiple categories. Proteins that did not match the predefined categories are shown under “No matching category.” Counts are descriptive and do not represent functional-enrichment tests.

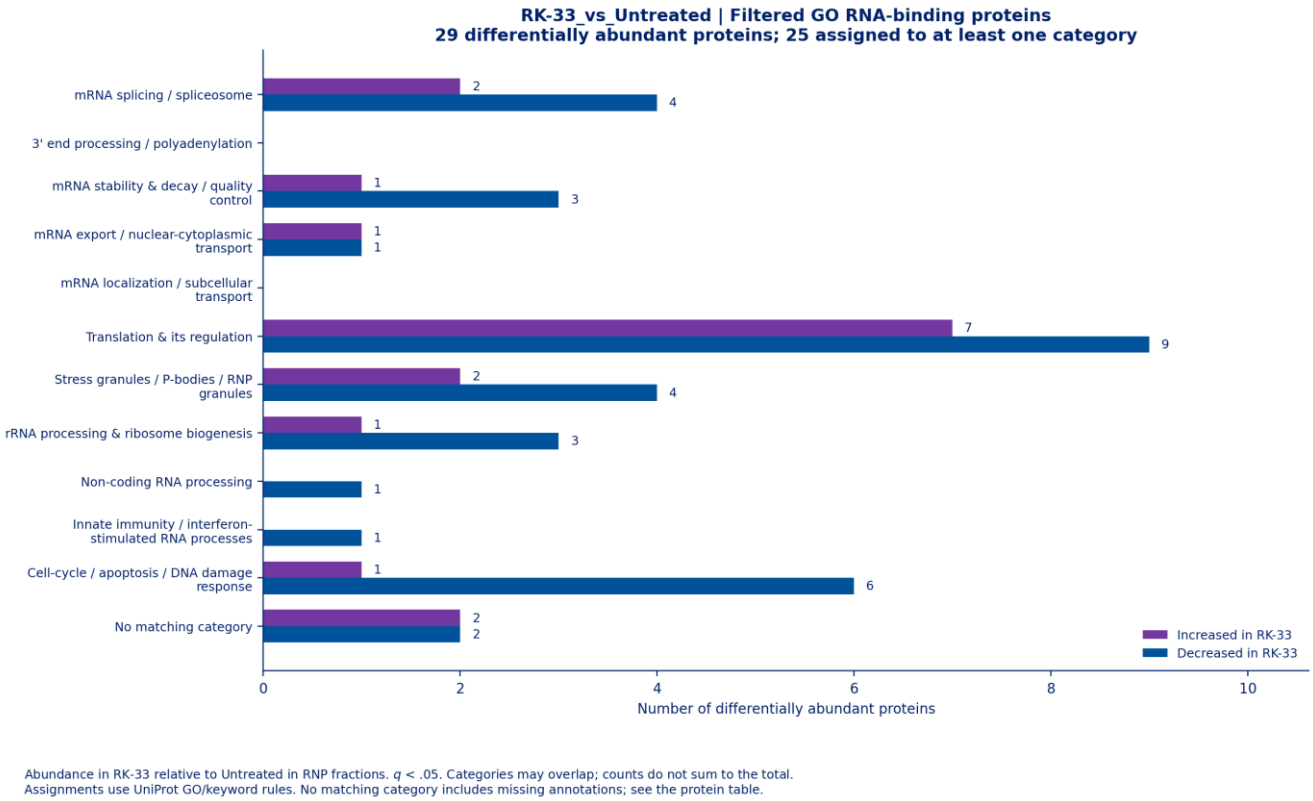


Figure 17. Annotated functions of differentially abundant proteins. Bar chart showing the numbers of differentially abundant filtered GO RNA-binding proteins assigned automatically to categories defined in-house using UniProtKB Gene Ontology annotations and keywords. Purple and blue bars indicate proteins with increased and decreased abundance in RK-33 relative to Untreated, respectively ($q < .05$). Categories overlap, and individual proteins may contribute to multiple categories. Proteins that did not match the predefined categories are shown under “No matching category.” Counts are descriptive and do not represent functional-enrichment tests.

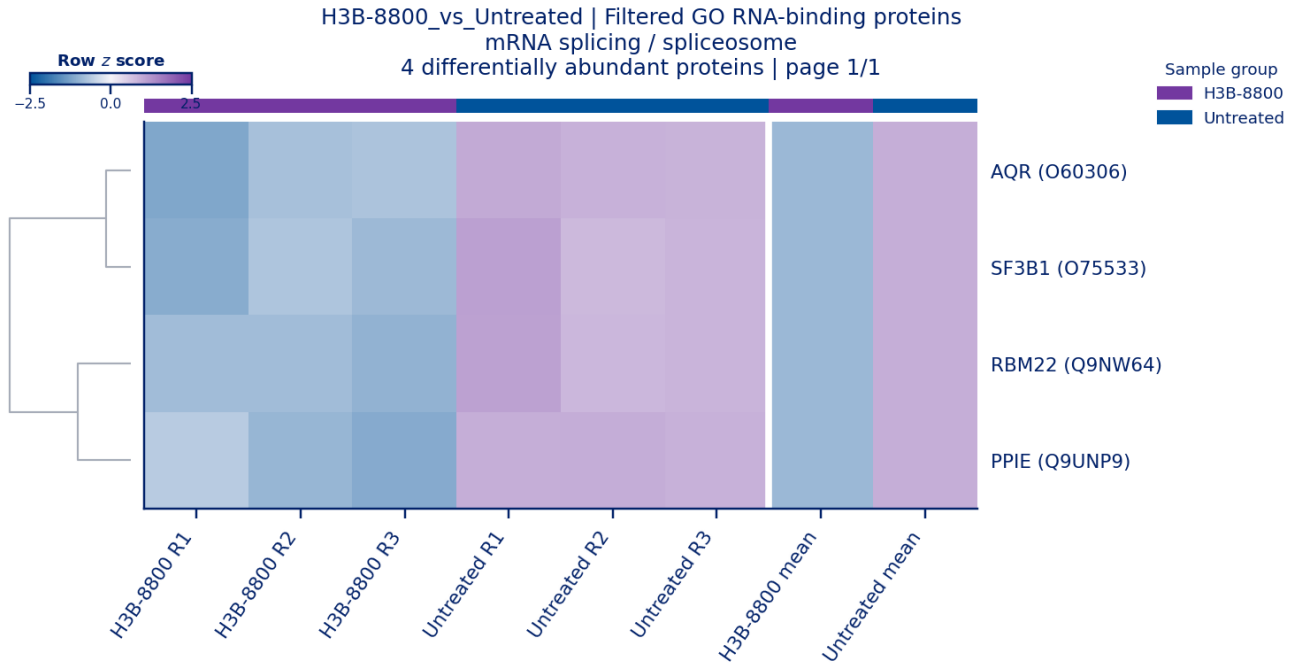


Figure 18. Protein abundance patterns within the mRNA splicing / spliceosome category. Heatmap showing $\log_2$(%TP) values in the analyzed RNP fractions, standardized within each protein across biological replicates (row *z* scores). Category membership was assigned automatically using in-house classification rules applied to positive UniProtKB Gene Ontology annotations and keywords relating to RNA splicing, the spliceosome, or U1, U2, U4, U5, or U6 snRNPs. Purple and blue indicate abundances above and below the mean for each protein, respectively; the color scale is limited to ±2.5. Rows were clustered using average linkage and correlation distance across replicate samples. The dendrogram branches show the hierarchical clustering of proteins by their abundance patterns; the merge positions reflect average correlation distances, not evidence of direct interactions. Sample columns retain their experimental order. The final columns show the group means of the row *z* scores and were excluded from clustering. Proteins may appear in more than one category.

Protein functions and features (Figure 18)

AQR (O60306). Involved in pre-mRNA splicing as component of the spliceosome; GO annotations include 3'-5' RNA helicase activity; mRNA splicing, via spliceosome. Annotated features: AAA domain; Intron-binding protein aquarius insert domain.

SF3B1 (O75533). Component of the 17S U2 SnRNP complex of the spliceosome, a large ribonucleoprotein complex that removes introns from transcribed pre-mRNAs. Annotated features: Splicing factor 3B subunit 1; PPP2R1A-like HEAT repeat (repeat).

RBM22 (Q9NW64). Required for pre-mRNA splicing as component of the activated spliceosome; GO annotations include U6 snRNA binding; positive regulation of protein import into nucleus. Annotated features: RBM22 CCCH zinc finger domain; RNA recognition motif.

PPIE (Q9UNP9). Involved in pre-mRNA splicing as component of the spliceosome; GO annotations include poly(A) binding; mRNA splicing, via spliceosome. Annotated features: Cyclophilin type peptidyl-prolyl cis-trans isomerase/CLD; RNA recognition motif.

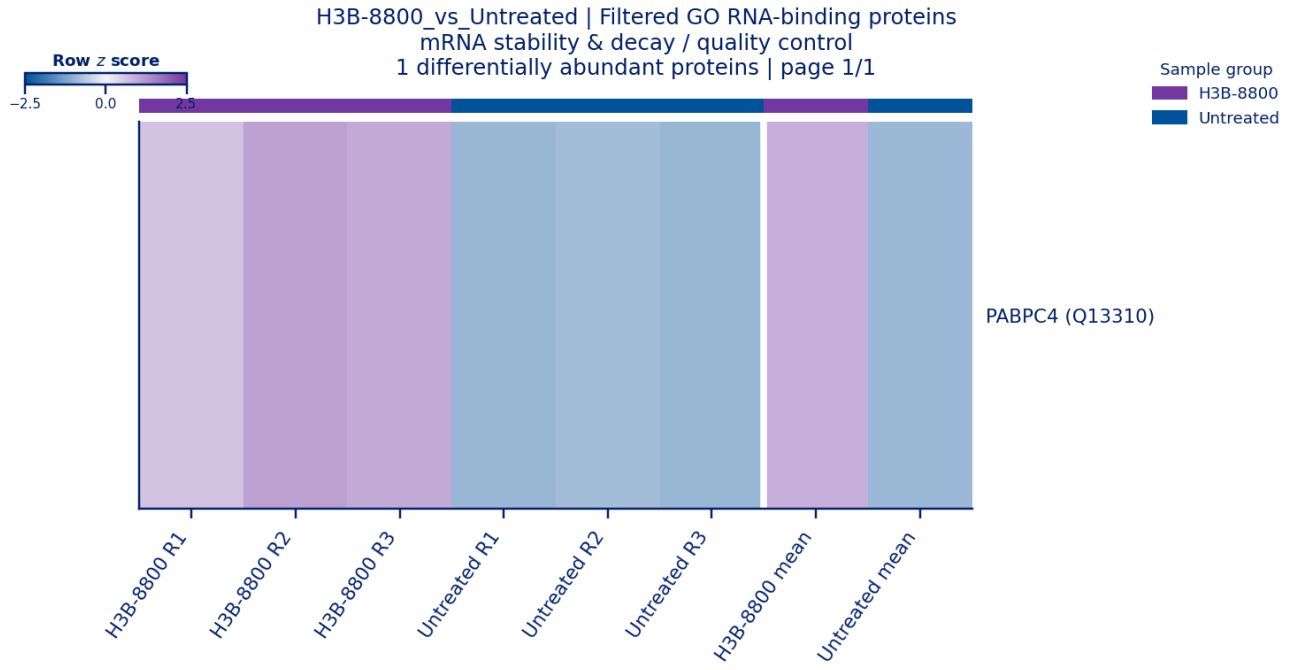


Figure 19. Protein abundance patterns within the mRNA stability & decay / quality control category. Heatmap showing $\log_2$(%TP) values in the analyzed RNP fractions, standardized within each protein across biological replicates (row *z* scores). Category membership was assigned automatically using in-house classification rules applied to positive UniProtKB Gene Ontology annotations and keywords relating to RNA stability, turnover, decay, degradation, or surveillance, including deadenylation, decapping, and translation-associated RNA decay. Purple and blue indicate abundances above and below the mean for each protein, respectively; the color scale is limited to ±2.5. Rows were clustered using average linkage and correlation distance across replicate samples. The dendrogram branches show the hierarchical clustering of proteins by their abundance patterns; the merge positions reflect average correlation distances, not evidence of direct interactions. Sample columns retain their experimental order. The final columns show the group means of the row *z* scores and were excluded from clustering. Proteins may appear in more than one category.

Protein functions and features (Figure 19)

PABPC4 (Q13310). Binds the poly(A) tail of mRNA; GO annotations include poly(A) binding; RNA catabolic process. Annotated features: MLLE domain; RNA recognition motif.

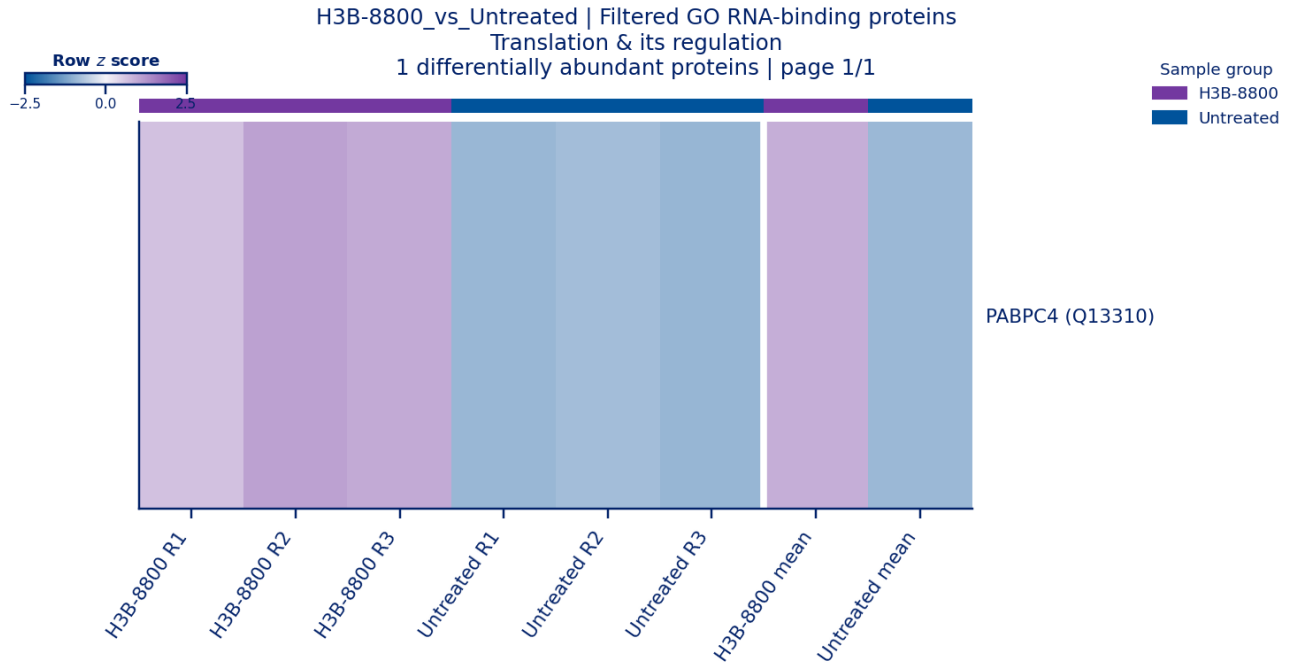


Figure 20. Protein abundance patterns within the Translation & its regulation category. Heatmap showing $\log_2$(%TP) values in the analyzed RNP fractions, standardized within each protein across biological replicates (row *z* scores). Category membership was assigned automatically using in-house classification rules applied to positive UniProtKB Gene Ontology annotations and keywords relating to translation or its regulation, ribosomal proteins, or structural constituents of the ribosome. Purple and blue indicate abundances above and below the mean for each protein, respectively; the color scale is limited to ±2.5. Rows were clustered using average linkage and correlation distance across replicate samples. The dendrogram branches show the hierarchical clustering of proteins by their abundance patterns; the merge positions reflect average correlation distances, not evidence of direct interactions. Sample columns retain their experimental order. The final columns show the group means of the row *z* scores and were excluded from clustering. Proteins may appear in more than one category.

Protein functions and features (Figure 20)

PABPC4 (Q13310). Binds the poly(A) tail of mRNA; GO annotations include poly(A) binding; RNA catabolic process. Annotated features: MLLE domain; RNA recognition motif.

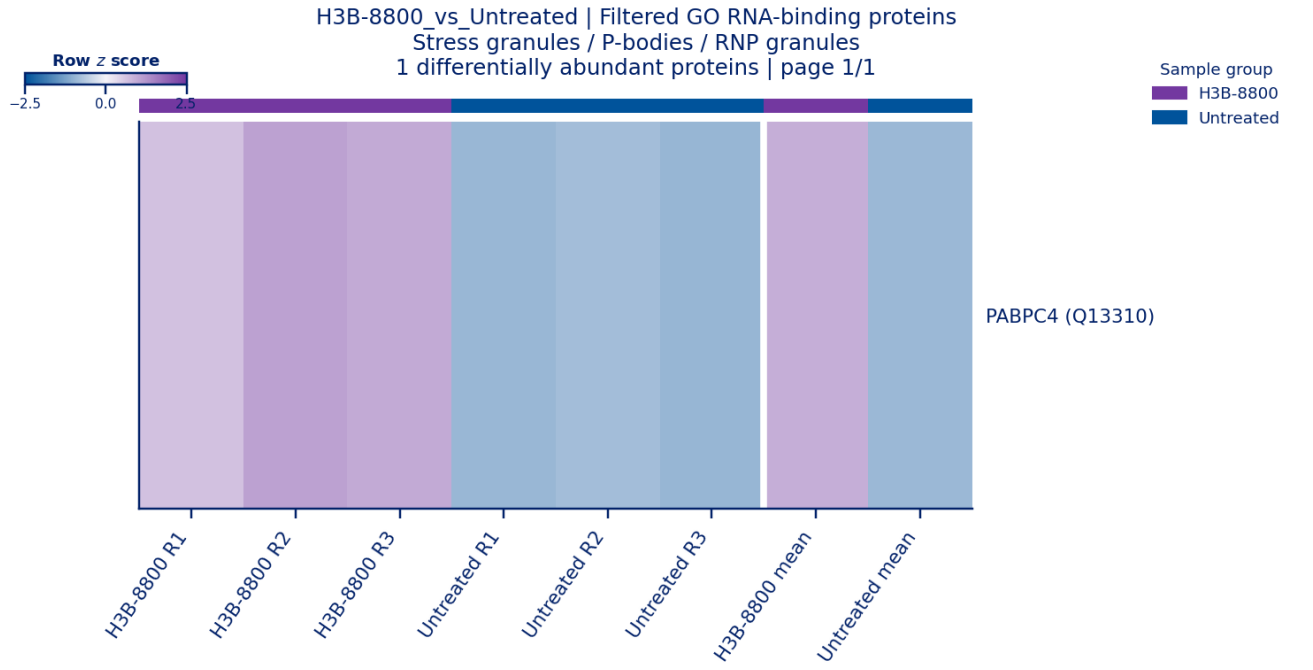


Figure 21. Protein abundance patterns within the Stress granules / P-bodies / RNP granules category. Heatmap showing $\log_2$(%TP) values in the analyzed RNP fractions, standardized within each protein across biological replicates (row *z* scores). Category membership was assigned automatically using in-house classification rules applied to positive UniProtKB Gene Ontology annotations and keywords describing stress granules, P-bodies, processing bodies, or ribonucleoprotein granules; membership can reflect cellular association rather than a demonstrated role in granule formation. Purple and blue indicate abundances above and below the mean for each protein, respectively; the color scale is limited to ±2.5. Rows were clustered using average linkage and correlation distance across replicate samples. The dendrogram branches show the hierarchical clustering of proteins by their abundance patterns; the merge positions reflect average correlation distances, not evidence of direct interactions. Sample columns retain their experimental order. The final columns show the group means of the row *z* scores and were excluded from clustering. Proteins may appear in more than one category.

Protein functions and features (Figure 21)

PABPC4 (Q13310). Binds the poly(A) tail of mRNA; GO annotations include poly(A) binding; RNA catabolic process. Annotated features: MLLE domain; RNA recognition motif.

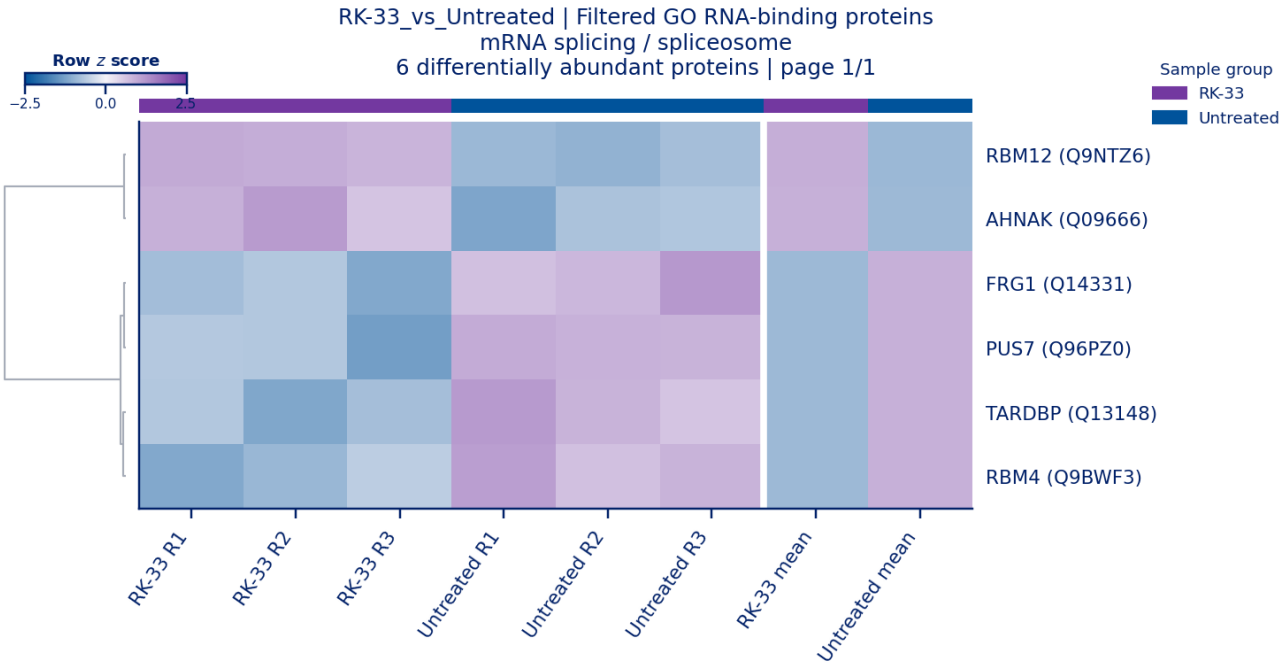


Figure 22. Protein abundance patterns within the mRNA splicing / spliceosome category. Heatmap showing $\log_2$(%TP) values in the analyzed RNP fractions, standardized within each protein across biological replicates (row *z* scores). Category membership was assigned automatically using in-house classification rules applied to positive UniProtKB Gene Ontology annotations and keywords relating to RNA splicing, the spliceosome, or U1, U2, U4, U5, or U6 snRNPs. Purple and blue indicate abundances above and below the mean for each protein, respectively; the color scale is limited to ±2.5. Rows were clustered using average linkage and correlation distance across replicate samples. The dendrogram branches show the hierarchical clustering of proteins by their abundance patterns; the merge positions reflect average correlation distances, not evidence of direct interactions. Sample columns retain their experimental order. The final columns show the group means of the row *z* scores and were excluded from clustering. Proteins may appear in more than one category.

Protein functions and features (Figure 22)

RBM12 (Q9NTZ6). RNA binding protein; GO annotations include nucleic acid binding; negative regulation of cAMP/PKA signal transduction. Annotated features: RNA recognition motif; RRM domain.

AHNAK (Q09666). May be required for neuronal cell differentiation; GO annotations include cadherin binding; positive regulation of plasma membrane repair. Annotated features: PDZ domain.

FRG1 (Q14331). Binds to mRNA in a sequence-independent manner; GO annotations include mRNA splicing, via spliceosome. Annotated features: FRG1-like domain.

PUS7 (Q96PZ0). Pseudouridylate synthase that catalyzes pseudouridylation of RNAs; GO annotations include tRNA pseudouridine(13) synthase activity; negative regulation of translation. Annotated features: Pseudouridine synthase, TruD, insertion domain.

TARDBP (Q13148). RNA-binding protein that is involved in various steps of RNA biogenesis and processing. Annotated features: RNA recognition motif; TAR DNA-binding protein 43, N-terminal domain.

RBM4 (Q9BWF3). RNA-binding factor involved in multiple aspects of cellular processes like alternative splicing of pre-mRNA and translation regulation. Annotated features: RNA recognition motif; Zinc knuckle.

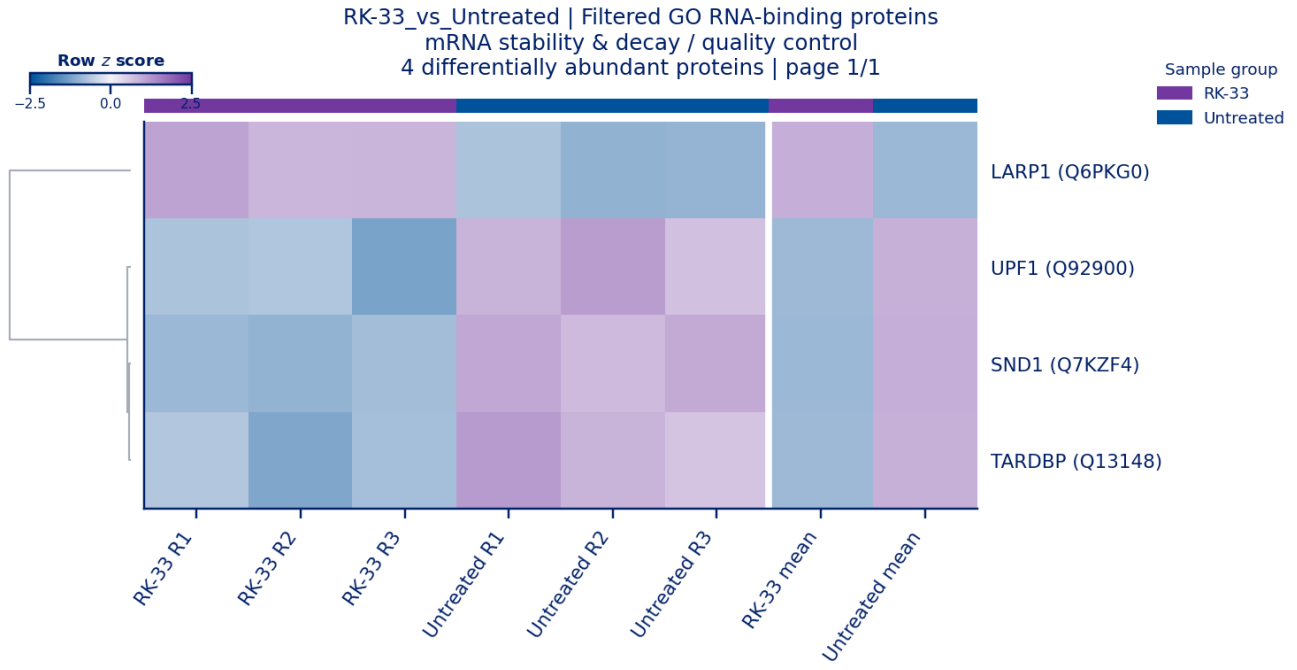


Figure 23. Protein abundance patterns within the mRNA stability & decay / quality control category. Heatmap showing $\log_2$(%TP) values in the analyzed RNP fractions, standardized within each protein across biological replicates (row *z* scores). Category membership was assigned automatically using in-house classification rules applied to positive UniProtKB Gene Ontology annotations and keywords relating to RNA stability, turnover, decay, degradation, or surveillance, including deadenylation, decapping, and translation-associated RNA decay. Purple and blue indicate abundances above and below the mean for each protein, respectively; the color scale is limited to ±2.5. Rows were clustered using average linkage and correlation distance across replicate samples. The dendrogram branches show the hierarchical clustering of proteins by their abundance patterns; the merge positions reflect average correlation distances, not evidence of direct interactions. Sample columns retain their experimental order. The final columns show the group means of the row *z* scores and were excluded from clustering. Proteins may appear in more than one category.

Protein functions and features (Figure 23)

LARP1 (Q6PKG0). RNA-binding protein that regulates the translation of specific target mRNA species downstream of the mTORC1 complex, in function of growth signals and nutrient availability. Annotated features: La domain; LARP1 HEAT repeat region (repeat).

UPF1 (Q92900). RNA-dependent helicase required for nonsense-mediated decay (NMD) of aberrant mRNAs containing premature stop codons and which modulates the expression level of normal mRNAs. Annotated features: AAA domain; RNA helicase (UPF2 interacting domain).

SND1 (Q7KZF4). Endonuclease that mediates miRNA decay of both protein-free and AGO2-loaded miRNAs; GO annotations include 3' overhang single-stranded DNA endonuclease activity; mRNA catabolic process. Annotated features: Staphylococcal nuclease homologue; Tudor domain.

TARDBP (Q13148). RNA-binding protein that is involved in various steps of RNA biogenesis and processing. Annotated features: RNA recognition motif; TAR DNA-binding protein 43, N-terminal domain.

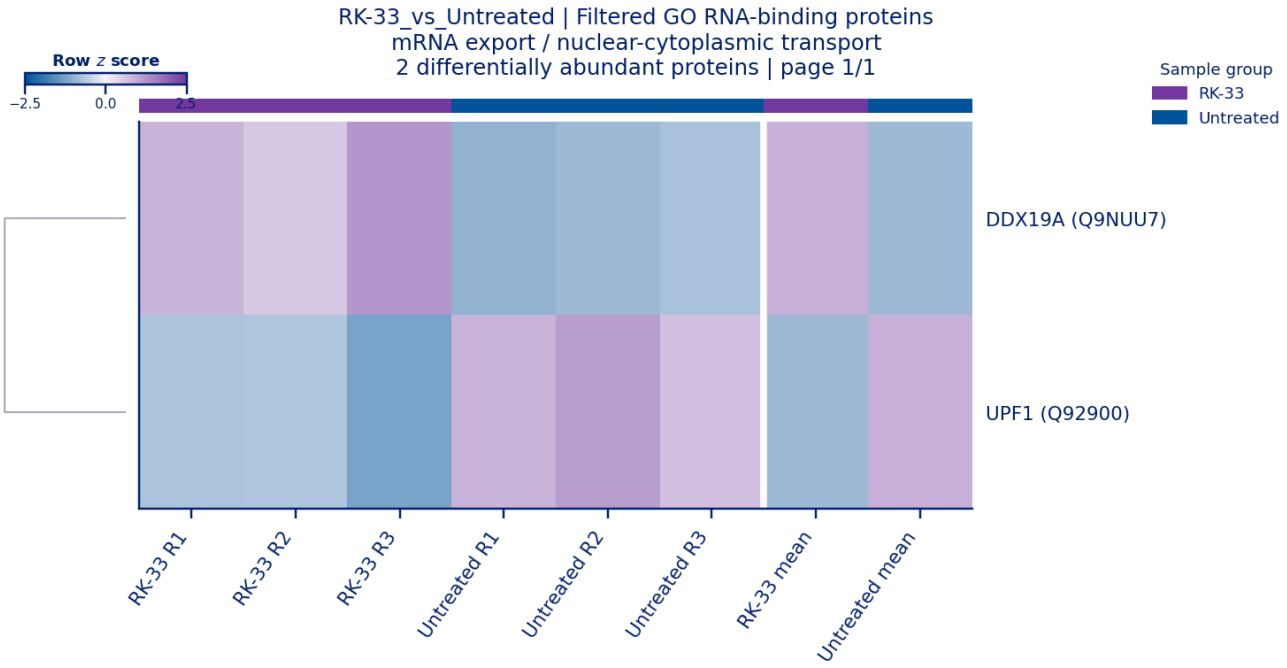


Figure 24. Protein abundance patterns within the mRNA export / nuclear-cytoplasmic transport category. Heatmap showing $\log_2$(%TP) values in the analyzed RNP fractions, standardized within each protein across biological replicates (row *z* scores). Category membership was assigned automatically using in-house classification rules applied to positive UniProtKB Gene Ontology annotations and keywords relating to RNA or ribonucleoprotein-complex export or nucleocytoplasmic transport; supporting annotations may describe a transport complex. Purple and blue indicate abundances above and below the mean for each protein, respectively; the color scale is limited to ±2.5. Rows were clustered using average linkage and correlation distance across replicate samples. The dendrogram branches show the hierarchical clustering of proteins by their abundance patterns; the merge positions reflect average correlation distances, not evidence of direct interactions. Sample columns retain their experimental order. The final columns show the group means of the row *z* scores and were excluded from clustering. Proteins may appear in more than one category.

Protein functions and features (Figure 24)

DDX19A (Q9NUU7). ATP-dependent RNA helicase involved in mRNA export from the nucleus (inferred by similarity). Annotated features: DEAD/DEAH box helicase; Helicase conserved C-terminal domain.

UPF1 (Q92900). RNA-dependent helicase required for nonsense-mediated decay (NMD) of aberrant mRNAs containing premature stop codons and which modulates the expression level of normal mRNAs. Annotated features: AAA domain; RNA helicase (UPF2 interacting domain).

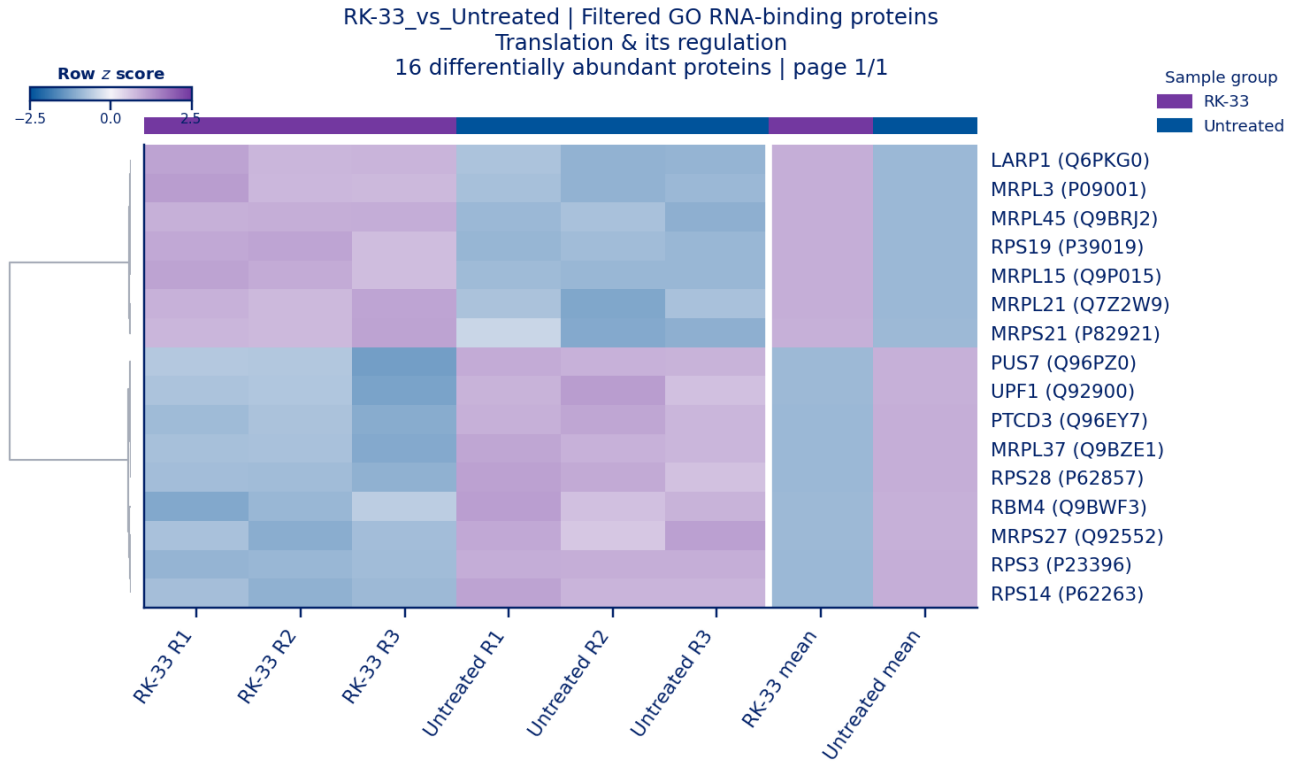


Figure 25. Protein abundance patterns within the Translation & its regulation category. Heatmap showing $\log_2$(%TP) values in the analyzed RNP fractions, standardized within each protein across biological replicates (row *z* scores). Category membership was assigned automatically using in-house classification rules applied to positive UniProtKB Gene Ontology annotations and keywords relating to translation or its regulation, ribosomal proteins, or structural constituents of the ribosome. Purple and blue indicate abundances above and below the mean for each protein, respectively; the color scale is limited to ±2.5. Rows were clustered using average linkage and correlation distance across replicate samples. The dendrogram branches show the hierarchical clustering of proteins by their abundance patterns; the merge positions reflect average correlation distances, not evidence of direct interactions. Sample columns retain their experimental order. The final columns show the group means of the row *z* scores and were excluded from clustering. Proteins may appear in more than one category.

Protein functions and features (Figure 25)

LARP1 (Q6PKG0). RNA-binding protein that regulates the translation of specific target mRNA species downstream of the mTORC1 complex, in function of growth signals and nutrient availability. Annotated features: La domain; LARP1 HEAT repeat region (repeat).

MRPL3 (P09001). GO annotations include structural constituent of ribosome; mitochondrial translation. Annotated features: Ribosomal protein L3 (family).

MRPL45 (Q9BRJ2). Component of the mitochondrial large ribosomal subunit (mt-LSU); GO annotations include mitochondrial translation. Annotated features: Tim44-like domain.

RPS19 (P39019). Component of the small ribosomal subunit; GO annotations include fibroblast growth factor binding; antimicrobial humoral immune response mediated by antimicrobial peptide. Annotated features: Ribosomal protein S19e (family).

MRPL15 (Q9P015). GO annotations include structural constituent of ribosome; mitochondrial translation. Annotated features: Ribosomal proteins 50S-L15, 50S-L18e, 60S-L27A.

MRPL21 (Q7Z2W9). GO annotations include structural constituent of ribosome; mitochondrial translation. Annotated features: Ribosomal prokaryotic L21 protein (family).

MRPS21 (P82921). GO annotations include structural constituent of ribosome; mitochondrial translation. Annotated features: Ribosomal protein S21 (family).

PUS7 (Q96PZ0). Pseudouridylate synthase that catalyzes pseudouridylation of RNAs; GO annotations include tRNA pseudouridine(13) synthase activity; negative regulation of translation. Annotated features: Pseudouridine synthase, TruD, insertion domain.

UPF1 (Q92900). RNA-dependent helicase required for nonsense-mediated decay (NMD) of aberrant mRNAs containing premature stop codons and which modulates the expression level of normal mRNAs. Annotated features: AAA domain; RNA helicase (UPF2 interacting domain).

PTCD3 (Q96EY7). Mitochondrial RNA-binding protein that has a role in mitochondrial translation. ; GO annotations include ribosomal small subunit binding; mitochondrial translation. Annotated features: Pentatricopeptide repeat domain (repeat); Small ribosomal subunit protein mS39, PPR (repeat).

MRPL37 (Q9BZE1). GO annotations include structural constituent of ribosome; mitochondrial translation. Annotated features: Mitochondrial 28S ribosomal protein S30 (PDCD9) (family).

RPS28 (P62857). Component of the small ribosomal subunit; GO annotations include structural constituent of ribosome; cytoplasmic translation. Annotated features: Ribosomal protein S28e.

RBM4 (Q9BWF3). RNA-binding factor involved in multiple aspects of cellular processes like alternative splicing of pre-mRNA and translation regulation. Annotated features: RNA recognition motif; Zinc knuckle.

MRPS27 (Q92552). RNA-binding component of the mitochondrial small ribosomal subunit (mt-SSU) that plays a role in mitochondrial protein synthesis. Annotated features: Mitochondrial 28S ribosomal protein S27 (repeat); Pentatricopeptide repeat (repeat).

RPS3 (P23396). Component of the small ribosomal subunit; GO annotations include class I DNA-(apurinic or apyrimidinic site) endonuclease activity; positive regulation of intrinsic apoptotic signaling pathway in response to DNA damage. Annotated features: KH domain; Ribosomal protein S3, C-terminal domain.

RPS14 (P62263). Component of the small ribosomal subunit; GO annotations include mRNA 5'-UTR binding; negative regulation of transcription by RNA polymerase II. Annotated features: Ribosomal protein S11 (family).

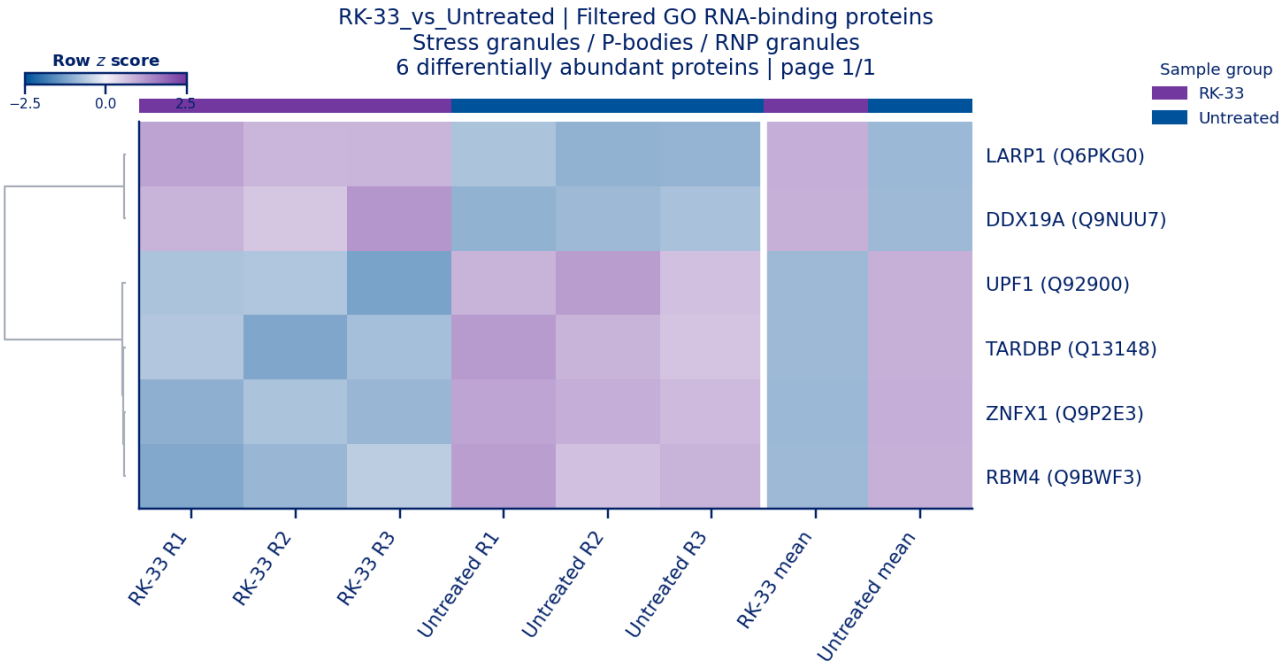


Figure 26. Protein abundance patterns within the Stress granules / P-bodies / RNP granules category. Heatmap showing $\log_2$(%TP) values in the analyzed RNP fractions, standardized within each protein across biological replicates (row *z* scores). Category membership was assigned automatically using in-house classification rules applied to positive UniProtKB Gene Ontology annotations and keywords describing stress granules, P-bodies, processing bodies, or ribonucleoprotein granules; membership can reflect cellular association rather than a demonstrated role in granule formation. Purple and blue indicate abundances above and below the mean for each protein, respectively; the color scale is limited to ±2.5. Rows were clustered using average linkage and correlation distance across replicate samples. The dendrogram branches show the hierarchical clustering of proteins by their abundance patterns; the merge positions reflect average correlation distances, not evidence of direct interactions. Sample columns retain their experimental order. The final columns show the group means of the row *z* scores and were excluded from clustering. Proteins may appear in more than one category.

Protein functions and features (Figure 26)

LARP1 (Q6PKG0). RNA-binding protein that regulates the translation of specific target mRNA species downstream of the mTORC1 complex, in function of growth signals and nutrient availability. Annotated features: La domain; LARP1 HEAT repeat region (repeat).

DDX19A (Q9NUU7). ATP-dependent RNA helicase involved in mRNA export from the nucleus (inferred by similarity). Annotated features: DEAD/DEAH box helicase; Helicase conserved C-terminal domain.

UPF1 (Q92900). RNA-dependent helicase required for nonsense-mediated decay (NMD) of aberrant mRNAs containing premature stop codons and which modulates the expression level of normal mRNAs. Annotated features: AAA domain; RNA helicase (UPF2 interacting domain).

TARDBP (Q13148). RNA-binding protein that is involved in various steps of RNA biogenesis and processing. Annotated features: RNA recognition motif; TAR DNA-binding protein 43, N-terminal domain.

ZNFX1 (Q9P2E3). RNA-activated non-canonical E3 ubiquitin ligase required for cell survival during interferon (IFN) responses. Annotated features: AAA domain; RZ type zinc finger domain.

RBM4 (Q9BWF3). RNA-binding factor involved in multiple aspects of cellular processes like alternative splicing of pre-mRNA and translation regulation. Annotated features: RNA recognition motif; Zinc knuckle.

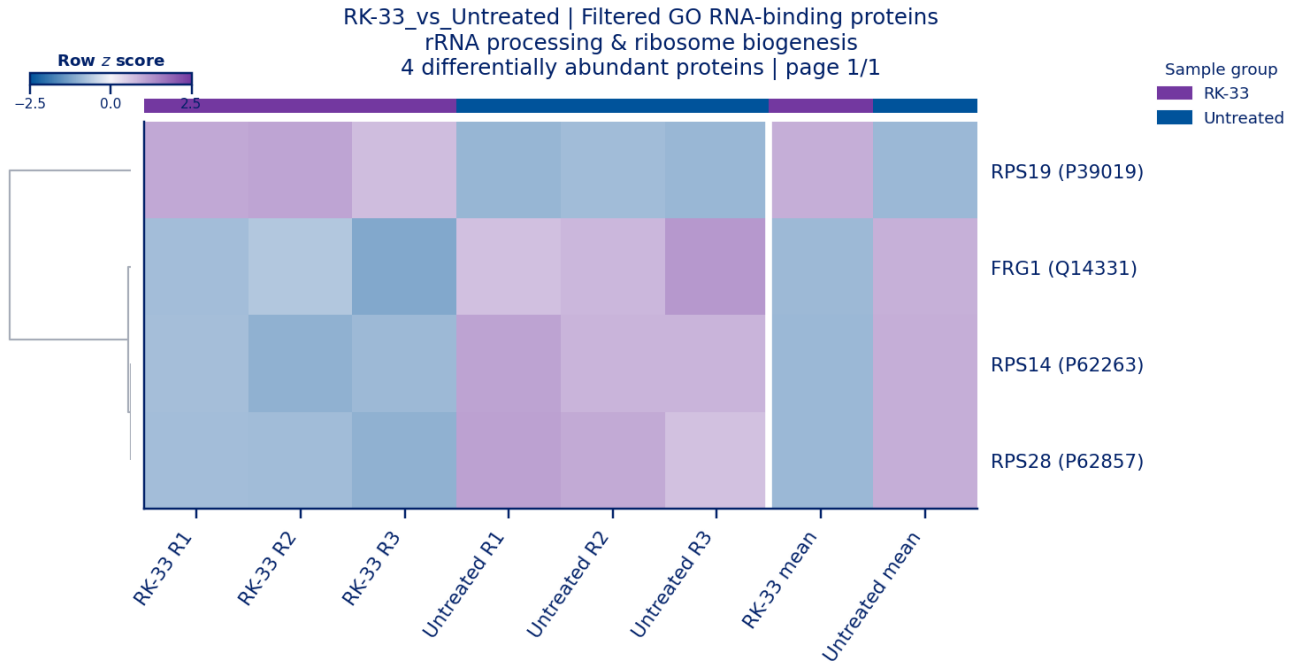


Figure 27. Protein abundance patterns within the rRNA processing & ribosome biogenesis category. Heatmap showing $\log_2$(%TP) values in the analyzed RNP fractions, standardized within each protein across biological replicates (row *z* scores). Category membership was assigned automatically using in-house classification rules applied to positive UniProtKB Gene Ontology annotations and keywords relating to rRNA processing, maturation, or modification, ribosome or ribosomal-subunit biogenesis or assembly, or the small-subunit processome. Purple and blue indicate abundances above and below the mean for each protein, respectively; the color scale is limited to ±2.5. Rows were clustered using average linkage and correlation distance across replicate samples. The dendrogram branches show the hierarchical clustering of proteins by their abundance patterns; the merge positions reflect average correlation distances, not evidence of direct interactions. Sample columns retain their experimental order. The final columns show the group means of the row *z* scores and were excluded from clustering. Proteins may appear in more than one category.

Protein functions and features (Figure 27)

RPS19 (P39019). Component of the small ribosomal subunit; GO annotations include fibroblast growth factor binding; antimicrobial humoral immune response mediated by antimicrobial peptide. Annotated features: Ribosomal protein S19e (family).

FRG1 (Q14331). Binds to mRNA in a sequence-independent manner; GO annotations include mRNA splicing, via spliceosome. Annotated features: FRG1-like domain.

RPS14 (P62263). Component of the small ribosomal subunit; GO annotations include mRNA 5'-UTR binding; negative regulation of transcription by RNA polymerase II. Annotated features: Ribosomal protein S11 (family).

RPS28 (P62857). Component of the small ribosomal subunit; GO annotations include structural constituent of ribosome; cytoplasmic translation. Annotated features: Ribosomal protein S28e.

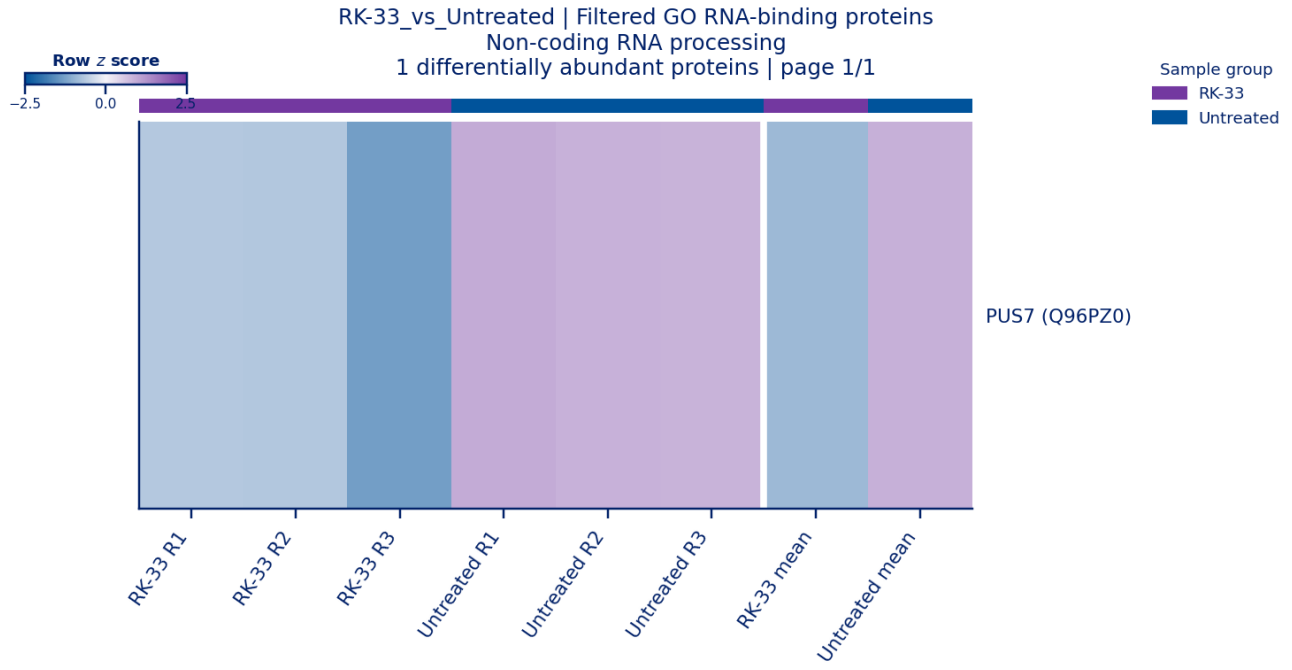


Figure 28. Protein abundance patterns within the Non-coding RNA processing category. Heatmap showing $\log_2$(%TP) values in the analyzed RNP fractions, standardized within each protein across biological replicates (row *z* scores). Category membership was assigned automatically using in-house classification rules applied to positive UniProtKB Gene Ontology annotations and keywords relating to processing, maturation, modification, aminoacylation, or splicing of tRNA, miRNA, snRNA, snoRNA, lncRNA, or other noncoding RNA. Purple and blue indicate abundances above and below the mean for each protein, respectively; the color scale is limited to ±2.5. Rows were clustered using average linkage and correlation distance across replicate samples. The dendrogram branches show the hierarchical clustering of proteins by their abundance patterns; the merge positions reflect average correlation distances, not evidence of direct interactions. Sample columns retain their experimental order. The final columns show the group means of the row *z* scores and were excluded from clustering. Proteins may appear in more than one category.

Protein functions and features (Figure 28)

PUS7 (Q96PZ0). Pseudouridylate synthase that catalyzes pseudouridylation of RNAs; GO annotations include tRNA pseudouridine(13) synthase activity; negative regulation of translation. Annotated features: Pseudouridine synthase, TruD, insertion domain.

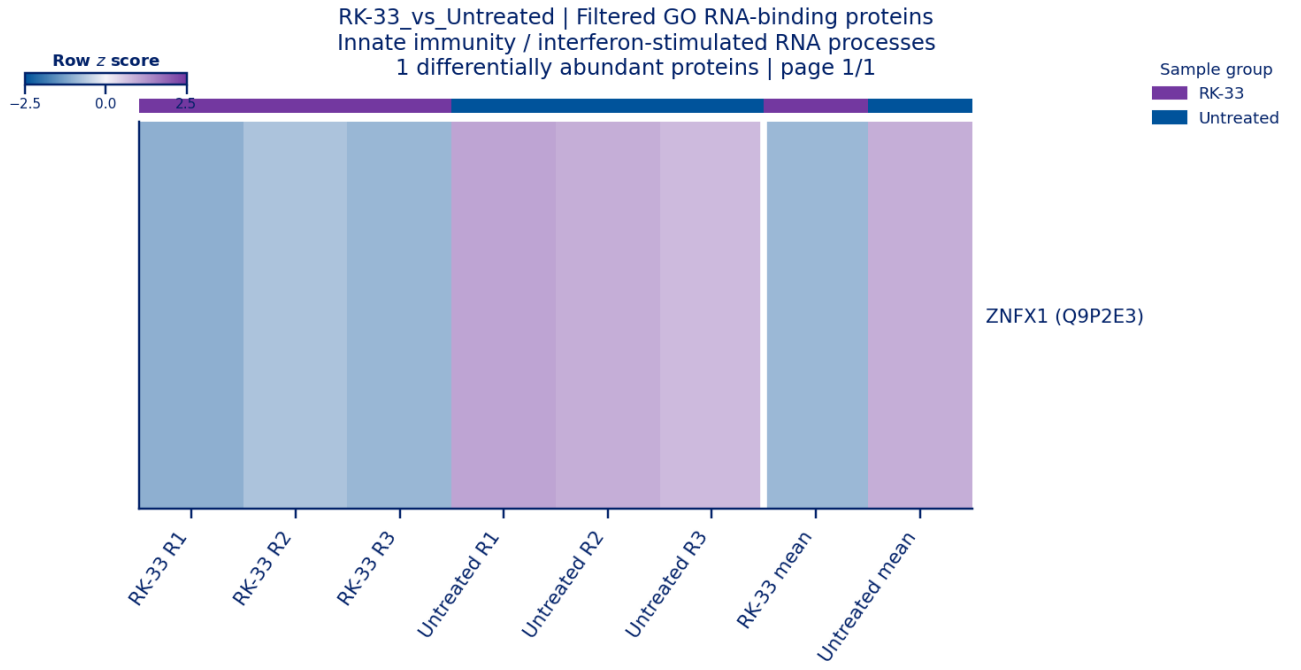


Figure 29. Protein abundance patterns within the Innate immunity / interferon-stimulated RNA processes category. Heatmap showing $\log_2$(%TP) values in the analyzed RNP fractions, standardized within each protein across biological replicates (row *z* scores). Category membership was assigned automatically using in-house classification rules applied to positive UniProtKB Gene Ontology annotations and keywords relating to interferon, innate immune responses, antiviral functions, viral RNA sensing, or RNA-mediated immunity. Purple and blue indicate abundances above and below the mean for each protein, respectively; the color scale is limited to ±2.5. Rows were clustered using average linkage and correlation distance across replicate samples. The dendrogram branches show the hierarchical clustering of proteins by their abundance patterns; the merge positions reflect average correlation distances, not evidence of direct interactions. Sample columns retain their experimental order. The final columns show the group means of the row *z* scores and were excluded from clustering. Proteins may appear in more than one category.

Protein functions and features (Figure 29)

ZNFX1 (Q9P2E3). RNA-activated non-canonical E3 ubiquitin ligase required for cell survival during interferon (IFN) responses. Annotated features: AAA domain; RZ type zinc finger domain.

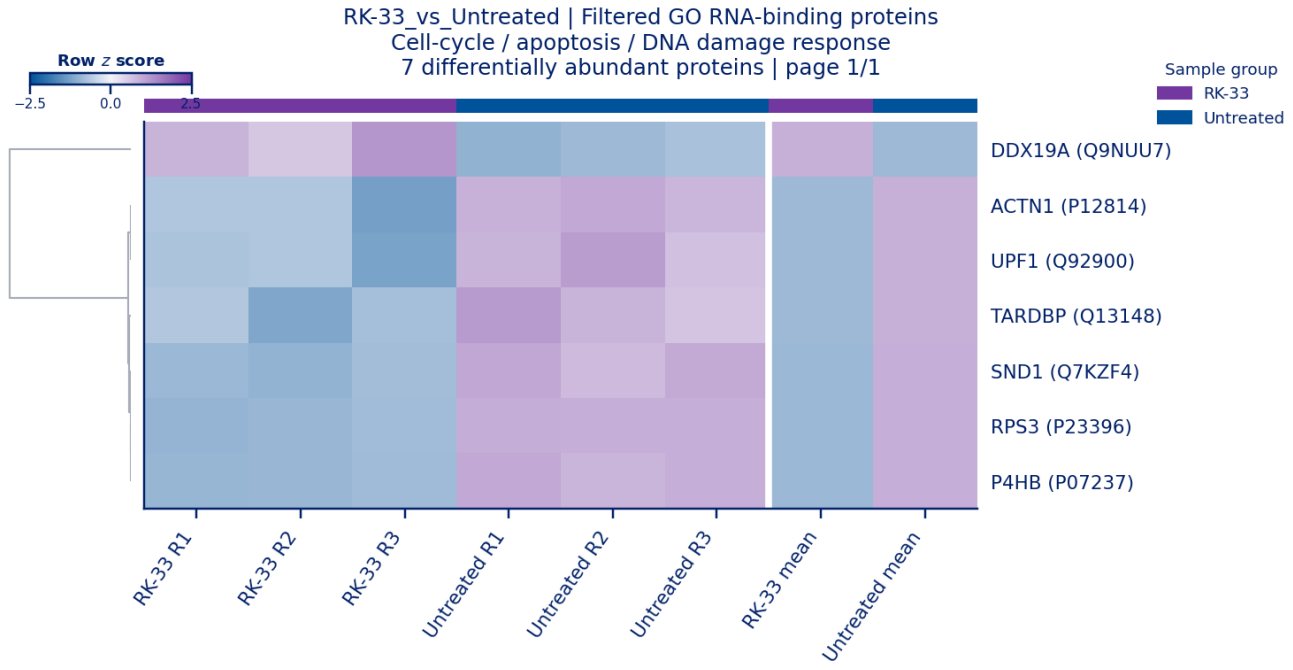


Figure 30. Protein abundance patterns within the Cell-cycle / apoptosis / DNA damage response category. Heatmap showing $\log_2$(%TP) values in the analyzed RNP fractions, standardized within each protein across biological replicates (row *z* scores). Category membership was assigned automatically using in-house classification rules applied to positive UniProtKB Gene Ontology annotations and keywords relating to the cell cycle, mitosis, apoptosis, programmed cell death, DNA-damage responses or checkpoints, or DNA repair. Purple and blue indicate abundances above and below the mean for each protein, respectively; the color scale is limited to ±2.5. Rows were clustered using average linkage and correlation distance across replicate samples. The dendrogram branches show the hierarchical clustering of proteins by their abundance patterns; the merge positions reflect average correlation distances, not evidence of direct interactions. Sample columns retain their experimental order. The final columns show the group means of the row *z* scores and were excluded from clustering. Proteins may appear in more than one category.

Protein functions and features (Figure 30)

DDX19A (Q9NUU7). ATP-dependent RNA helicase involved in mRNA export from the nucleus (inferred by similarity). Annotated features: DEAD/DEAH box helicase; Helicase conserved C-terminal domain.

ACTN1 (P12814). F-actin cross-linking protein which is thought to anchor actin to a variety of intracellular structures. Annotated features: Ca2+ insensitive EF hand; Calponin homology (CH) domain.

UPF1 (Q92900). RNA-dependent helicase required for nonsense-mediated decay (NMD) of aberrant mRNAs containing premature stop codons and which modulates the expression level of normal mRNAs. Annotated features: AAA domain; RNA helicase (UPF2 interacting domain).

TARDBP (Q13148). RNA-binding protein that is involved in various steps of RNA biogenesis and processing. Annotated features: RNA recognition motif; TAR DNA-binding protein 43, N-terminal domain.

SND1 (Q7KZF4). Endonuclease that mediates miRNA decay of both protein-free and AGO2-loaded miRNAs; GO annotations include 3' overhang single-stranded DNA endonuclease activity; mRNA catabolic process. Annotated features: Staphylococcal nuclease homologue; Tudor domain.

RPS3 (P23396). Component of the small ribosomal subunit; GO annotations include class I DNA-(apurinic or apyrimidinic site) endonuclease activity; positive regulation of intrinsic apoptotic signaling pathway in response to DNA damage. Annotated features: KH domain; Ribosomal protein S3, C-terminal domain.

P4HB (P07237). This multifunctional protein catalyzes the formation, breakage and rearrangement of disulfide bonds. Annotated features: Thioredoxin; Thioredoxin-like domain.

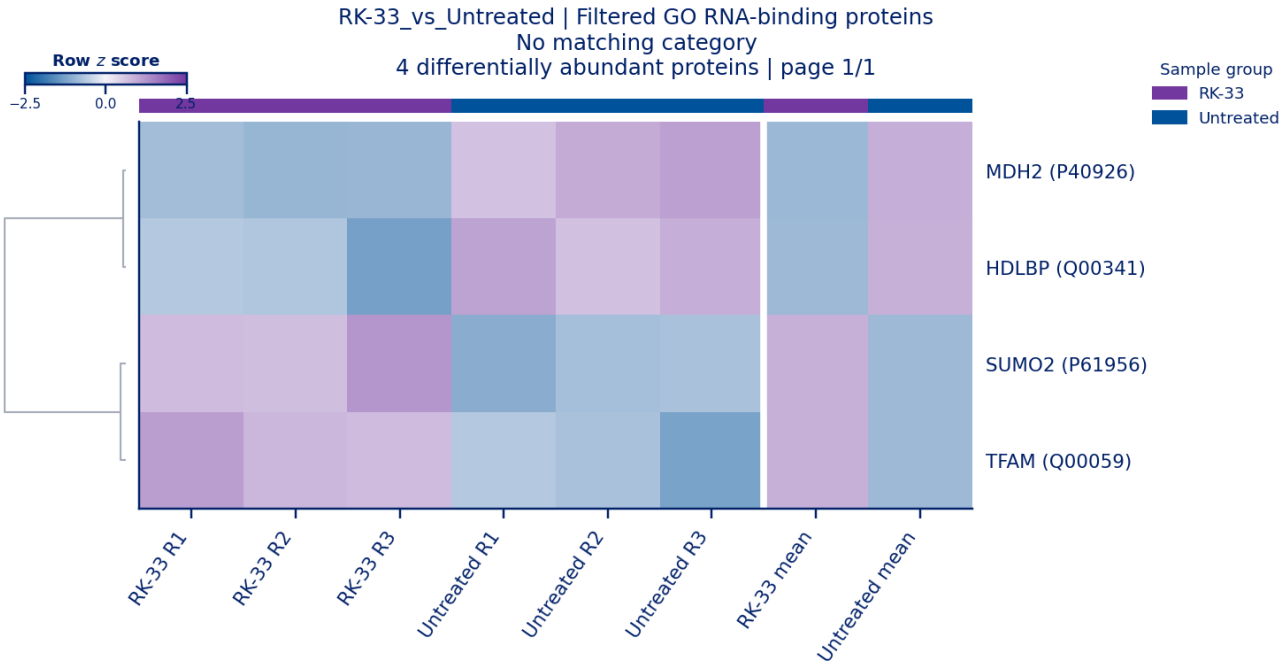


Figure 31. Protein abundance patterns of proteins without a matching functional category. Heatmap showing $\log_2$(%TP) values in the analyzed RNP fractions, standardized within each protein across biological replicates (row *z* scores). These proteins did not match the predefined annotation categories; this does not indicate an absence of known functions. Purple and blue indicate abundances above and below the mean for each protein, respectively; the color scale is limited to ±2.5. Rows were clustered using average linkage and correlation distance across replicate samples. The dendrogram branches show the hierarchical clustering of proteins by their abundance patterns; the merge positions reflect average correlation distances, not evidence of direct interactions. Sample columns retain their experimental order. The final columns show the group means of the row *z* scores and were excluded from clustering. Proteins may appear in more than one category.

Protein functions and features (Figure 31)

MDH2 (P40926). Mitochondrial malate dehydrogenase that catalyzes the reversible conversion of malate to oxaloacetate using NAD(+) as a cofactor. Annotated features: lactate/malate dehydrogenase, NAD binding domain; lactate/malate dehydrogenase, alpha/beta C-terminal domain.

HDLBP (Q00341). Appears to play a role in cell sterol metabolism; GO annotations include cadherin binding; cholesterol metabolic process. Annotated features: KH domain; Vigilin KH domain.

SUMO2 (P61956). Ubiquitin-like protein that can be covalently attached to proteins as a monomer or as a lysine-linked polymer. Annotated features: Rad60/SUMO-like domain; Ubiquitin-like domain.

TFAM (Q00059). Binds to the mitochondrial light strand promoter and functions in mitochondrial transcription regulation. Annotated features: HMG (high mobility group) box; HMG-box domain.

10. Over-representation and Gene Set Enrichment Analyses

H3B-8800 versus Untreated

Functional enrichment was evaluated using genes corresponding to tested proteins. The comparison included 790 unique, unambiguously mapped genes, of which 5 corresponded to differentially abundant proteins (1 with increased and 4 with decreased %TP in H3B-8800 relative to Untreated). Missing or ambiguous gene symbols were excluded without alias substitution. Multiple protein entries mapping to the same gene were counted once; their signed *t* statistics were averaged for ranked enrichment.

Gene sets were obtained from GOA/QuickGO, Enrichr, Reactome, and InterPro/UniProtKB as listed below (retrieved 2026-11-14). Enrichr library years identify provider exports; the upstream release is not necessarily specified. Direct Reactome and InterPro library labels identify recorded source releases; InterPro domain assignments use reviewed human UniProtKB cross-references. GO gene sets use positive human GOA protein annotations, all evidence codes, and is_a and part_of propagation within each GO aspect using the recorded QuickGO ontology release. These gene sets were analyzed separately from the descriptive categories in Section 9.

RK-33 versus Untreated

Functional enrichment was evaluated using genes corresponding to tested proteins. The comparison included 757 unique, unambiguously mapped genes, of which 29 corresponded to differentially abundant proteins (12 with increased and 17 with decreased %TP in RK-33 relative to Untreated). Missing or ambiguous gene symbols were excluded without alias substitution. Multiple protein entries mapping to the same gene were counted once; their signed *t* statistics were averaged for ranked enrichment.

Gene sets were obtained from GOA/QuickGO, Enrichr, Reactome, and InterPro/UniProtKB as listed below (retrieved 2026-11-14). Enrichr library years identify provider exports; the upstream release is not necessarily specified. Direct Reactome and InterPro library labels identify recorded source releases; InterPro domain assignments use reviewed human UniProtKB cross-references. GO gene sets use positive human GOA protein annotations, all evidence codes, and is_a and part_of propagation within each GO aspect using the recorded QuickGO ontology release. These gene sets were analyzed separately from the descriptive categories in Section 9.

Over-representation analysis

Over-representation analysis was performed separately for all differentially abundant proteins and for each abundance direction, using all 790 tested genes as the background. Gene sets containing 3–500 background genes were tested using a one-sided hypergeometric test. The Benjamini–Hochberg procedure was applied across all eligible terms, including terms with no overlap, separately for each library and selected list. The adjusted *p* values are reported as *q* values ($q < .05$). Fold enrichment is the observed overlap divided by its expectation under random selection from the tested background.

H3B-8800 versus Untreated

Gene-set library	Terms tested	Significant terms: all proteins	Significant terms: increased in H3B-8800	Significant terms: decreased in H3B-8800
GO biological process (2026-11-13)	1479	0	0	0
GO molecular function (2026-11-13)	366	0	0	0

Gene-set library	Terms tested	Significant terms: all proteins	Significant terms: increased in H3B-8800	Significant terms: decreased in H3B-8800
GO cellular component (2026-11-13)	340	8	0	9
Reactome pathways (98)	458	4	0	10
KEGG 2026	71	1	0	1
InterPro domains (111.0)	108	0	0	0

The final three columns give the numbers of terms meeting $q < .05$ in each selected list. Increased and decreased refer to H3B-8800 relative to Untreated. Terms overlap, and counts are not numbers of independent biological processes. All libraries and selected lists are included, including those with no significant terms.

Over-representation analysis was performed separately for all differentially abundant proteins and for each abundance direction, using all 757 tested genes as the background. Gene sets containing 3–500 background genes were tested using a one-sided hypergeometric test. The Benjamini–Hochberg procedure was applied across all eligible terms, including terms with no overlap, separately for each library and selected list. The adjusted *p* values are reported as *q* values ($q < .05$). Fold enrichment is the observed overlap divided by its expectation under random selection from the tested background.

RK-33 versus Untreated

Gene-set library	Terms tested	Significant terms: all proteins	Significant terms: increased in RK-33	Significant terms: decreased in RK-33
GO biological process (2026-11-13)	1383	3	3	0
GO molecular function (2026-11-13)	344	0	0	0
GO cellular component (2026-11-13)	320	17	13	0
Reactome pathways (98)	414	7	5	0
KEGG 2026	65	1	0	0
InterPro domains (111.0)	104	0	0	0

The final three columns give the numbers of terms meeting $q < .05$ in each selected list. Increased and decreased refer to RK-33 relative to Untreated. Terms overlap, and counts are not numbers of independent biological processes. All libraries and selected lists are included, including those with no significant terms.

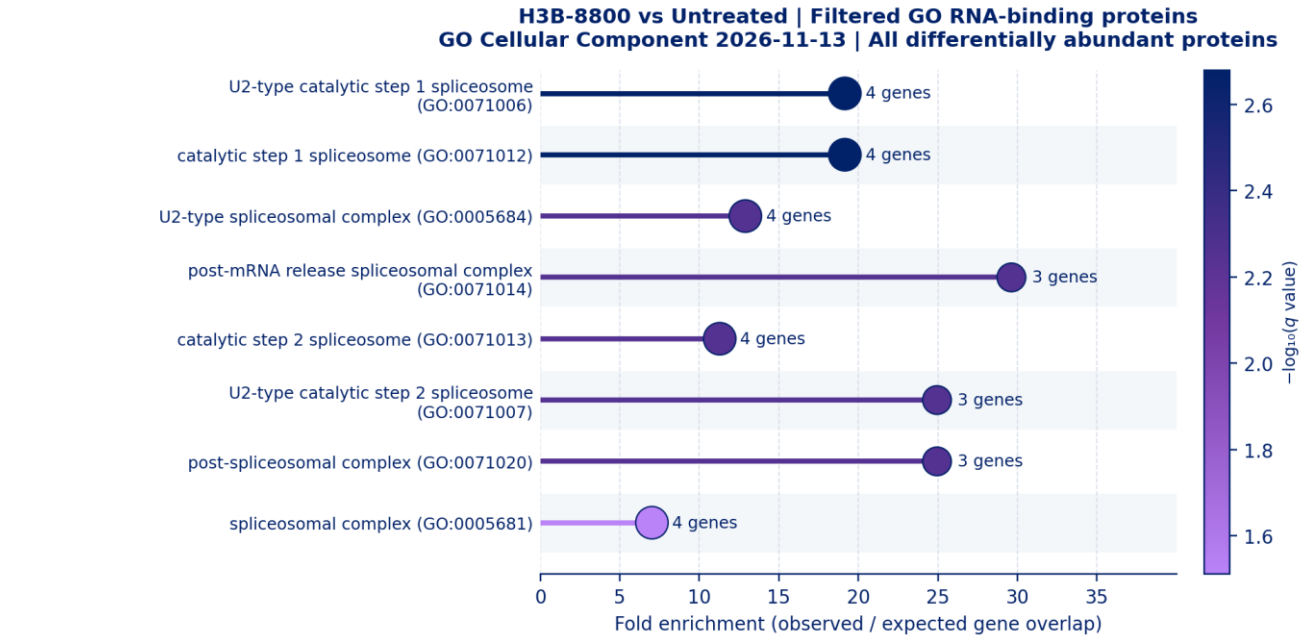


Figure 32. Over-representation of GO cellular component (2026-11-13) terms among all differentially abundant proteins. Shown are all 8 significant terms, ordered by *q* value, then *p* value and term name. Horizontal positions indicate fold enrichment (observed divided by expected gene overlap); dot size indicates the number of overlapping genes, and color indicates $-\log_{10}(q)$. Terms meet $q < .05$ after correction across 340 eligible terms in this library and selected list. Complete results and supporting genes are provided in the corresponding over-representation tables.

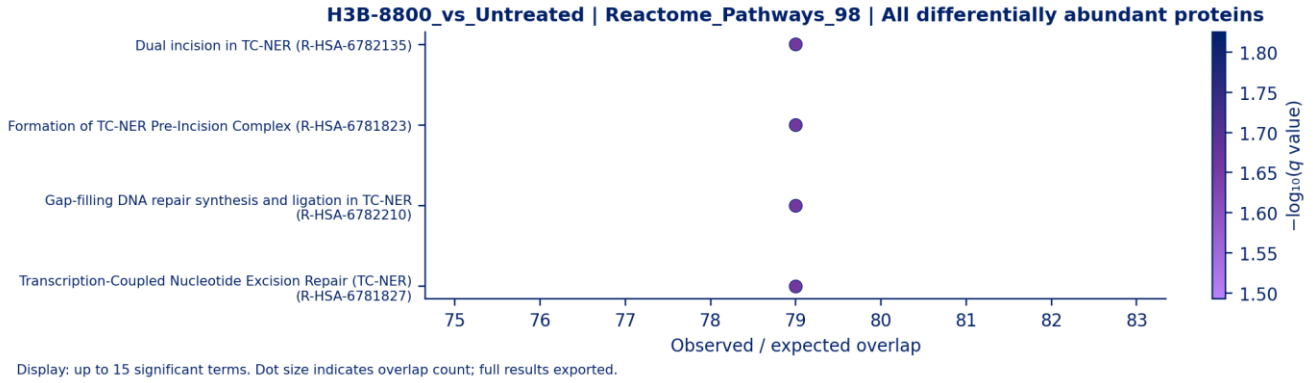


Figure 33. Over-representation of Reactome pathways (98) terms among all differentially abundant proteins. Shown are all 4 significant terms, ordered by *q* value, then *p* value and term name. Horizontal positions indicate fold enrichment (observed divided by expected gene overlap); dot size indicates the number of overlapping genes, and color indicates $-\log_{10}(q)$. Terms meet $q < .05$ after correction across 458 eligible terms in this library and selected list. Complete results and supporting genes are provided in the corresponding over-representation tables.

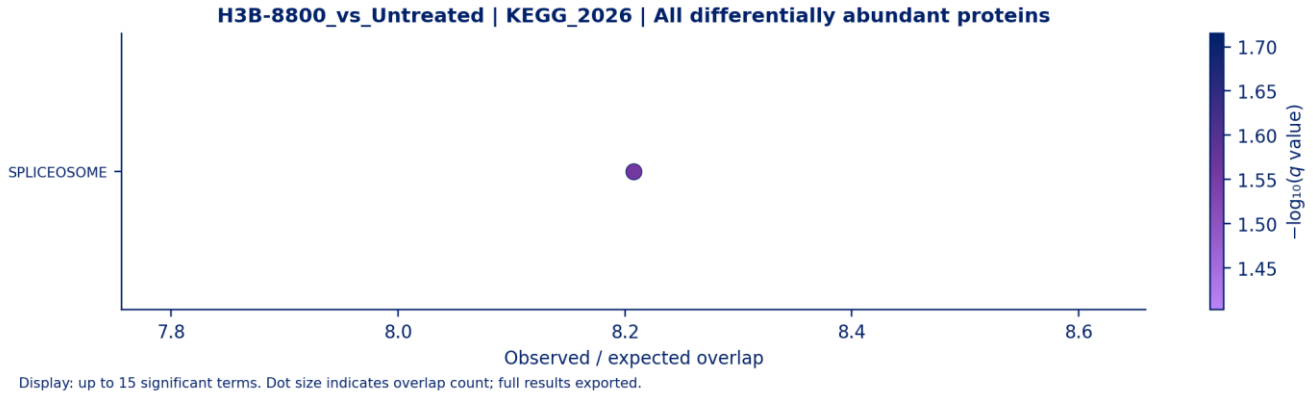


Figure 34. Over-representation of KEGG 2026 terms among all differentially abundant proteins. Shown is the significant term, ordered by *q* value, then *p* value and term name. Horizontal positions indicate fold enrichment (observed divided by expected gene overlap); dot size indicates the number of overlapping genes, and color indicates $-\log_{10}(q)$. Terms meet $q < .05$ after correction across 71 eligible terms in this library and selected list. Complete results and supporting genes are provided in the corresponding over-representation tables.

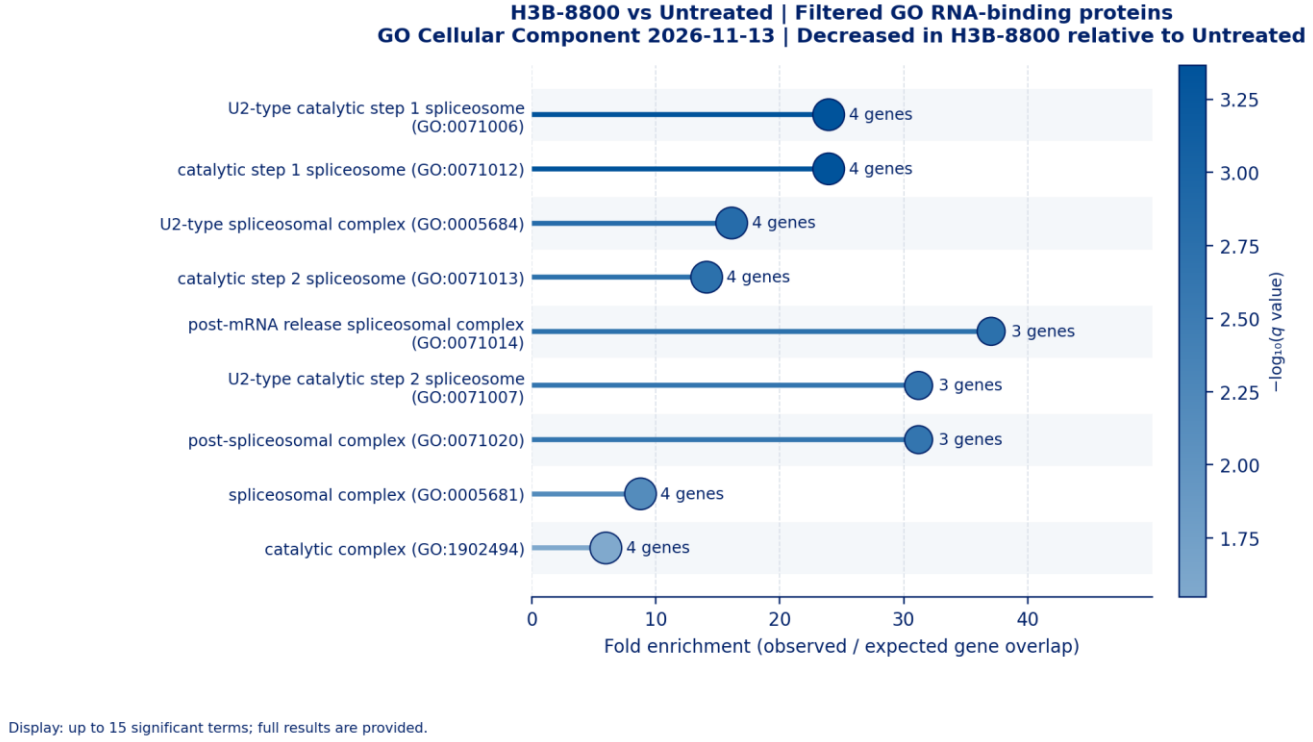


Figure 35. Over-representation of GO cellular component (2026-11-13) terms among proteins with decreased %TP in H3B-8800 relative to Untreated. Shown are all 9 significant terms, ordered by *q* value, then *p* value and term name. Horizontal positions indicate fold enrichment (observed divided by expected gene overlap); dot size indicates the number of overlapping genes, and color indicates $-\log_{10}(q)$. Terms meet $q < .05$ after correction across 340 eligible terms in this library and selected list. Complete results and supporting genes are provided in the corresponding over-representation tables.

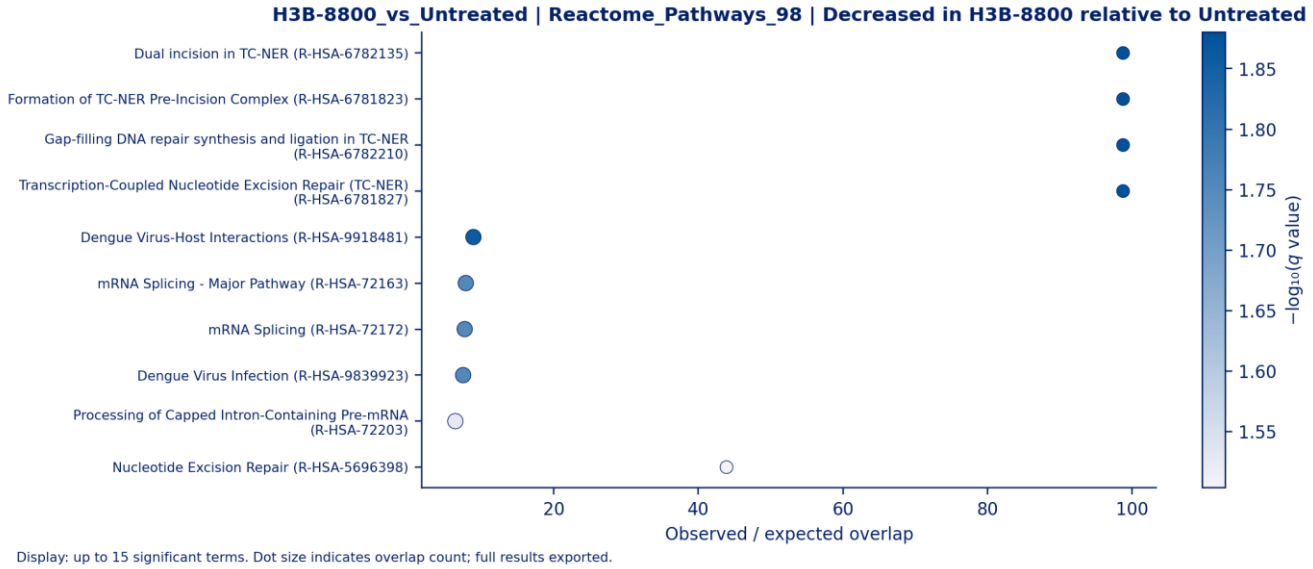


Figure 36. Over-representation of Reactome pathways (98) terms among proteins with decreased %TP in H3B-8800 relative to Untreated. Shown are all 10 significant terms, ordered by *q* value, then *p* value and term name. Horizontal positions indicate fold enrichment (observed divided by expected gene overlap); dot size indicates the number of overlapping genes, and color indicates $-\log_{10}(q)$. Terms meet $q < .05$ after correction across 458 eligible terms in this library and selected list. Complete results and supporting genes are provided in the corresponding over-representation tables.

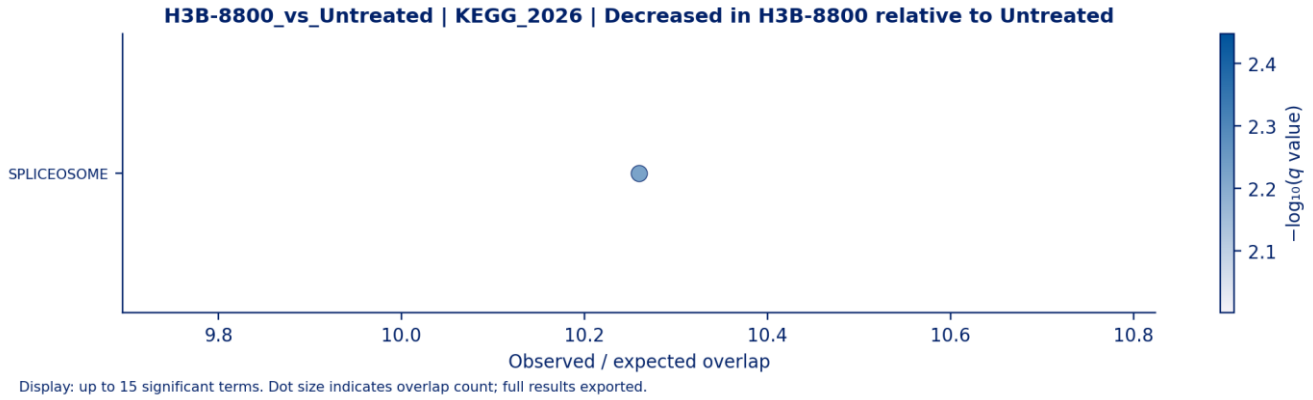


Figure 37. Over-representation of KEGG 2026 terms among proteins with decreased %TP in H3B-8800 relative to Untreated. Shown is the significant term, ordered by *q* value, then *p* value and term name. Horizontal positions indicate fold enrichment (observed divided by expected gene overlap); dot size indicates the number of overlapping genes, and color indicates $-\log_{10}(q)$. Terms meet $q < .05$ after correction across 71 eligible terms in this library and selected list. Complete results and supporting genes are provided in the corresponding over-representation tables.

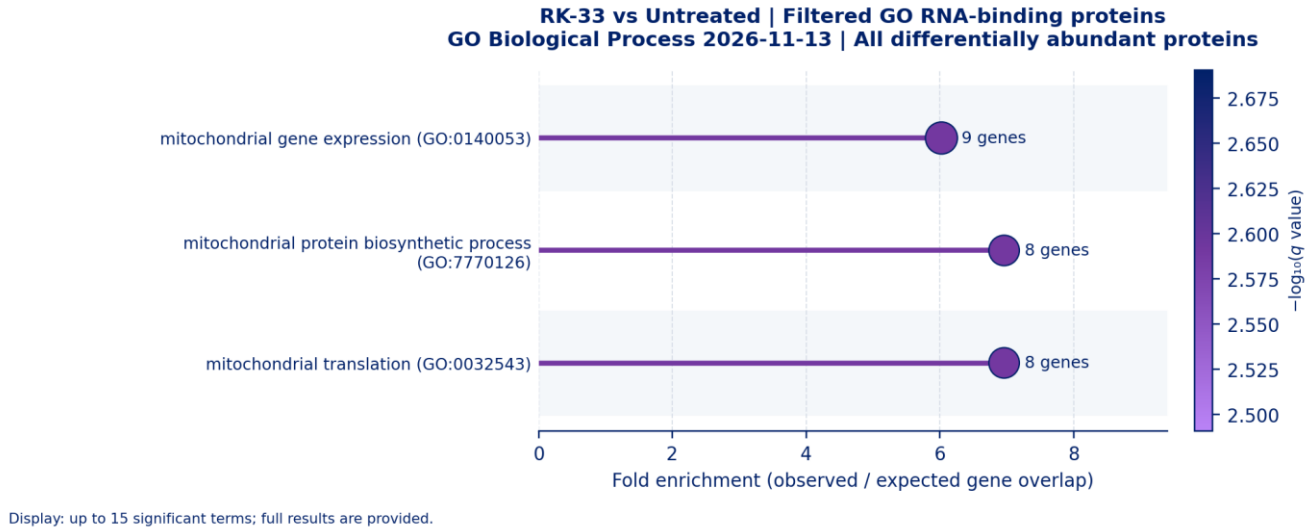


Figure 38. Over-representation of GO biological process (2026-11-13) terms among all differentially abundant proteins. Shown are all 3 significant terms, ordered by *q* value, then *p* value and term name. Horizontal positions indicate fold enrichment (observed divided by expected gene overlap); dot size indicates the number of overlapping genes, and color indicates $-\log_{10}(q)$. Terms meet $q < .05$ after correction across 1383 eligible terms in this library and selected list. Complete results and supporting genes are provided in the corresponding over-representation tables.

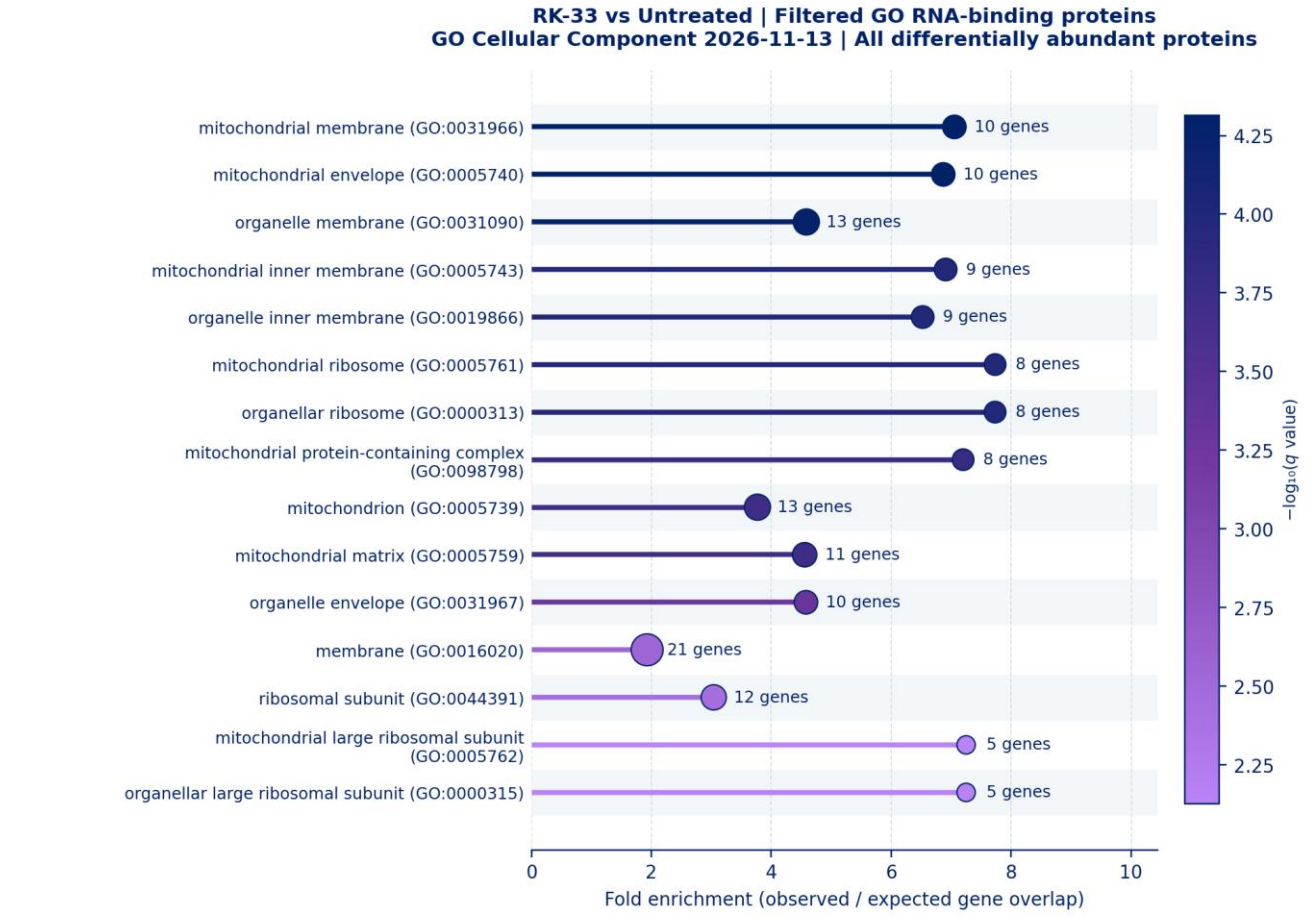


Figure 39. Over-representation of GO cellular component (2026-11-13) terms among all differentially abundant proteins. Shown are 15 of 17 significant terms, ordered by *q* value, then *p* value and term name. Horizontal positions indicate fold enrichment (observed divided by expected gene overlap); dot size indicates the number of overlapping genes, and color indicates $-\log_{10}(q)$. Terms meet $q < .05$ after correction across 320 eligible terms in this library and selected list. Complete results and supporting genes are provided in the corresponding over-representation tables.

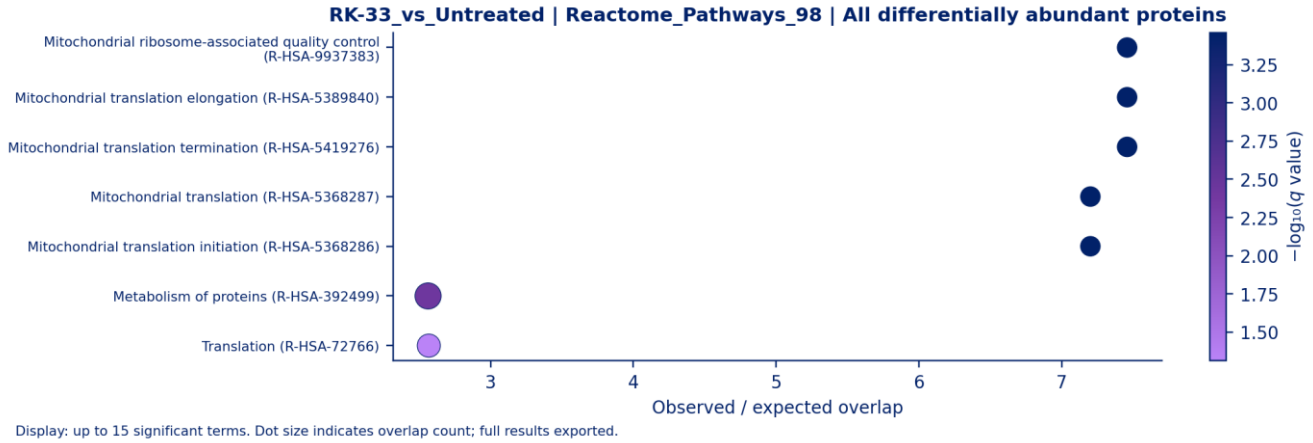


Figure 40. Over-representation of Reactome pathways (98) terms among all differentially abundant proteins. Shown are all 7 significant terms, ordered by *q* value, then *p* value and term name. Horizontal positions indicate fold enrichment (observed divided by expected gene overlap); dot size indicates the number of overlapping genes, and color indicates $-\log_{10}(q)$. Terms meet $q < .05$ after correction across 414 eligible terms in this library and selected list. Complete results and supporting genes are provided in the corresponding over-representation tables.

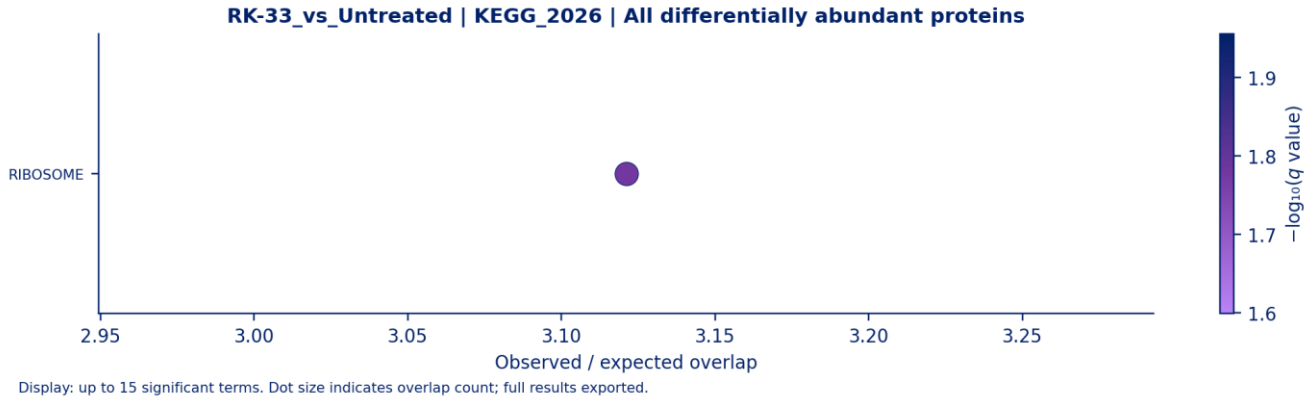


Figure 41. Over-representation of KEGG 2026 terms among all differentially abundant proteins. Shown is the significant term, ordered by *q* value, then *p* value and term name. Horizontal positions indicate fold enrichment (observed divided by expected gene overlap); dot size indicates the number of overlapping genes, and color indicates $-\log_{10}(q)$. Terms meet $q < .05$ after correction across 65 eligible terms in this library and selected list. Complete results and supporting genes are provided in the corresponding over-representation tables.

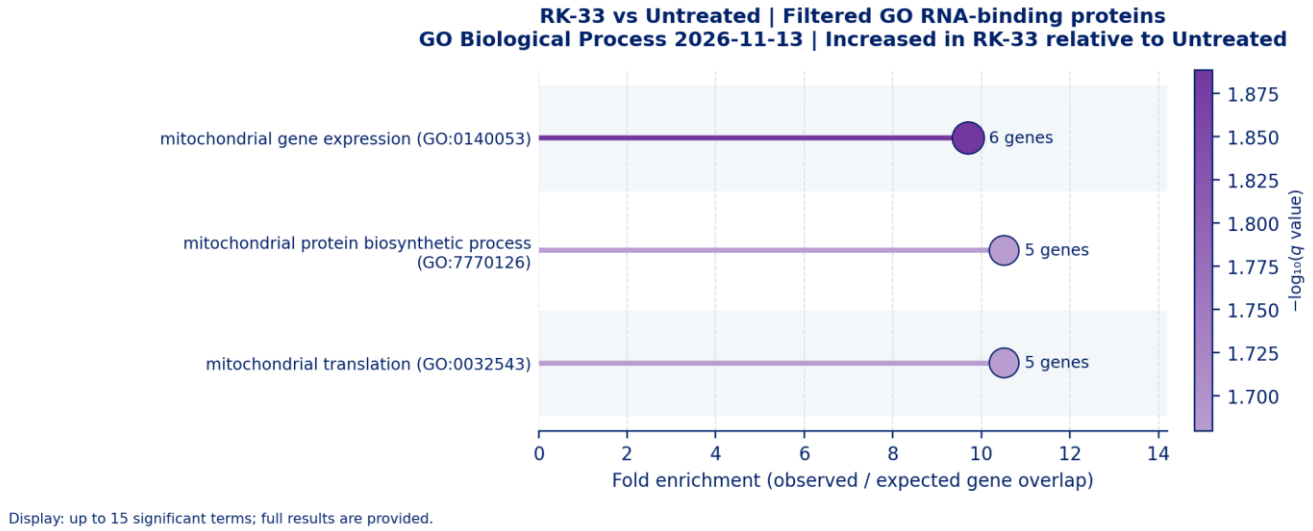


Figure 42. Over-representation of GO biological process (2026-11-13) terms among proteins with increased %TP in RK-33 relative to Untreated. Shown are all 3 significant terms, ordered by *q* value, then *p* value and term name. Horizontal positions indicate fold enrichment (observed divided by expected gene overlap); dot size indicates the number of overlapping genes, and color indicates $-\log_{10}(q)$. Terms meet $q < .05$ after correction across 1383 eligible terms in this library and selected list. Complete results and supporting genes are provided in the corresponding over-representation tables.

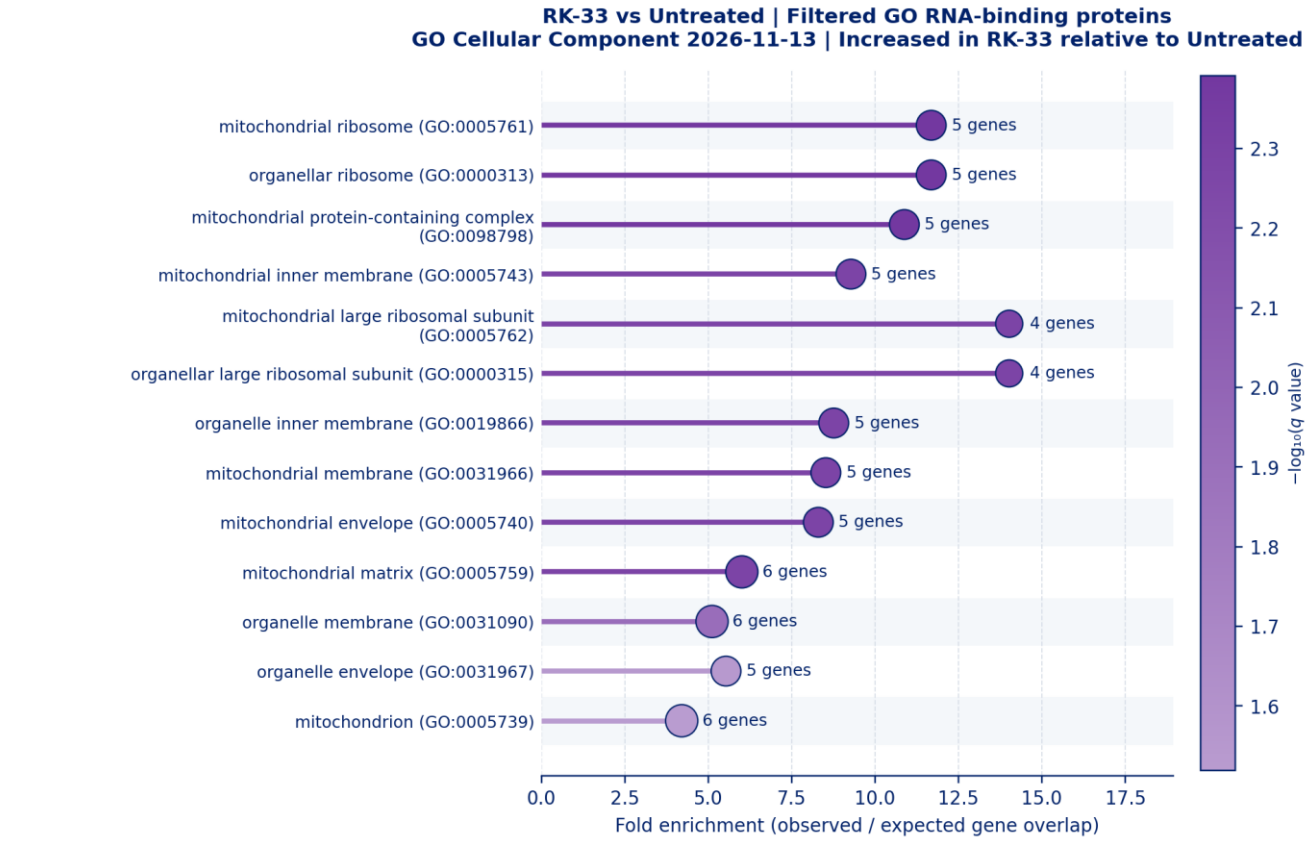


Figure 43. Over-representation of GO cellular component (2026-11-13) terms among proteins with increased %TP in RK-33 relative to Untreated. Shown are all 13 significant terms, ordered by *q* value, then *p* value and term name. Horizontal positions indicate fold enrichment (observed divided by expected gene overlap); dot size indicates the number of overlapping genes, and color indicates $-\log_{10}(q)$. Terms meet $q < .05$ after correction across 320 eligible terms in this library and selected list. Complete results and supporting genes are provided in the corresponding over-representation tables.

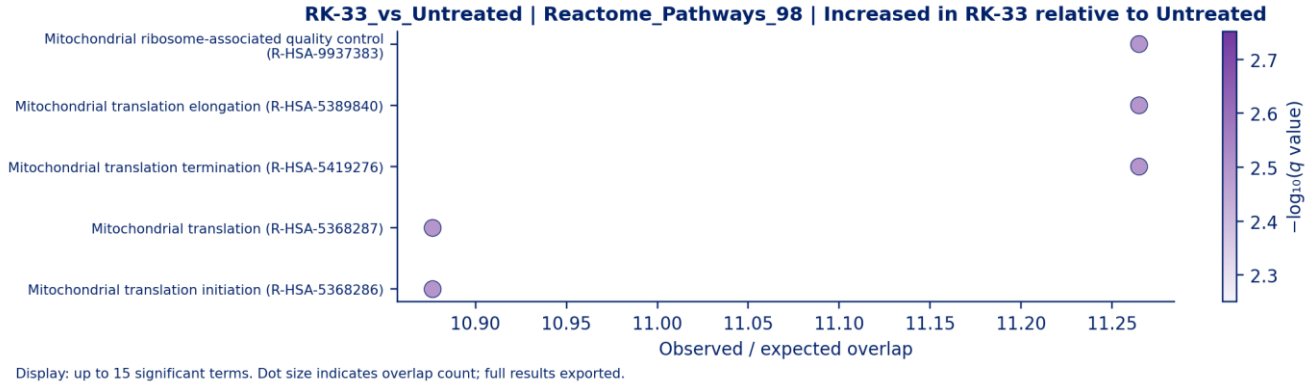


Figure 44. Over-representation of Reactome pathways (98) terms among proteins with increased %TP in RK-33 relative to Untreated. Shown are all 5 significant terms, ordered by *q* value, then *p* value and term name. Horizontal positions indicate fold enrichment (observed divided by expected gene overlap); dot size indicates the number of overlapping genes, and color indicates $-\log_{10}(q)$. Terms meet $q < .05$ after correction across 414 eligible terms in this library and selected list. Complete results and supporting genes are provided in the corresponding over-representation tables.

Ranked gene set enrichment analysis

Preranked gene set enrichment analysis (GSEA) used the full gene list ordered by decreasing signed *t* statistic. Positive and negative scores indicate increased and decreased relative protein abundance in H3B-8800 relative to Untreated, respectively. Gene sets containing 15–500 ranked genes were eligible. Weighted enrichment scores (weight = 1) were evaluated using 1,000 gene-set permutations (seed = 1729); sample-group labels were not permuted. GSEA's permutation-based adjusted *p* values are reported as *q* values and were estimated separately within each library ($q < .05$). Leading-edge genes are the subset contributing to a gene set's enrichment score; they need not be individually differentially abundant. Enrichment FDR is distinct from the protein-level Benjamini–Hochberg correction and is not pooled across libraries.

H3B-8800 versus Untreated

Gene-set library	Sets tested	Significant sets: NES > 0	Significant sets: NES < 0
GO biological process (2026-11-13)	396	0	4
GO molecular function (2026-11-13)	123	0	0
GO cellular component (2026-11-13)	125	0	13
Reactome pathways (98)	101	0	6
KEGG 2026	8	0	1
InterPro domains (111.0)	10	1	1

The final two columns give the numbers of gene sets with $q < .05$, separated by enrichment direction. All libraries are included. Summary figures show up to 15 significant sets per library; complete results and supporting genes are retained in the data package.

Preranked gene set enrichment analysis (GSEA) used the full gene list ordered by decreasing signed *t* statistic. Positive and negative scores indicate increased and decreased relative protein abundance in RK-33 relative to Untreated, respectively. Gene sets containing 15–500 ranked genes were eligible. Weighted enrichment scores (weight = 1) were evaluated using 1,000 gene-set permutations (seed = 1729); sample-group labels were not permuted. GSEA's permutation-based adjusted *p* values are reported as *q* values and were estimated separately within each library ($q < .05$). Leading-edge genes are the subset contributing to a gene set's enrichment score; they need not be individually differentially abundant. Enrichment FDR is distinct from the protein-level Benjamini–Hochberg correction and is not pooled across libraries.

RK-33 versus Untreated

Gene-set library	Sets tested	Significant sets: NES > 0	Significant sets: NES < 0
GO biological process (2026-11-13)	382	0	2
GO molecular function (2026-11-13)	118	0	0
GO cellular component (2026-11-13)	122	2	0
Reactome pathways (98)	100	0	0
KEGG 2026	8	0	0
InterPro domains (111.0)	10	0	0

The final two columns give the numbers of gene sets with $q < .05$, separated by enrichment direction. All libraries are included. Summary figures show up to 15 significant sets per library; complete results and supporting genes are retained in the data package.

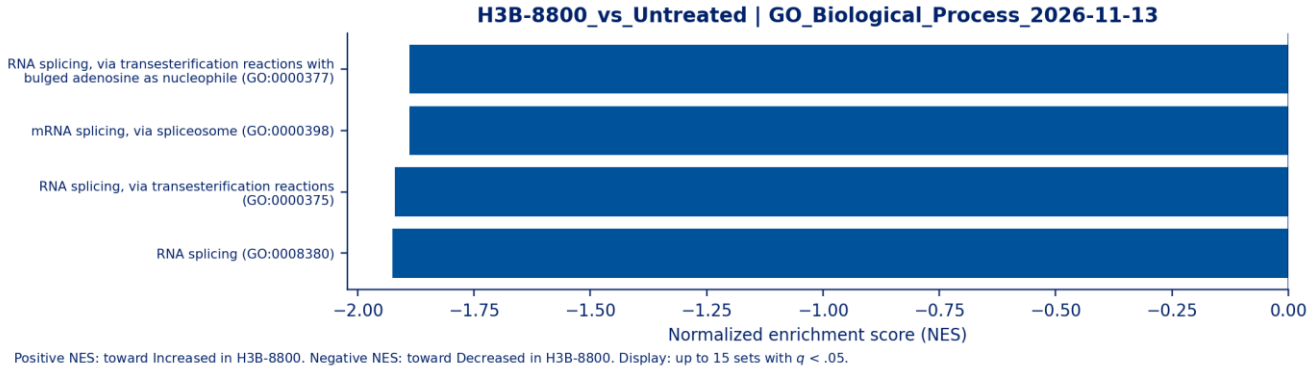


Figure 45. Ranked enrichment of GO biological process (2026-11-13) gene sets. Shown are all 4 significant gene sets, ordered by *q* value, then nominal *p* value and term name. Bars show normalized enrichment scores (NES). Positive and negative NES indicate enrichment toward the H3B-8800 and Untreated ends of the signed *t*-statistic ranking, respectively. Gene sets meet $q < .05$ within this library (396 sets tested). Complete results, ranked genes, leading-edge genes, and running enrichment curves are provided in the corresponding ranked-enrichment folder.

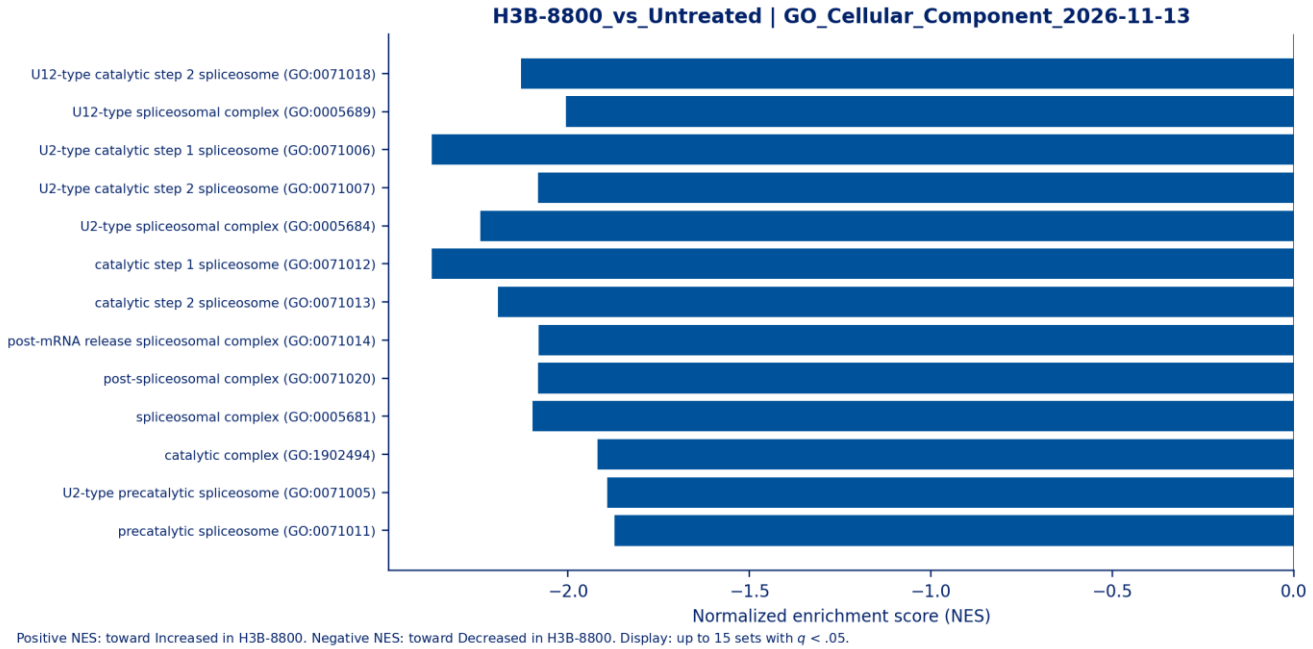


Figure 46. Ranked enrichment of GO cellular component (2026-11-13) gene sets. Shown are all 13 significant gene sets, ordered by *q* value, then nominal *p* value and term name. Bars show normalized enrichment scores (NES). Positive and negative NES indicate enrichment toward the H3B-8800 and Untreated ends of the signed *t*-statistic ranking, respectively. Gene sets meet $q < .05$ within this library (125 sets tested). Complete results, ranked genes, leading-edge genes, and running enrichment curves are provided in the corresponding ranked-enrichment folder.

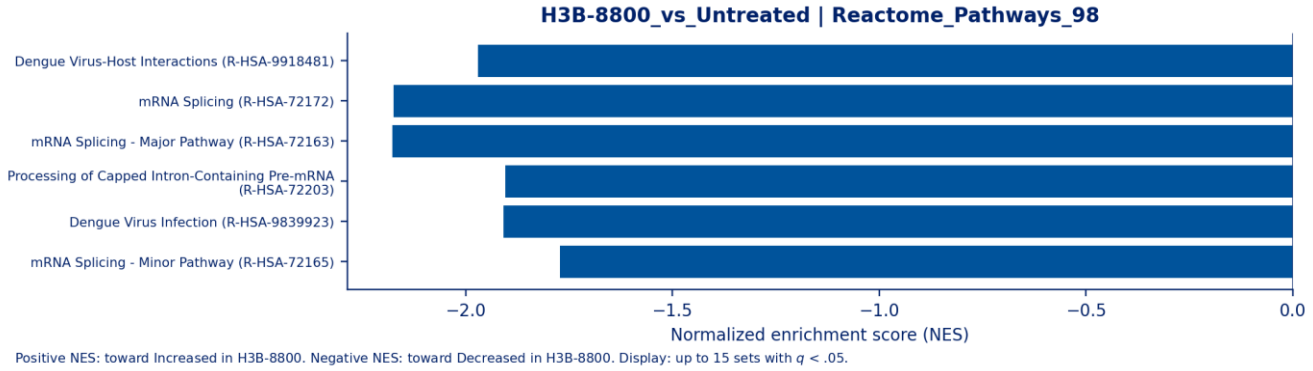


Figure 47. Ranked enrichment of Reactome pathways (98) gene sets. Shown are all 6 significant gene sets, ordered by *q* value, then nominal *p* value and term name. Bars show normalized enrichment scores (NES). Positive and negative NES indicate enrichment toward the H3B-8800 and Untreated ends of the signed *t*-statistic ranking, respectively. Gene sets meet $q < .05$ within this library (101 sets tested). Complete results, ranked genes, leading-edge genes, and running enrichment curves are provided in the corresponding ranked-enrichment folder.

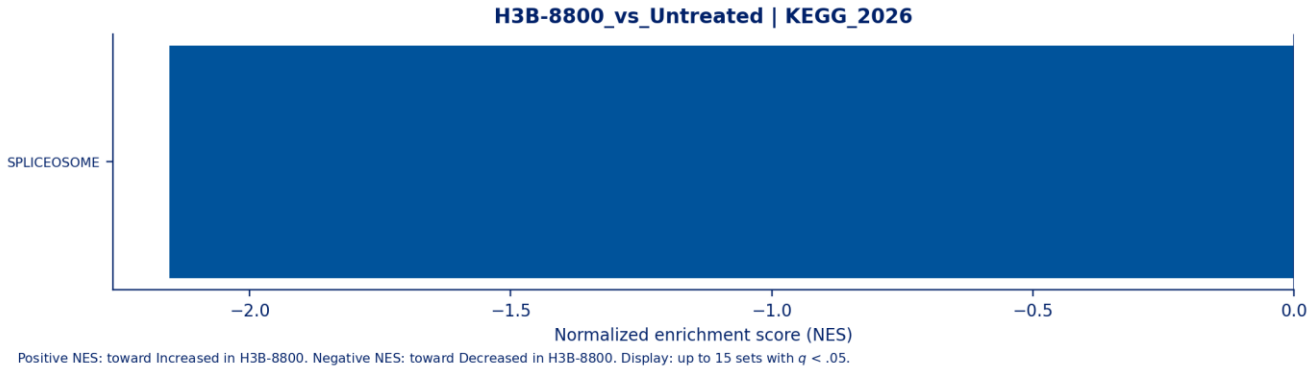


Figure 48. Ranked enrichment of KEGG 2026 gene sets. Shown is the significant gene set, ordered by *q* value, then nominal *p* value and term name. Bars show normalized enrichment scores (NES). Positive and negative NES indicate enrichment toward the H3B-8800 and Untreated ends of the signed *t*-statistic ranking, respectively. Gene sets meet $q < .05$ within this library (8 sets tested). Complete results, ranked genes, leading-edge genes, and running enrichment curves are provided in the corresponding ranked-enrichment folder.

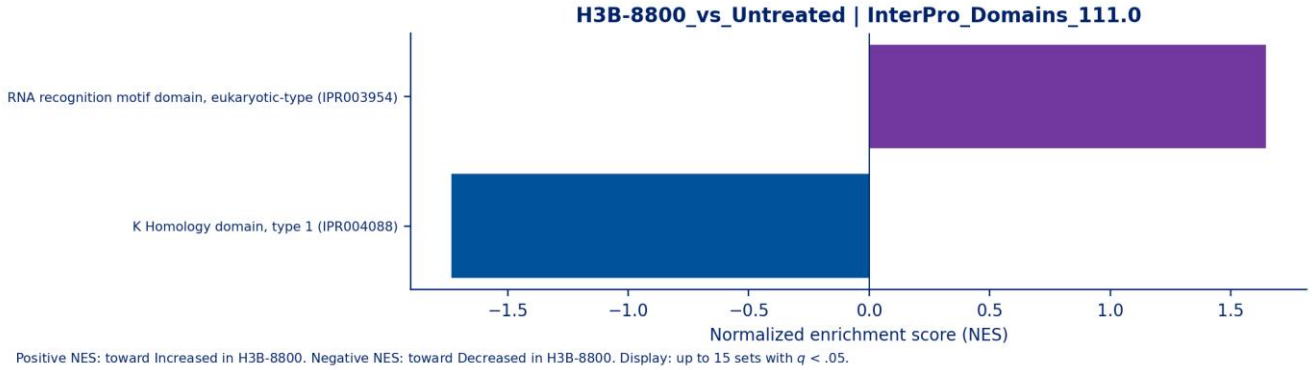


Figure 49. Ranked enrichment of InterPro domains (111.0) gene sets. Shown are all 2 significant gene sets, ordered by *q* value, then nominal *p* value and term name. Bars show normalized enrichment scores (NES). Positive and negative NES indicate enrichment toward the H3B-8800 and Untreated ends of the signed *t*-statistic ranking, respectively. Gene sets meet $q < .05$ within this library (10 sets tested). Complete results, ranked genes, leading-edge genes, and running enrichment curves are provided in the corresponding ranked-enrichment folder.

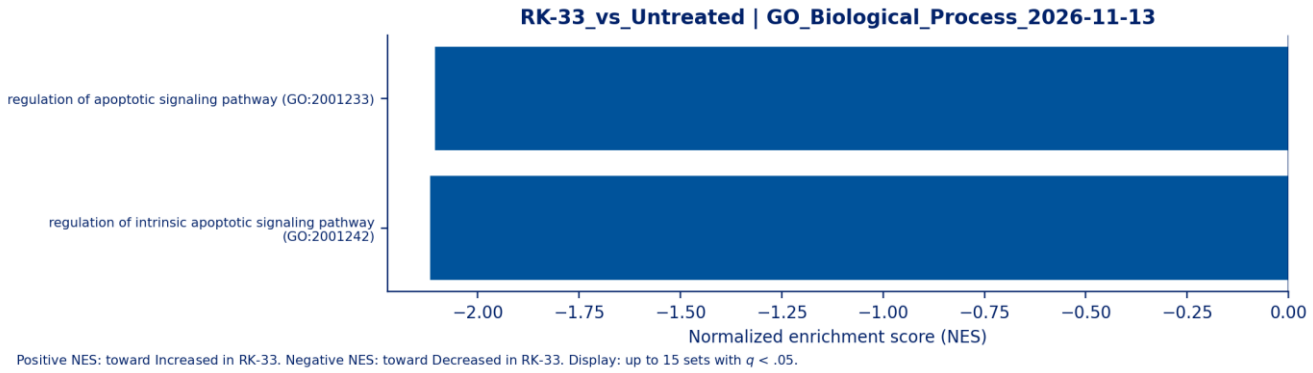


Figure 50. Ranked enrichment of GO biological process (2026-11-13) gene sets. Shown are all 2 significant gene sets, ordered by *q* value, then nominal *p* value and term name. Bars show normalized enrichment scores (NES). Positive and negative NES indicate enrichment toward the RK-33 and Untreated ends of the signed *t*-statistic ranking, respectively. Gene sets meet $q < .05$ within this library (382 sets tested). Complete results, ranked genes, leading-edge genes, and running enrichment curves are provided in the corresponding ranked-enrichment folder.

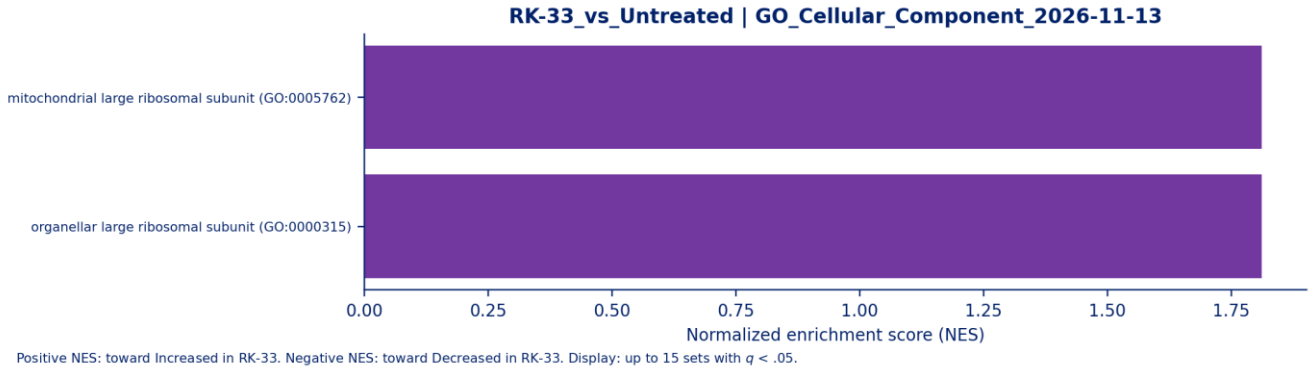


Figure 51. Ranked enrichment of GO cellular component (2026-11-13) gene sets. Shown are all 2 significant gene sets, ordered by *q* value, then nominal *p* value and term name. Bars show normalized enrichment scores (NES). Positive and negative NES indicate enrichment toward the RK-33 and Untreated ends of the signed *t*-statistic ranking, respectively. Gene sets meet $q < .05$ within this library (122 sets tested). Complete results, ranked genes, leading-edge genes, and running enrichment curves are provided in the corresponding ranked-enrichment folder.

Functional enrichment describes the distribution of annotations among selected or ranked proteins in the analyzed fractions. Overlapping terms may reflect the same proteins. These results do not establish changes in total cellular protein abundance, RNA-binding occupancy, or pathway activity.

11. Protein Networks

STRING functional-association networks show proteins with BH-adjusted $q < .05$ in each selected comparison and protein panel. Colored lines show the sources of evidence for reference associations; node and line colors do not show the direction of the measured change. The mapping and association tables accompany the figures. No additional proteins were added.

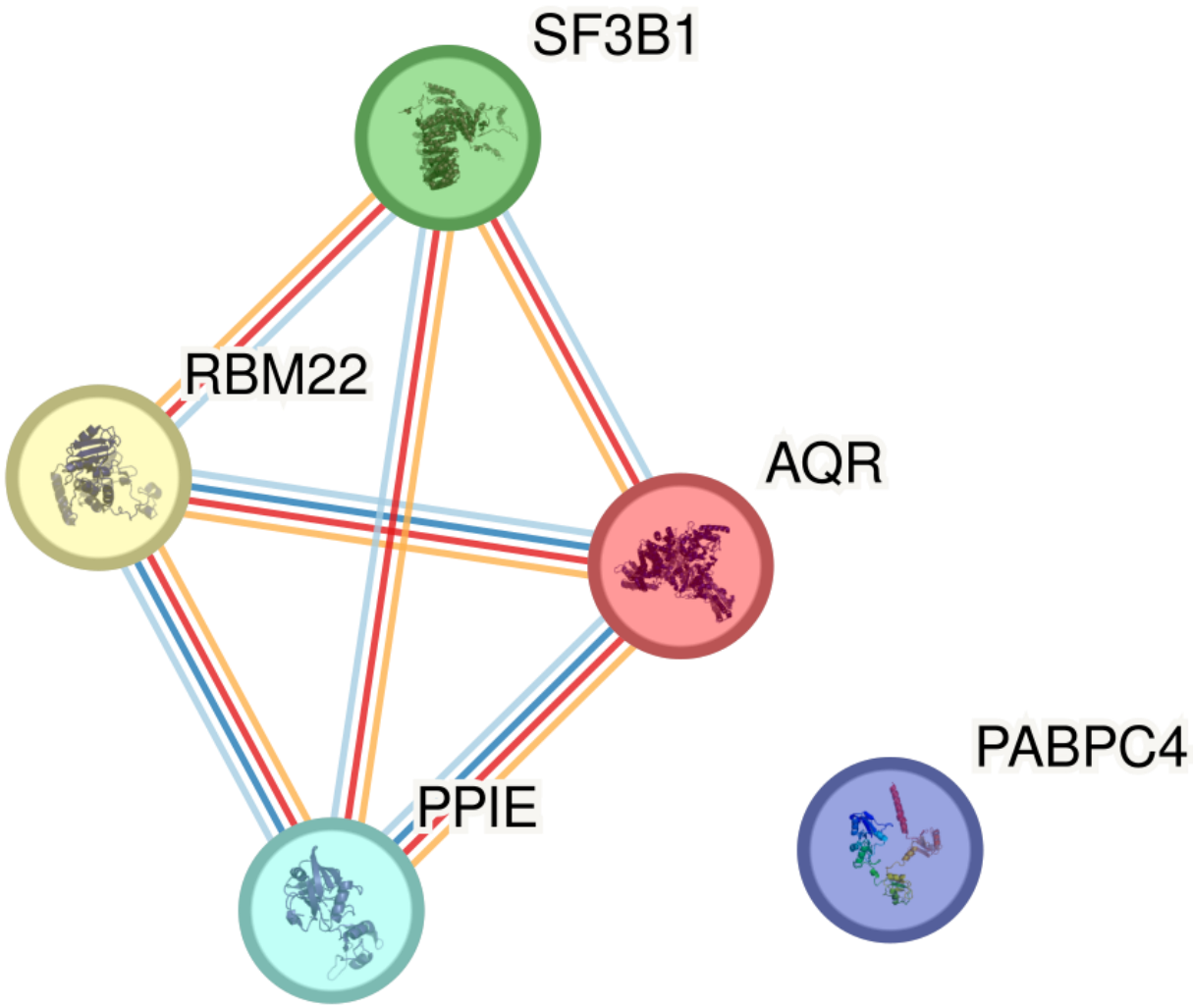


Figure 52. STRING functional-association network for H3B-8800 versus Untreated. The input comprises 5 proteins with protein-level BH-adjusted $q < .05$; 5 mapped uniquely to STRING. Colored lines identify evidence sources; nodes and line colors do not encode fold-change direction. STRING v12.5; combined confidence ≥ 0.40; no additional proteins were added. Protein mappings and association scores are provided in the source tables. The report image is cropped to remove transparent margins. STRING network image and data: https://string-db.org, CC BY 4.0.

STRING line colors: ● light blue: curated databases; ● purple: experiments; ● yellow: text mining; ● black: co-expression; ● green: gene neighborhood; ● red: gene fusion; ● blue: gene co-occurrence. Multiple colors can support the same association. Node colors distinguish proteins and do not indicate the direction of change.

Source data: protein nodes; connections; selection

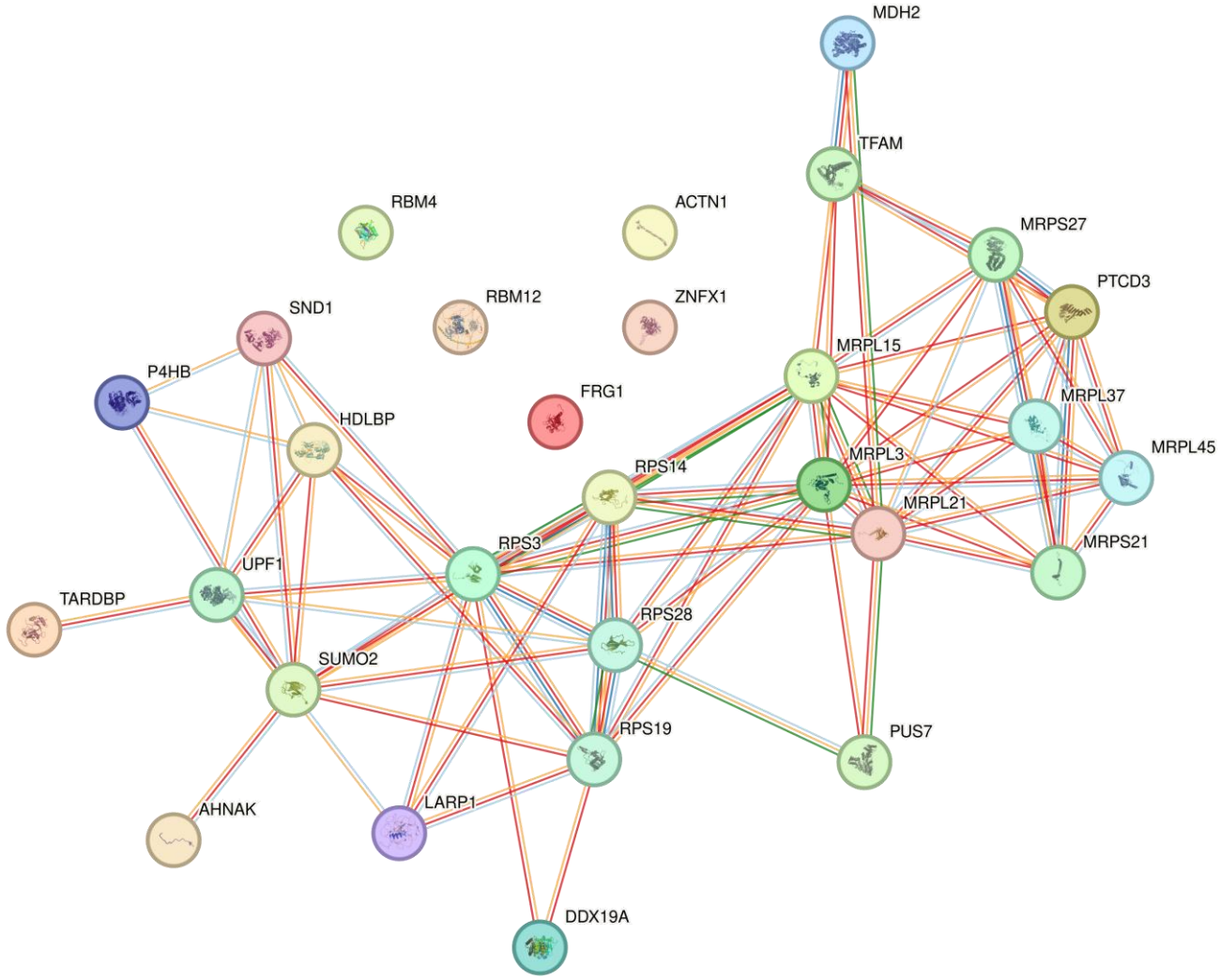


Figure 53. STRING functional-association network for RK-33 versus Untreated. The input comprises 29 proteins with protein-level BH-adjusted *q* < .05; 29 mapped uniquely to STRING. Colored lines identify evidence sources; nodes and line colors do not encode fold-change direction. STRING v12.5; combined confidence ≥ 0.40; no additional proteins were added. Protein mappings and association scores are provided in the source tables. The report image is cropped to remove transparent margins. STRING network image and data: https://string-db.org, CC BY 4.0.

STRING line colors: ● light blue: curated databases; ● purple: experiments; ● yellow: text mining; ● black: co-expression; ● green: gene neighborhood; ● red: gene fusion; ● blue: gene co-occurrence. Multiple colors can support the same association. Node colors distinguish proteins and do not indicate the direction of change.

Source data: protein nodes; connections; selection

12. Treatment Selectivity

Selectivity scores summarize the fraction of evaluated proteins whose abundance in the analyzed RNP fractions changes by at least the stated fold threshold relative to the explicitly nominated control. Increases and reciprocal decreases are counted without a *p*-value or *q*-value filter. These counts are separate from the differential-abundance calls in Section 8.

The following summary uses the common eligible protein set across nominated comparisons sharing the same control and protein panel. Lower scores describe a response concentrated among fewer evaluated proteins at that threshold. Comparison-specific scores, complete protein values and response memberships are provided in the data package. Scores describe the recorded treatment conditions.

Treatment	Control	*N*	S(1.25-fold)	S(1.5-fold)	S(2-fold)
H3B-8800	Untreated	750	0.1013	0.0467	0.0173
RK-33	Untreated	750	0.2333	0.0880	0.0267

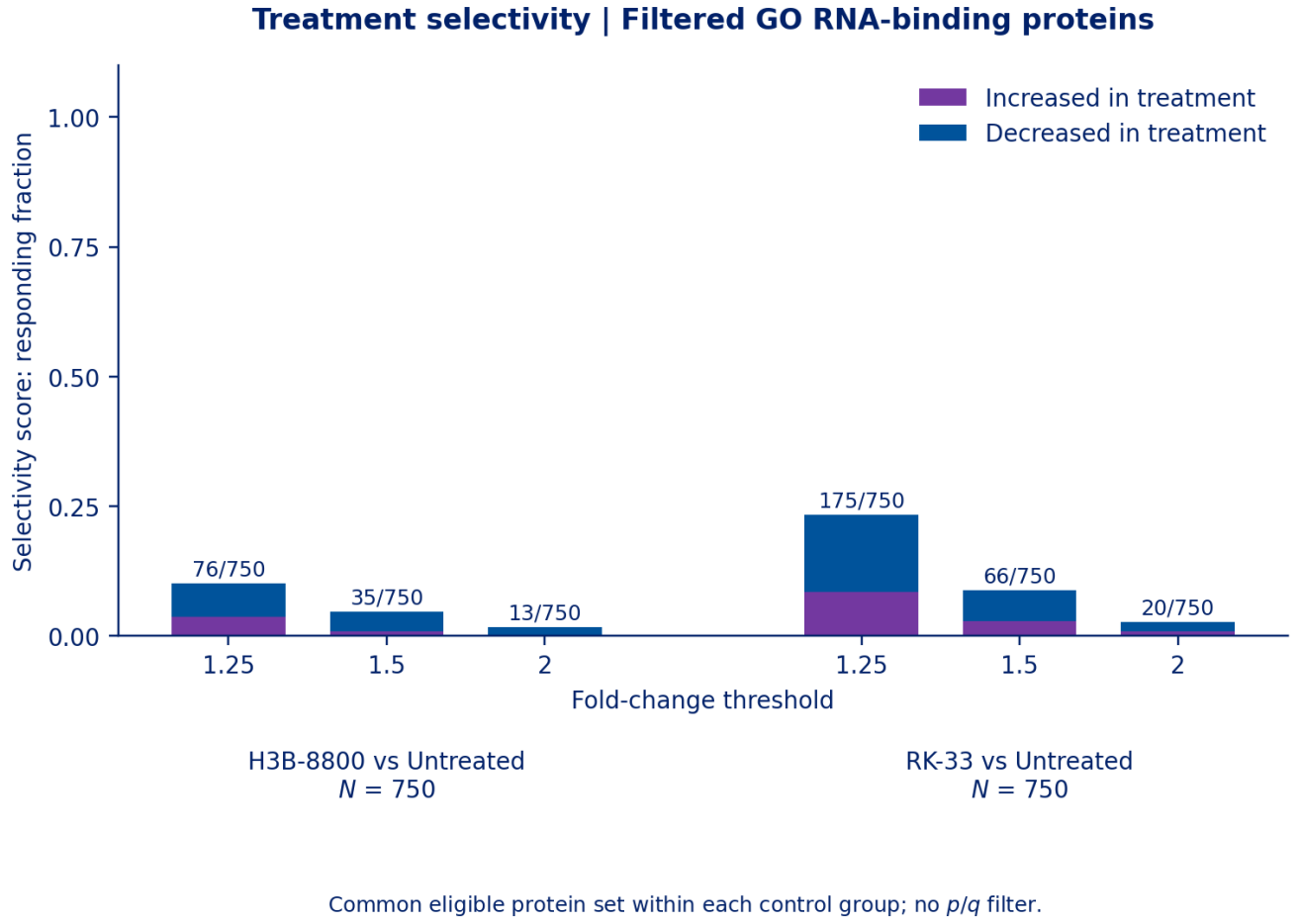


Figure 54. Treatment selectivity across fold-change thresholds. Stacked bars show the fraction of evaluated proteins with an increase (purple) or decrease (blue) of at least 1.25, 1.5, 2-fold relative to the nominated control. The total bar height is S(f-fold); no *p*-value or *q*-value filter is applied. The denominator is the common eligible protein set across nominated comparisons sharing a control and protein panel, with its size shown as *N*. Reciprocal decreases are counted: for example, a twofold decrease corresponds to a treatment/control ratio of 0.5. Fold changes retain the original %TP normalization. The source tables contain counts, scores, complete evaluated protein values, and threshold memberships; comparison-specific scores are also provided.

13. Additional Detection Evidence

Comparison	Panel	Criterion met in	Additional proteins
H3B-8800_vs_Untreated	Filtered GO RNA-binding proteins	H3B-8800	17
H3B-8800_vs_Untreated	Filtered GO RNA-binding proteins	Untreated	24
RK-33_vs_Untreated	Filtered GO RNA-binding proteins	RK-33	8
RK-33_vs_Untreated	Filtered GO RNA-binding proteins	Untreated	57

These proteins meet the peptide criterion in every replicate of one group and fail it in at least one replicate of the other. They are listed separately from differential-abundance results. Missing detection does not demonstrate biological absence; no imputed fold changes or significance values are assigned.

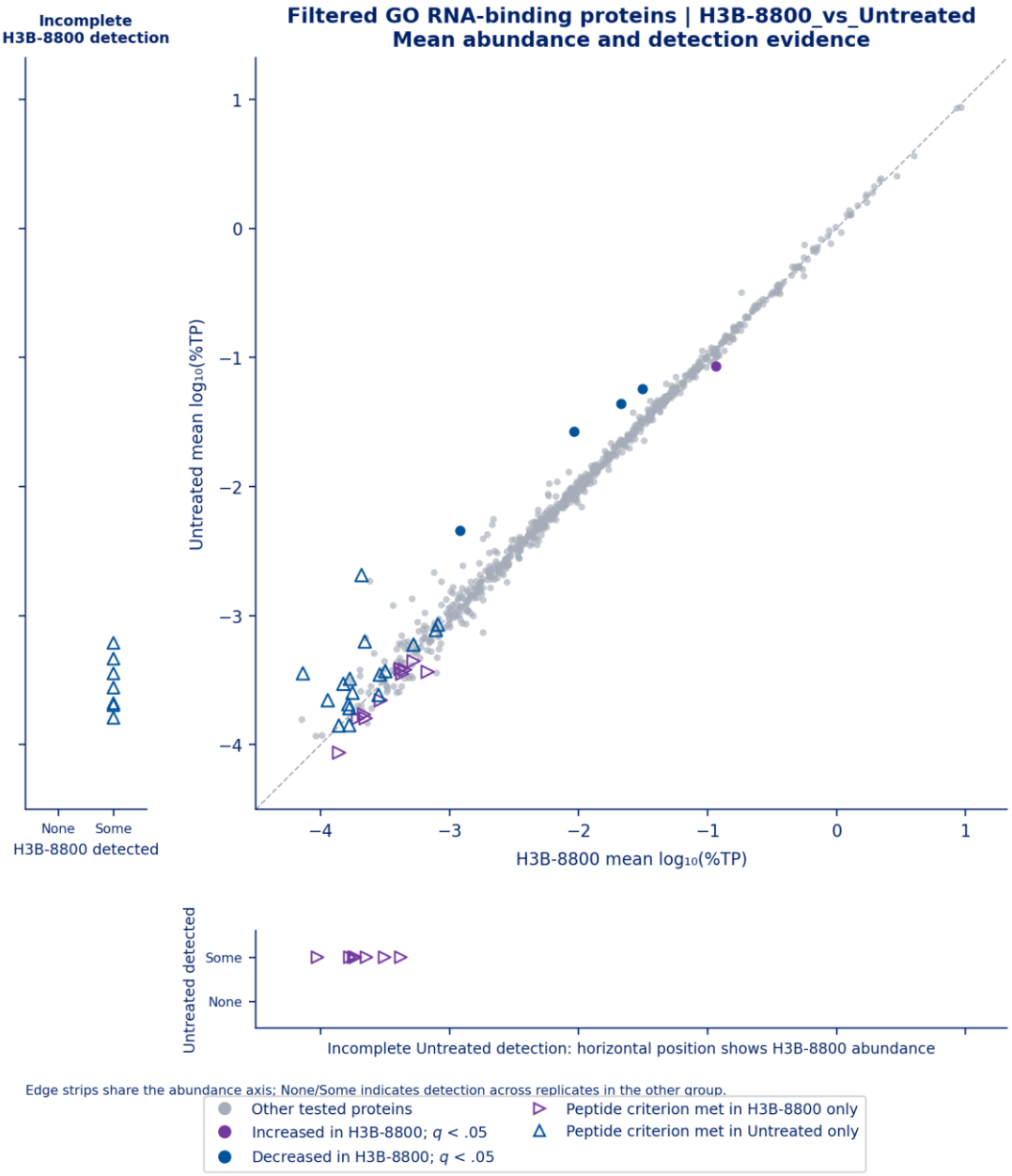


Figure 55. H3B-8800_vs_Untreated: measured abundance and incomplete detection evidence. Proteins meeting the peptide criterion in only one group are descriptive observations and have no assigned differential-abundance *p* values or fold changes.

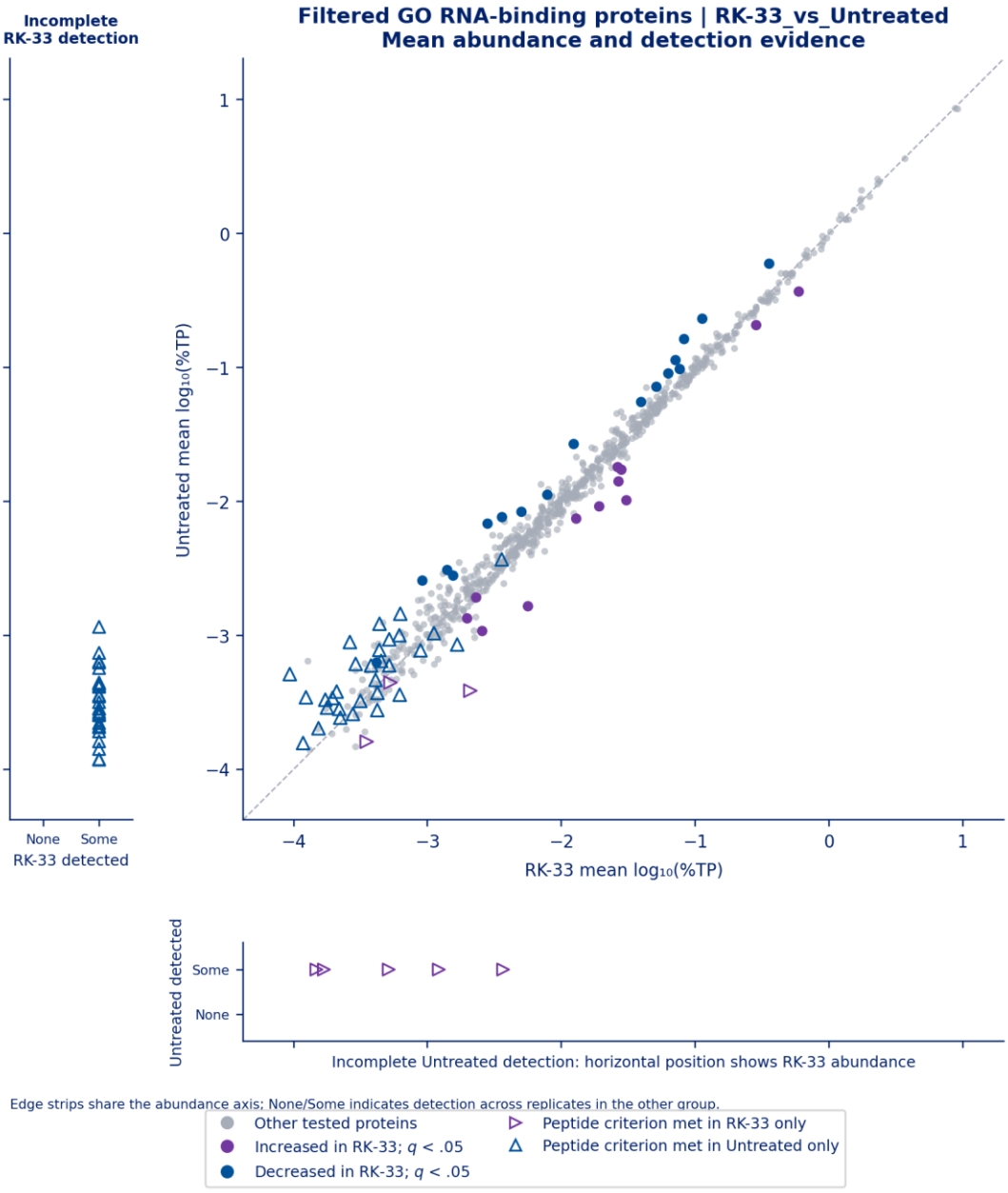


Figure 56. RK-33_vs_Untreated: measured abundance and incomplete detection evidence. Proteins meeting the peptide criterion in only one group are descriptive observations and have no assigned differential-abundance *p* values or fold changes.

14. Interpretation

This study profiles the cellular responses of HCT116 cells to H3B-8800 and RK-33. The two compounds produced distinct response patterns across the filtered GO RNA-binding protein panel. H3B-8800 was associated with changes in SF3B1 and other spliceosome proteins, while RK-33 was associated with changes in mitochondrial and cytoplasmic ribosomal proteins. These compound-responsive proteins provide candidate markers of cellular activity, and their functional relationships help place the responses in the context of the compounds' reported mechanisms.

H3B-8800 (10 µM, 90 minutes) was associated with differential abundance of five of 790 tested proteins ($q < .05$). SF3B1 (0.55-fold), AQR (0.35-fold), RBM22 (0.49-fold), and PPIE (0.27-fold) were decreased in the RNP fractions. H3B-8800 targets the SF3b complex, inhibits U2 snRNP assembly in biochemical studies, and modulates splicing in cell models (Seiler et al., 2018). The coordinated response of SF3B1 and other spliceosome proteins is consistent with activity involving the reported target complex and provides a potential compound-response signature. Negative ranked enrichment of spliceosome-related sets also included PRPF8 and additional spliceosome proteins; these related sets share proteins and should be interpreted as overlapping evidence for the same functional theme.

PABPC4, a cytoplasmic poly(A)-binding protein, was increased 1.37-fold in the H3B-8800 comparison ($q < .05$). PABP4 has been shown to bind poly(A) and support translation in a vertebrate developmental model (Gorgoni et al., 2011). PABPC4 and PABPC1 also contributed to a positively enriched RNA-recognition-motif gene set in the present study. This response identifies a potential activity marker outside the decreased spliceosome group; the published developmental system differs from the HCT116 treatment studied here.

RK-33 (10 µM, 90 minutes) was associated with differential abundance of 29 of 757 tested proteins ($q < .05$). MRPL15 (3.00-fold), MRPL21 (3.41-fold), MRPL3 (1.74-fold), and MRPL45 (1.46-fold) were increased, whereas MRPL37 (0.71-fold), PTCD3 (0.71-fold), RPS3 (0.49-fold), RPS14 (0.46-fold), and RPS28 (0.36-fold) were decreased. Mitochondrial translation-related annotations were over-represented among the differentially abundant proteins; the mitochondrial large-ribosomal-subunit gene set was also positively enriched in the ranked analysis (NES = 1.81, $q = .027$). The annotations overlap and include MRPL15, MRPL21, MRPL3, and MRPL45. Together with the cytoplasmic ribosomal proteins, they identify translation-related proteins as a prominent component of the RK-33 response.

RK-33 was developed as a DDX3 inhibitor (Bol et al., 2015). In breast cancer models, Heerma van Voss et al. (2018) reported that RK-33 treatment or DDX3 depletion affected mitochondrial translation and reduced mitochondrial translation-related proteins. The present HCT116 results likewise highlight mitochondrial ribosomal proteins, although the RNP-fraction measurements, treatment duration, and directions of individual protein changes differ from those prior experiments. DDX3X did not meet the protein-level significance threshold in this comparison. Hecht and Parker (2026) reported RK-33-associated cellular effects that persisted after DDX3 depletion in another model. The mitochondrial protein pattern is therefore a candidate signature of RK-33 activity, while its target dependence remains to be established.

The selectivity scores summarize response breadth across the 750 proteins eligible in both comparisons without applying a protein-level significance filter. At the twofold threshold, 13 proteins responded to H3B-8800 and 20 responded to RK-33. These scores describe the breadth of relative abundance changes under the tested conditions rather than direct compound binding or target specificity.

Under the signal-to-noise (*S*/*N*) analytical framework underlying the analyses in this report, differential abundance can serve as a proxy for altered relative RNA-interaction levels (Kristofich & Nicchitta, 2023, Supplementary Notes 4f and 6b–c). The filtered panel excludes proteins with historical *S*/*N* < 3 and retains proteins without historical measurements. Current-study protein-specific *S*/*N* was not measured; cellular protein abundance and the shared %TP denominator can also influence these relative measurements.

References

Bol, G. M., Vesuna, F., Xie, M., Zeng, J., Aziz, K., Gandhi, N., Levine, A., Irving, A., Korz, D., Tantravedi, S., Heerma van Voss, M. R., Gabrielson, K., Bordt, E. A., Polster, B. M., Cope, L., van der Groep, P., Kondaskar, A., Rudek, M. A., Hosmane, R. S., … Raman, V. (2015). Targeting DDX3 with a small molecule inhibitor for lung cancer therapy. *EMBO Molecular Medicine*, *7*(5), 648–669. https://doi.org/10.15252/emmm.201404368

Gorgoni, B., Richardson, W. A., Burgess, H. M., Anderson, R. C., Wilkie, G. S., Gautier, P., Martins, J. P. S., Brook, M., Sheets, M. D., & Gray, N. K. (2011). Poly(A)-binding proteins are functionally distinct and have essential roles during vertebrate development. *Proceedings of the National Academy of Sciences*, *108*(19), 7844–7849. https://doi.org/10.1073/pnas.1017664108

Heerma van Voss, M. R., Vesuna, F., Bol, G. M., Afzal, J., Tantravedi, S., Bergman, Y., Kammers, K., Lehar, M., Malek, R., Ballew, M., ter Hoeve, N., Abou, D., Thorek, D., Berlinicke, C., Yazdankhah, M., Sinha, D., Le, A., Abrahams, R., Tran, P. T., … Raman, V. (2018). Targeting mitochondrial translation by inhibiting DDX3: a novel radiosensitization strategy for cancer treatment. *Oncogene*, *37*(1), 63–74. https://doi.org/10.1038/onc.2017.308

Hecht, C. J. S., & Parker, R. R. (2026). RK-33 inhibits the OC43 coronavirus and induces stress granules via DDX3X-independent mechanisms. *RNA*, *32*(5), 724–735. https://doi.org/10.1261/rna.080931.125

Kristofich, J., & Nicchitta, C. V. (2023). Signal-noise metrics for RNA binding protein identification reveal broad spectrum protein-RNA interaction frequencies and dynamics. *Nature Communications*, *14*(1), 5868. https://doi.org/10.1038/s41467-023-41284-9

Seiler, M., Yoshimi, A., Darman, R., Chan, B., Keaney, G., Thomas, M., Agrawal, A. A., Caleb, B., Csibi, A., Sean, E., Fekkes, P., Karr, C., Klimek, V., Lai, G., Lee, L., Kumar, P., Lee, S. C.-W., Liu, X., Mackenzie, C., … Buonamici, S. (2018). H3B-8800, an orally available small-molecule splicing modulator, induces lethality in spliceosome-mutant cancers. *Nature Medicine*, *24*(4), 497–504. https://doi.org/10.1038/nm.4493

Supporting Data and Methods

README.md describes the package contents. Methods_and_Data_Analysis.docx contains the separate methods. The numbered panel folders contain complete result tables and available figures, including figures not selected for this report. SHA256SUMS.txt records package file checksums.